



With the support of the
Erasmus+ Programme
of the European Union



University of Évora

ARCHMAT

(ERASMUS MUNDUS MASTER IN ARCHaeological MATerials Science)

Mestrado em Arqueologia e Ambiente (Erasmus Mundus – ARCHMAT)

Preserving Archaeological Heritage through Roman Mortars of Villa Horta da Torre (Fronteira, Portugal)

Mizuki Takahashi

m50800

Supervisors | Patrícia Sofia Martins Moita
Paula Cristina Gonçalves Pereira Galacho
André Miguel Serra Carneiro



UNIVERSIDADE
DE ÉVORA

Evora, December 2023



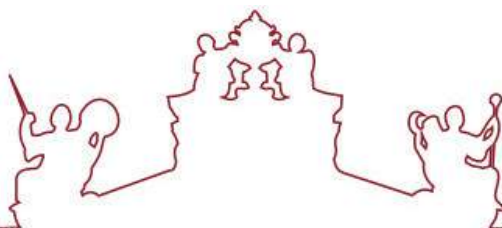
SAPIENZA
UNIVERSITÀ DI ROMA



SAPIENZA
UNIVERSITÀ DI ROMA



ARISTOTLE
UNIVERSITY OF
THESSALONIKI



**Universidade de Évora - Instituto de Investigação e Formação Avançada
Università degli Studi di Roma "La Sapienza" Aristotle University of
Thessaloniki**

Mestrado em Ciência dos Materiais Arqueológicos (ARCHMAT)

Dissertação

**Preservação do património arqueológico através do estudo
das argamassas romanas da villa Horta da Torre (Fronteira,
Portugal)**

Mizuki Takahashi

Orientador(es) | Patrícia Sofia Moita
André Miguel Carneiro
Cristina Galacho

Évora 2023

Esta dissertação não inclui as críticas e as sugestões feitas pelo júri.



PANEL OF JURY

Dados

Data da proposta: 06/12/2023

Data de homologação: 07/12/2023

Observações: GD/50551/2023-Proposta de Júri

Presidente do júri

Nome: Cristina Maria Barrocas Dias

Email: cmbd@uevora.pt

Departamento: Departamento de Química e Bioquímica

Vogais

Nome: Catarina Amélia Pereira Miguel de Sousa Cabral (Vogal)

Email: cpm@uevora.pt

Departamento: Laboratório HERCULES - Herança Cultural, Estudos e Salvaguarda

Nome: Ioannis Karapanagiotis (Vogal)

Email: y.karapanagiotis@aeath.gr

Nome: Eleni Pavlidou (Vogal)

Instituição: Aristotle University of Thessaloniki

Nome: Cristina Lemorini (Vogal)

Email: cristina.lemorini@uniroma1.it

Instituição: Università di Roma La Sapienza

Nome: Paula Cristina Gonçalves Pereira Galacho (Co-orientador)

Email: pcg@uevora.pt

Departamento: Departamento de Química e Bioquímica

Nome: Carlos Alexandre da Silva Ribeiro (Arguente)

Email: cribeiro@uevora.pt

Departamento: Departamento de Geociências

ABSTRACT

The Roman villa Horta da Torre was built around 3 - 4 century A.D. The archaeological site is located at Cabeço de Vide (Fronteira), Alto Alentejo Region, Portugal. The Roman villa is estimated to be around 30,000 square meters including the parts that have not gone under excavation. Located between two ancient cities, Augusta Emerita (Merida, Spain) and Olisippo (Lisbon, Portugal), Horta da Torre played a significant role as a median site between the two major cities on the Antonine Itinerary.

The aim of this study is to address the construction phase(s), production technology and provenance of materials by a multi-analytical approach to study textural, mineralogical, and chemical characterization of the selected mortars.

To address the construction(s) phase(s), production technology and provenance of materials, a total of 18 samples of mortar walls were collected from Horta da Torre, including renders and fillers. A multi-analytical approach to study textural, mineralogical, and chemical characterization of the selected mortars was developed by using Optical Microscopy, Scanning Electron Microscopy - Energy Dispersive X-ray Spectroscopy (SEM-EDS), X-ray Diffraction (XRD), Thermogravimetric analysis (TGA-DTG), Acid Attack, and Granulometric Analysis.

The research revealed that the excavated part of the villa agrees with three construction phases. Three groups of mortars were addressed based on their aggregates; granitic, basic, and mixed, used as filling and render. The production technology of mortars appears to have followed Vitruvius's recipe considering volume proportions but not for mural painting. The study also revealed that the aggregates likely come from two local sources; 2 km north of the site and 3.5 km south of the site, whereas lime raw material was available at a distance of within a kilometer of the site.

Key Words: Horta da Torre, mortars, Roman Villa, Characterization, Aerial, Hydraulic, Archaeometry.

RESUMO

A villa Romana Horta da Torre terá sido edificada por volta dos séculos III a IV d.C. O sítio arqueológico situa-se em Cabeço de Vide (Fronteira), região do Alto Alentejo, Portugal. Estima-se que a villa Romana tivesse cerca de 30.000 metros quadrados, incluindo as partes por escavar. Situada entre duas cidades antigas, Augusta Emerita (atual Mérida, Espanha) e Olisippo (atual Lisboa, Portugal), a villa Romana Horta da Torre desempenhou um papel importante como local intermédio entre estas duas grandes cidades do Itinerário Antonino.

O objetivo do trabalho foi a caracterização de argamassas Romanas da villa Romana da Horta da Torre, do ponto de vista textural, mineralógico e químico, visando a obtenção de informações sobre as fases de construção, a composição, a tecnologia de produção, as matérias-primas utilizadas e a sua proveniência.

No total, foram recolhidas 18 amostras de argamassas da villa Horta da Torre, incluindo argamassas de reboco e argamassas de enchimento. Para a caracterização das amostras foi usada uma abordagem arqueométrica multianalítica: Microscopia Ótica (Estereomicroscopia e Petrografia), Microscopia Eletrónica de Varrimento – Espectroscopia de Energia Dispersiva de Raios-X (MEV-EDS), Difração de Raios-X (DRX),-Análise Termogravimétrica (ATG-DTG), Ataque Ácido e Análise Granulométrica.

O estudo revelou que a parte escavada da villa foi construída em, possivelmente, três fases. As amostras foram divididas em três grupos, com base no tipo de agregados mais abundantes nomeadamente em graníticas, básicas e mistas. A tecnologia de produção das argamassas parece ter seguido, em alguns casos, a “receita” do arquiteto Romano Vitruvius. O estudo revelou ainda que os agregados eram, muito provavelmente, oriundos de duas fontes locais, situadas a 2 km a norte do sítio e a 3,5 km a sul do mesmo, enquanto a matéria-prima para a cal se encontrava disponível à distância de aproximadamente 1 km.

Palavras-chave: Horta da Torre, Argamassas, villa Romana, Caracterização, Aéreas, Hidráulicas, Arqueometria.

ACKNOWLEDGMENTS

Firstly, I would like to express my deepest gratitude to my supervisor, Professor Patrícia Moita, co-supervisor Professor Cristina Galacho, and co-supervisor Professor André Carneiro for their thorough guidance, expertise, aspiring insights, encouragement, and patience throughout the process. I am thankful to the supervisors for giving me the support that I needed throughout the entire process of this thesis and for always being available for discussions. It would have never been possible to accomplish this achievement without the professors, and they make a wonderful team in the study of historical mortars.

I would like to thank Ms. Sandra Velez and Ms. Aida Graça, assistant technicians at the University of Évora, for spending five weeks guiding me through the making of thin sections and assisting me with my preparation for the laboratory work, and the committed support in achieving the best results.

I am grateful to Massimo Beltrame, Anna Tsoupra, Dora Boieiro, Silvia Bottura-Scardina, and all other researchers, technicians, and professors at the HERCULES laboratory at the University of Évora for always being available to assist me in my needs by providing technical support and feedback at the laboratory.

I would like to thank Professor Nick Schiavon and the ARCHMAT Committee, for giving me the opportunity to participate in this program. I am grateful to all the professors who equipped us with the valuable knowledge and skill sets to develop and lead the future of archaeometry and heritage science.

Special thanks to Professor Carlos Ribeiro, Geosciences Department, for reviewing my work and giving me feedback to finalize this thesis.

Lastly, I would like to thank my colleagues, friends, and family for unconditionally encouraging and supporting me.

LIST OF FIGURES

Figure 2.1: Map of Portugal and Alto Alentejo region. created based on Google Maps.. 8

Figure 2.2: Diagram of Hispania with location of Horta da Torre Roman villa and Antonine Itinerary near the site in third century B.C. not to scale. created by author based on Iberian peninsula map (Carneiro, 2022), location of the site fig. 1 (Carneiro, A., Sanchez, J. G., Stek, T. D et al., 2020), and index map of Roman roads (Arias, 2004). 9

Figure 2.3: Locations of Roman settlement in the Fronteira territory (Carneiro, 2022). 10

Figure 2.4: Room plan of Horta da Torre Roman villa: a) *cenatio aestivalis*, b) large peristyle, c) small peristyle, d) and e) *cubiculum*, f) hypocaust. Locations of structures: a) *stibadium*, b) water channel, c) *impluvium* d) Y-shaped drainpipe. Schematic plan of structures - Roman villa of Horta da Torre (Fronteira). Research project under the responsibility of André Carneiro. Created by Ana Martins. Provided by André Carneiro. 12

Figure 2.5: Horta da Torre site photos. Captured at sampling on March 2, 2023. a) *stibadium* and double apse b) Y-shaped drainpipe c) large peristyle d) small peristyle. 13

Figure 2.6: Render of *cenatio aestivalis* filled with water. 3D proposal made by Gonçalo Lopes, Carlos Carpetudo and André Carneiro (Carneiro, 2019.) Roof proposal is tentative. 14

Figure 2.7: Aerial view of excavated southeast corner at the end of the 2019 campaign. Drone photo by Jesus García Sánchez (Carneiro, 2020.)..... 16

Figure 2.8: Geological map around Horta da Torre Roman villa based on Portalegre [32-B, top], Sousel [32-D, bottom] (Gonçalves, 1973; Gonçalves et al, 1975, and Marques, 2017). The location of a stream near Horta da Torre is indicated by light blue line..... 18

| | |
|--|----|
| Figure 3.1: Analytical methodology diagram..... | 24 |
| Figure 3.2: Sample locations and function..... | 25 |
| Figure 3.3: Sample preparation diagram. | 26 |
| Figure 4.1: Representative micrographs of granitic, basic, and mixed groups. | 38 |
| Figure 4.2: Mixed group samples demonstrating different layers in cross section (left) and thin sections (right). | 39 |
| Figure 4.3: Sample locations indicating sample groups and functions based on the petrographic analysis..... | 41 |
| Figure 4.4: Representative micrographs of mural render mortar (MHT-9). Red arrows indicate lime layer. Dashed lines indicate limestone fragments. | 44 |
| Figure 4.5: SEM-EDS representative images of granitic, basic, and mixed groups. BSE images and elemental map distribution. | 45 |
| Figure 4.6: TG Curve Comparisons by Granitic, Basic and Mixed Groups (A, B, and C) and TG/DTG Curves of Different Steps (C, D, and E)..... | 49 |
| Figure 4.7: Diffractograms by groups (granitic, basic, and mixed) and functions (render and filling). | 53 |
| Figure 4.8: Soluble fraction (%) compared by groups and functions. | 57 |
| Figure 4.9: Average percentage of insoluble residue and soluble fraction from acid attack analysis..... | 58 |
| Figure 4.10: Comparison between acid attack soluble fractions and TGA carbonates (%) by groups and functions. | 58 |
| Figure 4.11: Grain size distribution grouped by granitic, basic, and mixed groups and their functions. | 60 |
| Figure 4.12: Gravel sand mud diagram obtained using GRADISTAT. | 62 |

Figure 5.1: Horta da Torre Roman villa aerial view indicating Ditta's sample (Ditta, 2017) and Madrid's sample (Madrid, 2019) locations. Ditta's samples (HT-40 and HT-60) and Madrid's samples (HHT-4 and PHHT-6) are shown with red arrows.

..... 76

LIST OF TABLES

| | |
|--|----|
| Table 3.1: Sample function and locations. | 27 |
| Table 4.1: Visual inspection results. | 36 |
| Table 4.2: Type of minerals and rocks found in petrographic analysis in comparison to the function of mortar..... | 40 |
| Table 4.3: Individual minerals observed by petrographic microscope in cross polarized light (xpl) [left] and plane polarized light (ppl) [right]. Thin sections are thick to preserve binder..... | 42 |
| Table 4.4: TGA mass loss (%) according to temperature range..... | 51 |
| Table 4.5: Mineralogical composition of the global fractions assessed by XRD..... | 54 |
| Table 4.6: Simplified compositions of the mortars determined according to the Jedrzeiewska method. Soluble fraction (Jedrzeiewska) = $100 - [(IR \text{ (from acid attack)} + \text{calcium carbonate (from TGA)})]$ | 57 |
| Table 4.7: Results from GRADISTAT particle size analysis software showing sieving errors and descriptions of insoluble fractions in each sample. | 62 |
| Table 4.8: Colors and shapes of aggregates based on insoluble residues obtained by stereozoom microscopy..... | 63 |
| Table 4.9: Representative samples of granitic group with only white and transparent fragments..... | 64 |
| Table 4.10: Representative samples of granitic group with light-orange or light-pink fragments..... | 64 |
| Table 4.11: Representative samples of granitic group with brown fragments. | 65 |
| Table 4.12: Representative samples of basic group with dark-colored fragments. | 65 |

| | |
|--|----|
| Table 4.13: Representative samples of mixed group with white/transparent and black/green fragments. | 66 |
| Table 5.1: Samples by functions, aggregate groups, subgroups, and binder types. | 70 |
| Table 5.2: Samples compared by key aspects that effect on strength of mortar..... | 78 |

LIST OF APPENDICES

Appendix I. Photos of samples from Horta da Torre.....I
Appendix II. TG and DTG Curves.II
Appendix III: X-ray Diffractograms of Global Fractions.....III
Appendix IV: X-ray Diffractograms of Fine Fractions.IV
Appendix V: Insoluble Residues Sorted by Sieving System for Granulometric Analysis
After Acid Attack.....V
Appendix VI: Cross Section of Samples Taken by Stereozoom Microscope.....VI
Appendix VII: Acid Attack Results.VII

TABLE OF CONTENTS

| | |
|---|-----------|
| PANEL OF JURY | i |
| ABSTRACT | ii |
| RESUMO | iii |
| ACKNOWLEDGMENTS | iv |
| LIST OF FIGURES | v |
| LIST OF TABLES | viii |
| LIST OF APPENDICES | x |
| TABLE OF CONTENTS | xiii |
| 1. INTRODUCTION | 1 |
| 1.1. OBJECT OF STUDY | 1 |
| 1.2. MORTARS | 1 |
| 1.3. AERIAL BINDERS | 2 |
| 1.3.1. Calcareous Lime Mortars: CaCO_3 | 2 |
| 1.3.2. Magnesian Lime Mortars: $\text{CaMg}(\text{CO}_3)_2$ | 4 |
| 1.4. HYDRAULIC BINDERS | 5 |
| 1.4.1 Natural Hydraulic Binders | 5 |
| 1.4.2 Artificial Hydraulic Binders | 5 |
| 1.5. AGGREGATES | 6 |
| 2. ARCHAEOLOGICAL CONTEXT | 8 |
| 2.1. THE SITE | 8 |
| 2.2. HISTORICAL BACKGROUND OF VILLA HORTA DA TORRE | 11 |
| 2.2.1 Initial Occupation | 11 |
| 2.2.2 Abandonment and Second Occupation | 15 |
| 2.3. EXCAVATION | 16 |
| 2.4. GEOLOGICAL CONTEXT | 17 |
| 3. SAMPLES AND METHODOLOGY | 19 |
| 3.1. ANALYTICAL TECHNIQUES AND METHODS | 19 |
| 3.1.1 Visual Analysis | 19 |
| 3.1.2 Optical Microscopy (OM) | 20 |

| | | |
|-----------|--|-----------|
| 3.1.3 | X-Ray Diffraction (XRD)..... | 20 |
| 3.1.4 | Thermogravimetric analysis (TGA-DTG) | 21 |
| 3.1.5 | Variable Pressure Scanning Electron Microscopy (VP-SEM-EDS) | 22 |
| 3.1.6 | Acid Attack and Granulometric Analysis | 23 |
| 3.2 | SAMPLING | 24 |
| 3.3 | SAMPLE PREPARATION..... | 27 |
| 3.3.1 | Cleaning for Visual Inspection | 27 |
| 3.3.2 | Sample Preparation for Optical Microscopy and SEM-EDS—Cross and Thin Sections | 28 |
| 3.3.3 | Sample Preparation for X-Ray Diffraction (XRD) and Thermogravimetric Analysis (TGA) - Powders..... | 30 |
| 3.3.4 | Sample Preparation for Acid Attack and Granulometric Analysis – Fractions | 30 |
| 3.4. | EXPERIMENTAL CONDITIONS..... | 30 |
| 3.4.1 | Experimental Conditions for Petrographic Analysis | 30 |
| 3.4.2 | Experimental Conditions for X-Ray Diffraction (XRD)..... | 31 |
| 3.4.3 | Experimental Conditions for Thermogravimetric Analysis (TGA-DTG)..... | 31 |
| 3.4.4 | Experimental Conditions for Variable Pressure Scanning Electron Microscopy (VP-SEM-EDS) | 32 |
| 3.4.5 | Experimental Conditions for Acid Attack and Granulometric Analysis..... | 32 |
| 4. | RESULTS..... | 34 |
| 4.1 | VISUAL INSPECTION | 34 |
| 4.2 | PETROGRAPHIC MICROSCOPE..... | 37 |
| 4.3 | VARIABLE PRESSURE SCANNING ELECTRON MICROSCOPY COUPLED TO ENERGY DISPERSIVE X-RAY SPECTROSCOPY (VP-SEM-EDS)..... | 43 |
| 4.4 | THERMOGRAVIMETRIC ANALYSIS (TGA)..... | 46 |
| 4.5 | X-RAY DIFFRACTION (XRD) – POWDER XRD | 51 |
| 4.5.1 | Diffractograms..... | 51 |
| 4.5.2 | Semi-Analytical Quantification | 54 |
| 4.6 | ACID ATTACK AND GRANULOMETRIC ANALYSIS | 55 |
| 4.6.1 | Acid Attack..... | 55 |
| 4.6.2 | Granulometric Analysis | 59 |
| 5. | DISCUSSION | 67 |
| 5.1 | SUMMARY OF RESEARCH AIMS..... | 67 |

| | | |
|-----------|--|-----------|
| 5.2 | KEY FINDINGS..... | 67 |
| 5.2.1 | Construction Phases based on Aggregate Groups..... | 67 |
| 5.2.2 | Raw Materials of Binders | 70 |
| 5.2.3 | Provenance of Materials | 71 |
| 5.2.4 | Production Technology of the Horta da Torre..... | 73 |
| 5.3. | FURTHER INTERPRETATION OF FINDINGS | 75 |
| 5.3.1 | Comparison with Existing Research | 75 |
| 5.3.2. | Different Behavior of Aggregates in Mortars..... | 76 |
| 5.4 | LIMITATIONS OF THIS RESEARCH AND RECOMMENDATIONS | 78 |
| 6. | CONCLUSION | 80 |
| 7. | BIBLIOGRAPHY | 83 |

1. INTRODUCTION

1.1. OBJECT OF STUDY

The study of cultural heritage is essential to understanding the past, current, and future of human behavior and society. The interdisciplinary studies of built heritage not only give us insights into past human lives and development but also help us understand today's construction techniques and architecture as a legacy of the past and contribute to designing a better future.

This project was researched at the HERCULES Laboratory of the University of Évora, Portugal, as a thesis topic of the Erasmus Mundus Archaeological Materials Sciences Joint Master's Degree (ARCHMAT). In this project, selected mortars from Horta da Torre, Roman Villa archaeological site located in Cabeço de Vide, Fronteira, Alentejo, Portugal were studied to understand the construction phases of the villa, the production technology, and the origin of the raw materials. These issues were approached using multi-technical analysis that is crucial to study mortars.

X-ray Diffraction (XRD) was used to reveal mineral phases, Thermal Gravimetric Analysis (TGA), Acid attack, and Granulometric Analysis for the study of binder and aggregates, Optical Microscopy (OM) and Variable Pressure Scanning Electron Microscopy coupled to Energy Dispersive X-ray Spectroscopy (SEM-EDS) for visual inspection and identification of minerals.

1.2. MORTARS

The earliest record of mortar used as a part of masonry system is as early as 6500 BC in the Indus Valley Civilization (Khan et al., 2013). Lime as a building material was developed during the Roman Age, around the third century BC. By the second century B.C, Pozzuoli, a volcanic material, was discovered and used to produce hydraulic mortar.

An excellent example of Roman use of concrete is the Pantheon in Rome, Italy, which showcases the mastery of the Roman techniques of creating vaults and domes (Wang, 2013).

Mortars can be used to bind construction bricks. This type of mortar that is used to lay the structure of walls is commonly known as filling mortar. Mortars can also be used to cover and regulate the surface of walls. This type of mortar is referred to as rendering. Depending on the use of the walls, render mortar can have specific properties. It can be a waterproof layer and/ or a preparation layer for applying pigments of mural paintings.

There are two categories of lime cement: aerial lime and hydraulic lime. Slaked lime, a type of air-hardening cementitious material commonly employed in lime mortar, is what is normally referred to as aerial lime (Zhang et al., 2018). Its primary ingredient is calcium hydroxide, $\text{Ca}(\text{OH})_2$. Calcium hydroxide reacts with the carbon dioxide in the air to produce calcium carbonate and release moisture. Traditional lime mortar has a strong water vapor permeability and small drying shrinkage building material, but it also has low early strength, slow condensation hardening that takes one to two days, weak water resistance, and ready dissociation in wet or water conditions (Zhang et al., 2018).

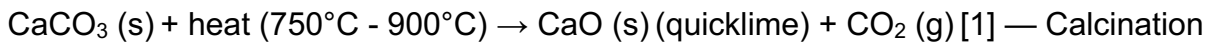
It is preferable to use hydraulic lime, a hydraulic cementitious material, to prepare bonding, plaster, or tick-off seam mortar for use as ancient building repair materials and external wall decorating mortar engineering. Hydraulic lime has both hydraulicity and air-hardening characteristics. The advantages of hydraulic lime include intermediate strength, faster hardening speed of 4 to 12 hours, strong water resistance, and resistance to salt erosion (Zhang et al., 2018).

1.3. AERIAL BINDERS

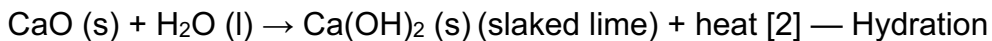
1.3.1. Calcareous Lime Mortars: CaCO_3

Pure lime mortars are set by the reaction with the carbon dioxide in the air (Faria et al., 2011). The main raw material of the lime mortar is limestone (CaCO_3), which is a sedimentary rock that can be obtained from the precipitation of carbonate on a sedimentary basin such as sea or lake water.

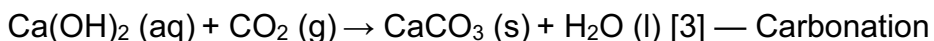
There are three chemical stages to obtaining mortars from limestones. Firstly, the limestone is heated by the fire with a temperature between 750°C - 900°C. This decomposition of limestone produces quicklime consisting of calcium oxide (CaO), along with CO₂ that escapes into the atmosphere. This chemical process is called calcination [1].



In the next step, the quicklime produced by calcination is mixed with added water (H₂O). This produces slaked lime, consisting of calcium hydroxide (Ca(OH)₂) [2]. As a result of adding water to the calcium oxide, an exothermic reaction occurs. The heat escapes, and only the slaked lime is left as a product. Since this step is to add water, it is called hydration.



The slaked lime produced in hydration [2] reacts with the CO₂ in the environment in step 3 [3]. As a result, calcite is produced along with water that evaporates into the atmosphere. This process is known as carbonation [3]. The carbonation of lime ensures that bonds are stronger and that the mortar is durable to sustain a building.



Although the chemical composition of the limestone (CaCO₃) and the calcite (CaCO₃) are the same, they are different substances in principle. Limestone is a sedimentary rock that is composed of calcium that includes calcite and dolomite, whereas calcite is a mineral composed of calcium carbonate. Limestone is a rock used at the beginning of the process, and calcite is a mineral as a result of the chemical reactions of limestone.

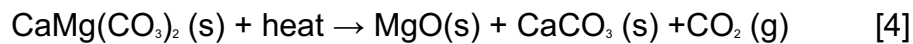
Unlike hydraulic mortars, aerial lime mortars need contact with CO₂ to set, as shown in the last step, carbonation [3]. The calcium hydroxide only hardens when exposed to the

air. Different types of aggregates are added depending on the purpose of use at the last step of making lime mortars.

1.3.2. Magnesian Lime Mortars: $\text{CaMg}(\text{CO}_3)_2$

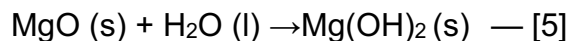
Magnesian lime is produced when dolostone instead of limestone is used to obtain lime. If the calcium oxide (CaO) in lime is less than 95%, the lime is considered dolostone or dolomitic lime. Dolostone contains magnesium and calcium carbonate, while lime only contains calcium carbonate. The results of firing dolostone are different from the process mentioned above of calcareous limestone, Despite the same process of calcination, hydration, and carbonation. Magnesium lime does not have evidence of hydraulic properties (Chever et al., 2010.).

In the calcination process [4], the firing temperature is at around 600°C , which is considerably lower than that of calcareous lime at around 900°C .

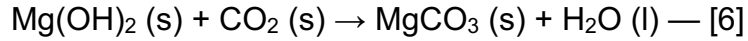


The calcite (CaCO_3) produced in [4] decomposes at a higher temperature as shown in equation [1].

In the second step, hydration, when water is added, Calcium Oxide (CaO) reacts with water and produces slaked lime, $\text{Ca}(\text{OH})_2$ as shown in equation [2]. Magnesium Oxide (MgO) reacts with water and produces brucite, $\text{Mg}(\text{OH})_2$; however, this hydration process of MgO takes much longer time than CaO (Chever et al., 2010) — [5].



In the final step of carbonation, the hardening of calcareous lime in contact with CO_2 in the environment takes days to months as in equation [3], whereas the hardening of magnesium lime can take a much longer time, sometimes for years [6].

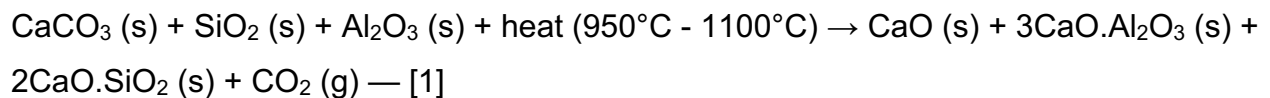


Just like calcareous lime, magnesium lime is ideal for building materials. Although magnesium lime can experience some shrinkage in volume, it requires less water to be added in production which can increase the workability of the mortar (Chever et al., 2010). Magnesium lime also has a relatively high mechanical strength in comparison to calcareous mortars, which makes it suitable as a building material (Chever et al., 2010).

1.4 HYDRAULIC BINDERS

1.4.1 Natural Hydraulic Binders

Natural hydraulic lime, or hydrated hydraulic lime, is the type of hydraulic lime that already has hydraulic properties without any additives. This type of hydraulic binder was most used in antiquity until the invention of Portland cement in the 19th century (Callebaut, 2001). It can be obtained by firing marl limestone at a temperature of 950-1100°C as shown in equation [7]. Marl limestone contains about 5 - 20% of clay, whereas regular lime or limestone contains only up to 5% of clay. The lower the CaCO₃, the higher the clay content to substitute it.



Hydraulic lime is composed of calcium silicates (2CaO.SiO₂) and calcium aluminates (3CaO.Al₂O₃) which harden in the presence of water or air and calcium oxide (CaO) which hardens by carbonation.

1.4.2 Artificial Hydraulic Binders

Portland cement, an artificial hydraulic binder, is made of clinker (85-95%), gypsum (4-6%), and other additives. According to the definition by the European Standard EN 197.1

Scope, "Portland cement clinker is a hydraulic material which shall consist of at least two-thirds by mass of calcium silicates ($2\text{CaO}\cdot\text{SiO}_2$), the remainder consisting of aluminum- and iron-containing clinker phases and other compounds. The ratio of CaO to SiO_2 shall not be less than 2:0. The magnesium content (MgO) shall not exceed 5.0% by mass (CEN, 2011)." Clinker is produced by the firing of clay, limestone, and sand (silicates), at temperatures around 1500°C (Saleh et al., 2020). Clay can contain silica (SiO_2), Aluminum oxides (Al_2O_3), and Iron Oxides (Fe_2O_3). As discussed in 1.2.1 Aerial Binder, limestone can contain calcium oxides (CaO) and Magnesium oxides (MgO). Heated at 1500°C , 20 to 30% of the mass is melted. Once the clinker is cooled, gypsum (calcium sulfate) is added. After the addition of gypsum to the clinker, the mixture is ground to powder (Hosam et al., 2020).

Portland cement emerged in 1824 and dominated the building material industry since then. Lime was mainly used in buildings before the invention of Portland cement (Callebaut, 2001). However, lime mortar has better durability and is reconsidered its brilliance as a building material in recent years (Zhang et al., 2018.).

1.5 AGGREGATES

Aggregates are additives that reduce plasticity and minimize the volume variation of mortars. Generally, one part of lime is mixed with three parts of aggregate for building mortars; however, this ratio depends on the use purpose of the mortar. The thicker the lime, the more aggregates should be added, as thick lime results in a larger change in the volume.

Aggregates can be quartz, calcareous, or hydraulic materials. Calcareous materials come from natural rocks, such as marble or travertine. Pozzolan, bricks, tufts, grogs, or glass are considered the hydraulic materials that add or improve the hydraulic property of the binders. The use of such hydraulic materials dates to the Roman time, when it is recorded on *The Ten Books on Architecture* by Vitruvius. He wrote about pozzolan on Book II, Chapter VI: "This substance, when mixed with lime and rubble, not only lends strength to buildings of other kinds, but even when piers of it are constructed in the sea, they set hard under water" (Morgan, 1914).

Mixing natural lime mortars with additives such as ceramic sherds, tile fragments, or brick pieces creates porosity, water absorption by capillarity rise, and permeability of vapor. The additives also assist the mortar in improving mechanical strength and stress resistance. The more additives were added, the more improvements to the hydraulic property (Torres et al., 2020).

2. ARCHAEOLOGICAL CONTEXT

2.1 THE SITE

Horta da Torre is an excavation site of a Roman Villa that dates to 1500 - 2000 years ago, estimated to have become active around the third and the fourth century A.D (Carneiro, 2019). The site is in the jurisdiction of Cabeço de Vide, near Fronteira, Alto Alentejo Region, Portugal (Figure 2.1) ($39^{\circ}07'12.0''N$ $7^{\circ}33'52.9''W$). This area was a part of the Lusitania province during the Roman period of which the capital city was Augusta Emerita, current-day Merida, Spain (Carneiro, 2019). The site is situated approximately halfway between Merida, Spain, and Lisbon, Portugal (Figure 2.2.). The currently excavated part is only a part of the vast Roman villa, specifically at the Southeastern corner of the site. The structure that has not been excavated yet is estimated to be 2 to 3 hectares or 20,000 - 30,000 square meters in total (Carneiro, 2022). The site is privately owned today, and the landowner agreed to the excavation and research by the University of Évora.



Map of Portugal and Alto Alentejo Region. Created based on ©Google Maps

Figure 2.1: Map of Portugal and Alto Alentejo region. created based on Google Maps.



Figure 2.2: Diagram of Hispania with location of Horta da Torre Roman villa and Antonine Itinerary near the site in third century B.C. not to scale. created by author based on Iberian peninsula map (Carneiro, 2022), location of the site fig. 1 (Carneiro, A., Sanchez, J. G., Stek, T. D et al., 2020), and index map of Roman roads (Arias, 2004).

The villa is located between two large ancient cities, Augusta Emerita (current day Mérida, Spain) and Olisippo (Lisbon, Portugal.) Having played an important role as an intermediate site between the two major cities, the villa had easy access to luxurious produce and goods from both cities. This information aligns with the Antonine Itinerary, one of the Roman itineraries that described Roman Empire roadways (Carneiro, 2020). Including Horta da Torre, several villas in the same area also seem to be located along this ancient itinerary (Figure 2.3.) (Carneiro, 2022).

The area is characterized by its soil with great agricultural potential and a thermal spa located northwest of the site and two kilometers away in the Sulfúrea Valley (Carneiro, 2019). The Antonine Itinerary connected the Villa and the Sulfúrea Valley, and the spa most likely drew people into the area as a local attraction. The thermal spa remains today in Cabeço de Vide and is known as Termas da Sulfúrea.

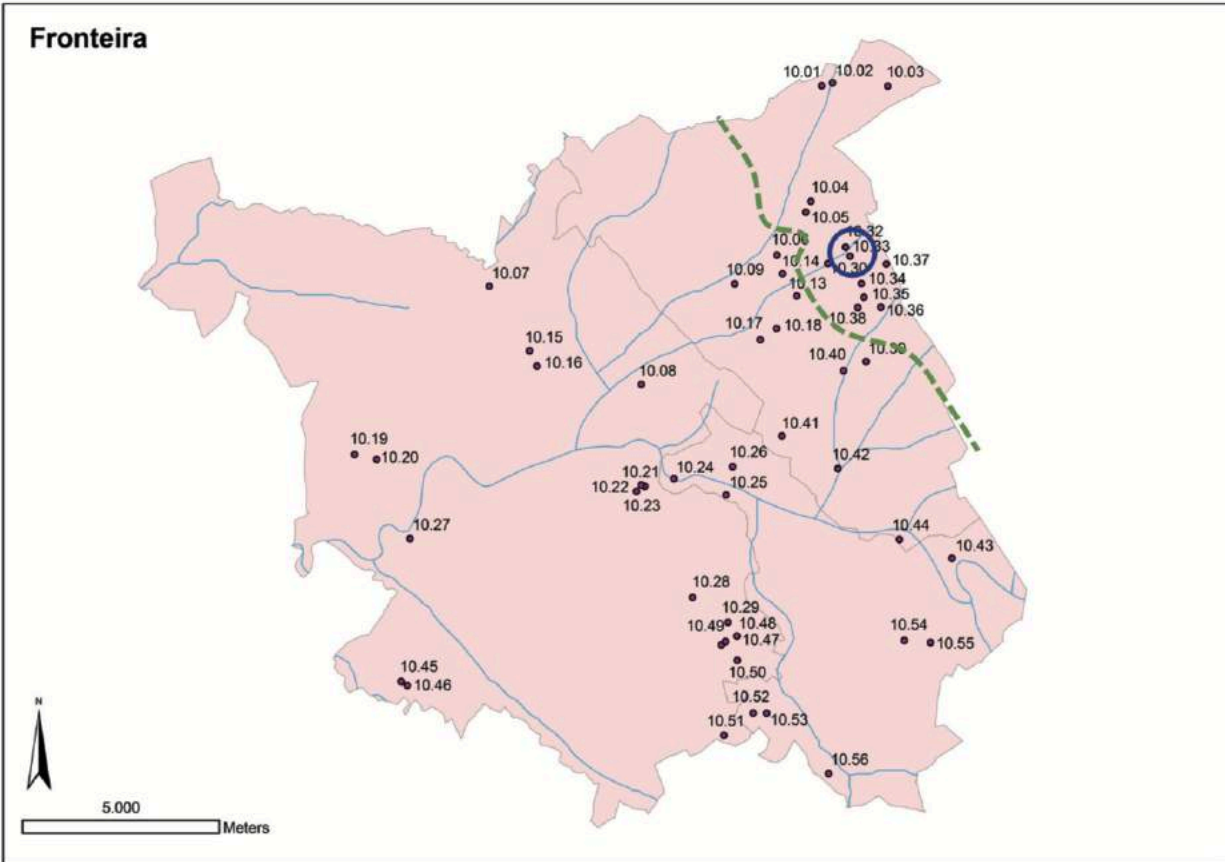


Figure 2.3: Locations of Roman settlement in the Fronteira territory (Carneiro, 2022).

Placing the villa on a gradually sloped site was also considered deliberate. The slope provided the site with visibility, protection from the wind, and effective reception of natural light (Carneiro, 2019). As a result of being built on a slope, parts of the villa rest on different topographic levels. The *cenatio aestivalis* (banquet room) and the large peristyle rest on one level, and the small peristyle rests on a lower level (Carneiro, 2019).

2.2 HISTORICAL BACKGROUND OF VILLA HORTA DA TORRE

2.2.1 Initial Occupation

It is probable that the villa was owned by a prosperous private owner(s) and was utilized as a summer retreat. Some of the traditional Roman villa typology traits can be seen in this villa such as the baths (*balneae*), the dining hall (*cenatio aestivalis*, Figure 2.4 A), the courtyard (peristyle, Figure 2.4 B), the small peristyle in tetra-style with four columns (Figure 2.4 C) with a water basin (impluvium, Figure 2.4 c), and the bedroom (cubiculum, Figure 2.4 D).

The *cenatio aestivalis* in this villa has a unique feature that the floor was most likely filled with a few centimeters of water. The study of the floor mortar revealed that it was hydraulic (Madrid, 2019). The water would have reflected the sun to create a special mirror effect and eased the severe heat of internal Portugal. This room, like a typical *cenatio aestivalis* of the era, would have functioned as a banquet room for summer ceremonies, encouraging social interactions between noble people to expand their business connections.

It is estimated that the owner(s) of the villa came from the city to the villa and stayed for a few days at a time. It was a typical daily life of elites to come from the cities and socialize at their villas located away from the cities. The villas were considered a more private, intimate, and relaxed environment in comparison to the city environment.

During the day, the owners and visitors would eat frugally. In the afternoon, a banquet would be held in the *cenatio aestivalis* (Figure 2.4 A) which lasted for several hours until nighttime (Carneiro, 2019). At the banquet, the people would eat on top of the semi-circular-shaped *stibadium* (Figure 2.4 a), a later form of Roman reclining chair, which remains intact at the site today (Figure 2.5 A). A moveable table was most likely brought in with food and drinks by the slaves. Performing artists such as poets, dancers, and theater groups were brought to the stage for entertainment, and the water was filled in

the hydraulic-mortar-paved stage floor (Figure 2.6). This created a water-mirror scenario and a unique atmosphere as well as relieving the unbearable heat in the summer.

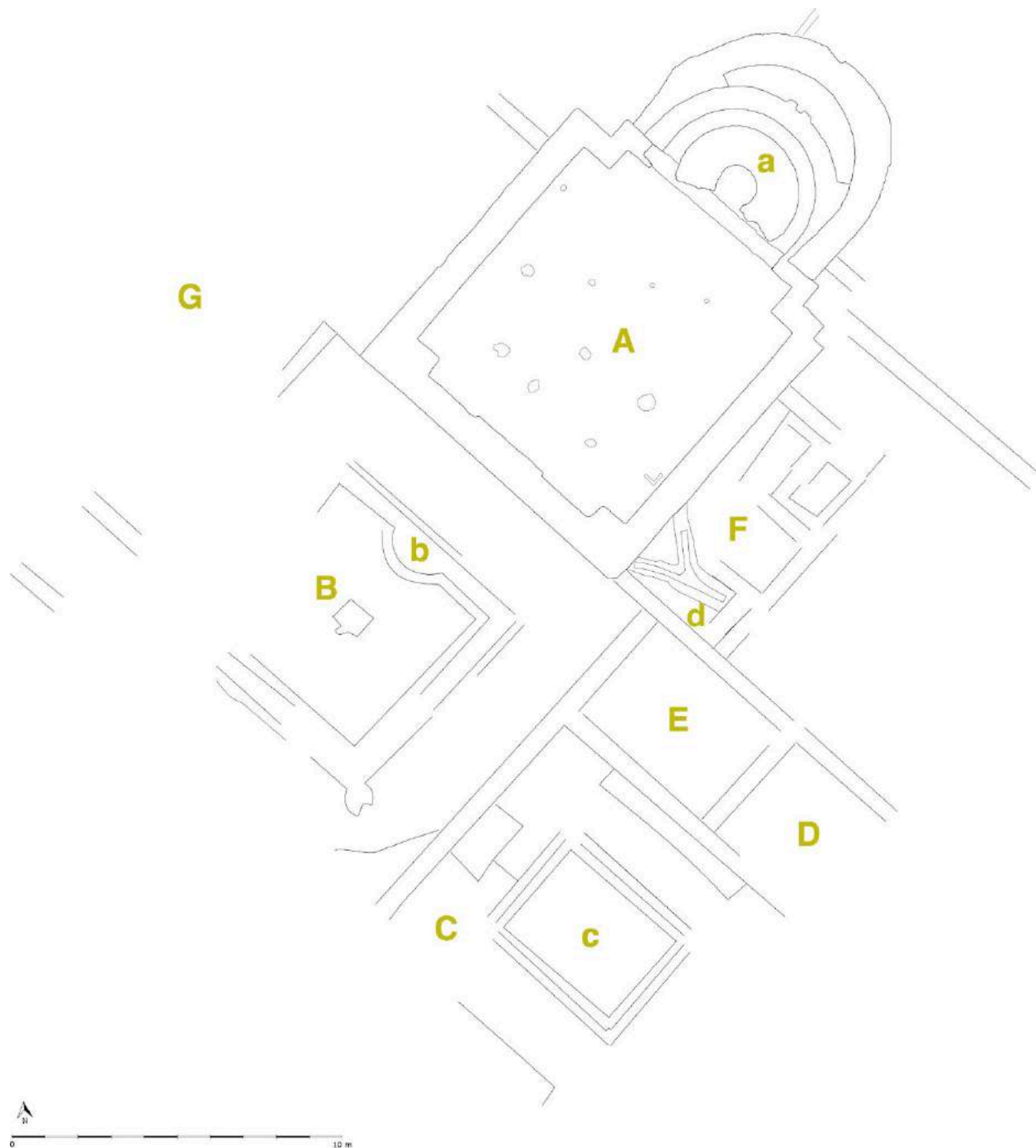


Figure 2.4: Room plan of Horta da Torre Roman villa: a) *cenatio aestivalis*, b) large peristyle, c) small peristyle, d) and e) *cubiculum*, f) hypocaust. Locations of structures: a) *stibadium*, b) water channel, c) *impluvium* d) Y-shaped drainpipe. Schematic plan of structures - Roman villa of Horta da Torre (Fronteira). Research project under the responsibility of André Carneiro. Created by Ana Martins. Provided by André Carneiro.



Figure 2.5: Horta da Torre site photos. Captured at sampling on March 2, 2023. a) *stibadium* and double apse b) Y-shaped drainpipe c) large peristyle d) small peristyle.

Although it is possible that a shading device existed over the performing area, few roof tiles to support this theory were discovered in excavations; furthermore, the remaining foundation around the *cenatio aestivalis* appears to be too small to support such a structure (Carneiro, 2019). The water-filled floor was connected to the Y-shaped drainage pipe system to the south of the site (Figure 2.4 d), (Figure 2.5 B) to control the water flow, connecting with the drainage from the large peristyle (Carneiro, 2019).

There were dumping areas on both sides of the dining apse area, on the north and the south (Carneiro, 2020). It is known from the study of the remains that varieties of animals such as cow, pig, rabbit, and deer meats and seafood such as oysters and clams were consumed by the people at the banquet (Carneiro, 2020). This proclaims the diet patterns

of the people and the transportation of marine products from cities accessible to the water. Fragments of *lucernae*, Roman oil lamps, were also discovered in this area which describes that the banquets lasted even after dark (Carneiro, 2019).



Figure 2.6: Render of *cenatio aestivalis* filled with water. 3D proposal made by Gonçalo Lopes, Carlos Carpetudo and André Carneiro (Carneiro, 2019.) Roof proposal is tentative.

Stepping down the *cenatio aestivalis*, it connects to a large peristyle surrounded by porticoes (Figure 2.4 B). This was a public area that the guests would have to pass by before entering the *cenatio aestivalis*. The columns were made of granite, and there was likely a statue in the center of the peristyle as the base of a statue remains in the center today (Figure 2.5 C). The peristyle was surrounded by a channel for a water feature (Figure 2.4 b), and the channel system was sloped so that the water would flow by gravity. There is evidence of the peristyle courtyard covered by the roof, as fragments of roof materials were excavated from the ground. The idea of this peristyle must have been to have a garden with a tranquil atmosphere with flowers and the sound of the water. On the south of this large peristyle, there is a small peristyle (Figure 2.4 C) that is also in the tetra-style, with four columns supporting the opening. Four potholes are observed where the columns must have been erected (Figure 2.5 D). Fragments of roof materials

were also discovered inside the impluvium (Figure 2.4 c) (Carneiro, 2020). This side of the site was considered private and typically not to be entered by guests, connecting with the cubiculum (Figure 2.4 E) that is situated adjacent to the small peristyle.

As mentioned at the beginning, this area which consists of the *cenatio aestivalis*, cubiculum, the two courtyards, and the hypocaust, is only a small part of the entire site. The villa most likely spread vastly towards the western side (Figure 2.4 G) and had its own economy to self-sustain the entire site. The villa incorporates Roman architectural ideology such as having its own baths and the distinction between public and private spaces. The incorporation of agricultural land that produced olive, cork, and grapes is also a trait of a Roman villa, with self-sustaining functionality such as an oil press room, wine cellar, living space for farm workers, and a horse stable. The site is clearly identified as the typology of a Roman villa, not only from the room functions but also from the structural measurements. The Roman feet system is used throughout the structure, and the strong symmetry along with the use of grids is visible in the placement of rooms.

2.2.2 Abandonment and Second Occupation

After the Roman period, a planned abandonment occurred to this site during the mid-fifth century. No signs of fire or any natural disasters that could have driven away the population was discovered at this specific time (Carneiro, 2020). After the abandonment, the site was reoccupied by a different population that domesticated animals in the sixth century A.D. This change in the occupying population was demonstrated by the archaeological records on the site that indicated a clear change in diet and economic habits (Carneiro, 2020). The circular holes on the floor of the *cenatio aestivalis* exhibit the possibility of wooden posts erected in the space to construct a hut. Bones of horses were collected from the same area without signs of human consumption, indicating a cohabitation of humans and horses inside the structure (Carneiro, 2022). Domestication of sheep and goat and cultivation of wheat was also indicated by the archeological remains discovered on the site. The excavations also revealed that dumping of waste

occurred all throughout the villa except the *cenatio aestivalis* during this time, which demonstrates the lack of planning by the population (Carneiro, 2020). The reuse of structure occurred only in a very pragmatic and minimal way to make the space habitable. The site was abandoned for good after this reoccupation period around the eighth century.

2.3 EXCAVATION

The currently excavated part of the Roman Villa is estimated to be around 1000 square meters (Carneiro, 2022.) Although it was assumed at the beginning that the exposed double apse is the central area of the villa, a geo-radar survey in 2018 as a part of the Fronteira Landscape Project confirmed that the site expands over 20,000 square meters underground (Carneiro, 2020). The double apse is a southeast corner of the entire structure (Figure 2.7), and on the west side that has not been excavated, a vast courtyard expands which was most likely used as agricultural land (Figure 2.4 G). The excavation has been in progress since 2012 (Carneiro, 2020).

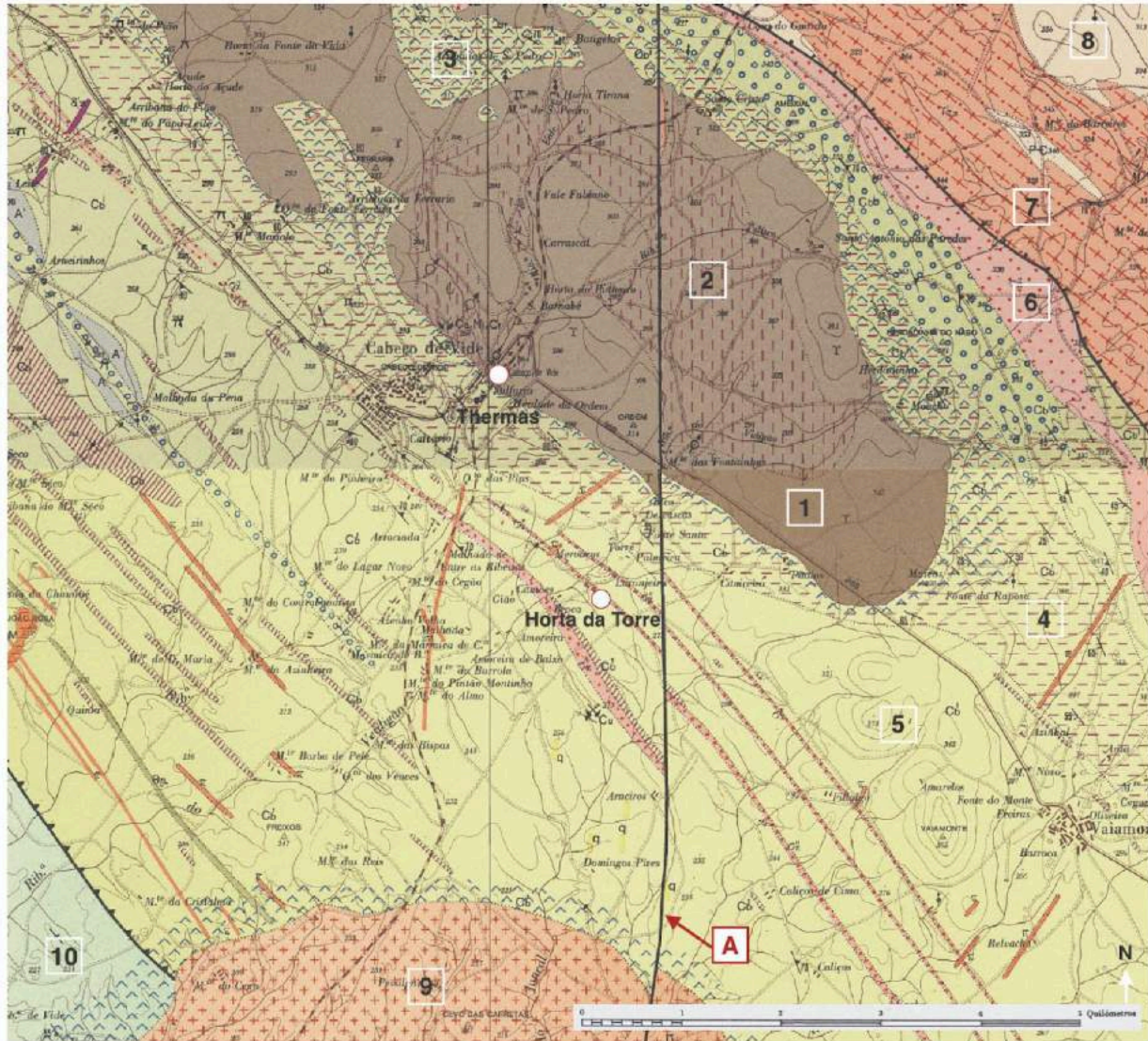


Figure 2.7: Aerial view of excavated southeast corner at the end of the 2019 campaign. Drone photo by Jesus García Sánchez (Carneiro, 2020.)

2.4 GEOLOGICAL CONTEXT

The site of Horta da Torre Roman Villa is in the contact metamorphism zone developed by the local mafic/ultramafic plutonic rocks (Marques et al., 2017). The area is rich in mineral thermal water at the intrusive contact between the mafic-ultramafic pluton and Cambrian carbonate metasediments. This thermal water was known as the Therma and attracted the population to settle in the area (Carneiro, 2019). The site, in the tectonic Ossa-Morena zone, has a geological trend of NE–SW elongated substrates throughout the northeast Alentejo region (Etiope et al., 2013).

The site is in a zone rich in schists, quartzites, graywackes, and conglomerates (Figure 2.8) (Gonçalves, 1973; Gonçalves et al, 1975, 1973). Within the 1 km radius of the site, crystalline limestones and dolomites (recrystallizations) enriched with silicon, porphyritic granite dykes (with chlorite and calcite, fine grains of quartz-feldspar), hyper alkaline granitic and syenitic orthogneiss, hornfels, and vulcanite (acid nature, rhyolitic, microgranitic or trachytic) are found. Within the 3 km radius, quartz veins and conglomerates (irregular quartz, alkaline feldspars, or calco-alkaline grains) are available. In the 5km radius, Calc-alkaline to alkaline granites, biotitic granitic orthogneiss, (metamorphosed syenitic rocks, with feldspars of albite and microperthite), holocene deposits, and hornblendic microtonalite dykes are observed. In the 7 km radius, schists and graywackes, marly limestones, feldspathic sandstones, and angular gravel (quartz, schist) with clays, metadolerite dykes, and a group of schists, quartzites, conglomerates and volcanic breccias, quartzites, and crystalline limestones are located (Figure 2.8) (Gonçalves, 1973; Gonçalves et al, 1975, 1973).



- | | |
|--|--|
| <p>1 Serpentinized Ultramafic Rocks</p> <p>2 Mafic And Ultramafic Rocks</p> <p>3 Hornfels</p> <p>4 Carbonate Rocks Displaying Contact Metamorphism: Limestones and Dolomites</p> <p>5 Cambrian Rocks: Schists, Quartzites And Greywackes</p> <p>A The Main Regional Trending Fault</p> | <p>6 Pre-cambrian Rocks: Metamorphic Schists And Greywackes</p> <p>7 Orthogneisses</p> <p>8 Orthogneisses And Hyperalkaline Syenites</p> <p>9 Calc-Alkaline to Alkaline Granites: Biotite, Porphyroid</p> <p>10 Shales With Interbedded Lites</p> |
|--|--|

Figure 2.8: Geological map around Horta da Torre Roman villa based on Portalegre [32-B, top], Sousel [32-D, bottom] (Gonçalves, 1973; Gonçalves et al, 1975, and Marques, 2017). The location of a stream near Horta da Torre is indicated by light blue line.

3. SAMPLES AND METHODOLOGY

3.1 ANALYTICAL TECHNIQUES AND METHODS

In archaeological findings, it is important to know the technological level and provenance of the artifacts. Historical mortar analysis generally provides us with the technological level of the time and the population. From the analysis of mortar, it is possible to obtain information such as the raw materials used, the ancient building technique, the surface treatment, and the firing conditions if applicable. As far as the provenance of material and production, in the case of building materials such as mortar, it is possible that both the material and the production are local. In ancient times, construction materials typically came from nearby sites, due to the difficulty in transporting the materials. Building materials are normally fixed on site and do not travel far and are not likely to be traded unless it is specific luxurious materials such as exotic stones or rare metals.

In the characterization of historic mortar, visual inspection, and other instrumental analysis techniques must be combined to obtain all this information. Data acquisition is made using the following techniques: Visual Analysis, X-ray Diffraction (XRD), Thermogravimetric Analysis (TGA), Secondary Electron Microscopy - Energy Dispersive Spectroscopy (SEM-EDS), and Optical Microscopy (OM), Acid Attack and Granulometric Analysis (Figure 3.1).

3.1.1 Visual Analysis

Visual analysis of samples holds a significant importance in mortar analysis; therefore, it needs to be done precisely and cautiously (Hughes, 2007). It is a non-destructive analytical method with a large gain at small cost. However, it should be noted that this must be done correctly by experienced professionals with knowledge in identifying materials and clarifying what issues on the site are to be addressed (Hughes, 2007). Visual analysis of samples shall be done before any other type of analyses (Hughes, 2007). Visual analysis should be conducted before altering the visual aspects of original samples by sample preparation.

3.1.2 Optical Microscopy (OM)

Optical Microscopy (OM) is used for the mineralogical characterization of mortar. It is suitable for observing the texture and identifying the aggregates. Visual differentiation of binder and aggregates in mortar is possible through this instrument, as well as identification of minerals, rocks, and other materials included in mortar as aggregates. The volumetric ratio of binder and aggregates can also be found by point-counting, giving the percentage of each component.

Optical Microscopy is applied on thin sections for the light to be able to penetrate amorphous and crystalline materials of mortar samples. This allows the observers to recognize materials in detail and leads to identification of the materials (Middendorf et al., 2005). The thin sections are observed using polarized transmitted light. The observation is done both in Plain Polarized Light (PPL) and Crossed Polarized Light (XPL). With PPL and XPL observations, it is possible to identify minerals by the specific optical features produced when the light transmits through thin sections of minerals and other materials.

3.1.3 X-Ray Diffraction (XRD)

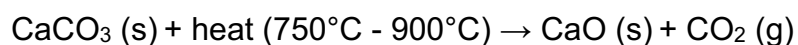
X-Ray Diffraction (XRD) works by radiating a sample by emitting an incident X-ray from an X-ray source and measuring the scattering angle and the intensity of the secondary X-ray released from the specimen. The intensity differs by the atom types and their positions of mass, and the diffraction angle is determined by the crystalline structure of the samples.

XRD analysis of historic mortar assists in identifying the general mineralogical composition of historic mortars binder and aggregate types and allows to obtain semi-quantitative data (Middendorf et al., 2005a). It also allows the identification of newly formed minerals during the firing that cannot be provided by any other instruments. XRD

is for analyzing extremely small crystals, in the form of powdered samples. Considering that XRD is performed on a pulverized sample, the analysis itself is a non-destructive technique that the powdered samples can be recovered after the analysis, thus the analysis using XRD shall be done before other destructive analyses.

3.1.4 Thermogravimetric analysis (TGA-DTG)

Thermogravimetric analysis (TGA-DTG) is used to track the phases that are decomposed by heat. For example, it is possible to identify the decomposition of calcium carbonates (CaCO_3) in the binder and/or carbonate aggregate such as calcite or limestone, if present.



The method is used for the quantification of calcite (CaCO_3). In TGA, the property of the sample measurement is mass (weight). CO_2 from CaCO_3 is typically lost at the temperature of $700^\circ\text{C} - 900^\circ\text{C}$. By identifying the amount of gas (CO_2) that escapes to the atmosphere at a certain temperature, the original mass of CaCO_3 can be calculated. Per 1 mol of CaCO_3 which is 100.082 grams in mass, 1 mol of CO_2 which is 44.02 grams is produced.

In the TGA at the HERCULES Laboratory, the instrument consists of two parts: oven and microbalance. The oven heats up powdered sample at a constant heating rate, while the microbalance detects the weight change which is recorded by a software, Proteus Analysis.

The TGA mainly consists of four steps. The first step is the blank analysis, which is performed when a new crucible is introduced. This is to minimize the interference of the crucible during the analysis. The second step is the cleaning run to remove impurities from crucibles. The cleaning run is done every time the crucible is used and after being washed with acid aqueous solution and distilled water. This is also performed at the beginning of the day to stabilize the instrument by heating up the oven. The third step is to analyze the sample, where the sample in powder form is placed in the crucible inside

the oven and gets heat up at a constant rate. In the last step, the crucible is cleaned by boiling in hydrochloric acid aqueous solution and distilled water. As these steps take time, generally only one sample per day is possible to be analyzed.

3.1.5 Variable Pressure Scanning Electron Microscopy (VP-SEM-EDS)

Variable Pressure Scanning Electron Microscopy coupled with Energy Dispersive X-ray Spectroscopy (VP-SEM-EDS) is utilized for characterization of materials. It is capable of imaging, elemental mapping, and quantification. VP-SEM-EDS offers higher magnification than Optical Microscopes and allows visual observation in detail. In addition, SEM-EDS can map out and quantify the elements on the selected local surfaces.

Using Variable Pressure Scanning Electron Microscopy (VP-SEM-EDS) produces a visual reconstruction of the surface image of the samples and allows observation of features such as texture, fabric, and the elemental composition of binder and aggregates. It is suitable for the observation of chemical and textural information of mortar as it can differentiate between binder and aggregates as well as identifying the compositions of binder and inclusions.

In SEM-EDS, the primary source of electrons creates a raster image. This primary beam results in two types of electron scattering: elastic and inelastic (Burnstock, 2000). In elastic, electrons collide and change directions which causes no loss of energy or velocity. The backscattered electrons produced are collected by a detector. When the image is reconstructed, the brighter the signal, the heavier the elements, as this means more numbers of electrons are ejected from the sample. In inelastic, the electrons interact with sample atoms, which results in energy and velocity loss of the electrons. The secondary electrons are lower in energy than the backscattered electrons. This provides a shallower depth of sample analysis. In any case, the samples should be electrically conductive to analyze; otherwise, the samples must be coated in metals (Burnstock, 2000).

There are different types of SEM: Conventional (High Vacuum) SEM, Low Vacuum (variable pressure) SEM, and Environmental SEM. In Conventional SEM, secondary

electrons are used to construct the image. The air should be removed because the presence of gas molecules scatters the electrons. Variable Pressure SEM enables imaging without coating. This enables analysis of valuable samples or samples delicate to high vacuum such as biological material. Environmental SEM has superior resolution by collecting more amplified secondary electrons (Burnstock, 2000). In this analysis, Low Vacuum variable pressure SEM (variable pressure) in back scattered electron mode was used.

3.1.6 Acid Attack and Granulometric Analysis

Acid attack is considered an analytical method that employs acid solution to dissolve binder and, as a result, separates acid-soluble binder and siliceous aggregates. This methodology must be applied after other petrographic and mineralogical analytical methods such as Optical Microscope, SEM-EDS, XRD and Thermogravimetric analysis, and the results of the wet chemical separation must be compared and agreed with those from the petrographic and mineralogical analyses (Middendorf et al., 2005b). The binder-aggregate ratio must be determined using both the results from acid attack and other techniques especially in the cases where aggregates contain acid-soluble materials. This affects the results from acid attack, and the acid-soluble part of aggregates must be taken into consideration when calculating the ratio of soluble fractions and insoluble residue (Middendorf et al., 2005b).

Much like other sample preparations, in acid attack analysis, it should be made sure that the samples used are representative of the structure where the samples were collected from. The analysis must be executed on samples cleaned and dried at or over 40°C. Once the soluble fractions and insoluble residue are separated after acid attack, the insoluble residue shall be sieved using test sieves to determine the particle sizes of the residues. Test sieves that will be used in this analysis is a set of ASTM test sieves (Gravimeta): 4, 2, 1, 0.5, 0.25, 0.125, and 0.063 mm. The residues that pass through 0.063mm sieves

are considered a part of binder, and the rest is considered aggregates (Middendorf et al., 2005b).

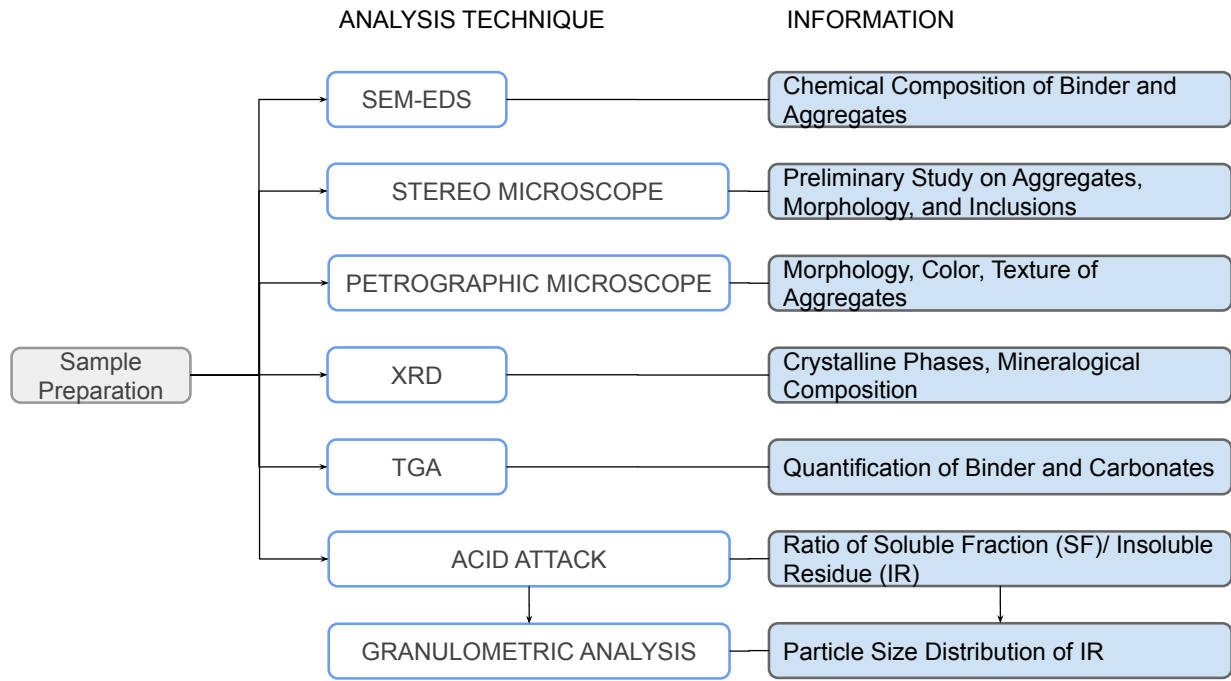


Figure 3.1: Analytical methodology diagram.

3.2 SAMPLING

A total of eighteen wall samples (Figure 3.2, Table 3.1,) were collected from the site of Horta da Torre Roman Villa, using a hammer and a chisel. Samples were chosen ensuring they represent the structure of the villa. Two samples are from the corridor located between the *cenatio aestivalis* and the peristyle (MHT-1, MHT-2), four samples are from the *cenatio aestivalis* (MHT-3, MHT-4, MHT-17, MHT-18), four samples from the peristyle (MHT-5, MHT-6, MHT-7, MHT-8), three samples from the small peristyle (MHT-9, MHT-10, MHT-11), three samples from the cubiculum (MHT-12, MHT-13, MHT-14), and two samples from hypocaust (MHT-15-EXT, MHT-16). Samples MHT-1 and MHT-2,

MHT-3 and MHT-4, and MHT-7 and MHT-8 are respectively pairs; one of them is render mortar and the other is filling from the same wall. Of nine render mortars, four have a mural painting on the surface (MHT-1, MHT-3, MHT-5, and MHT-9.) The mural paintings appear to be created with black, red, and green pigments on a white preparation layer. The combination of pigment colors depends on each wall from which the samples were collected.



Figure 3.2: Sample locations and function.

The samples collected at the site were placed inside resealable bags with reference numbers. The samples were then transported to and were cleaned at the HERCULES laboratory.

Finally, each sample was prepared into four appropriate forms (Figure 3.3) for further analysis using instruments: powder (XRD and TGA), particles under 125 μ m (XRD), two-10-gram bags of small fragments (Acid Attack and Granulometric Analysis), and resin bound (Optical Microscope and SEM-EDS).

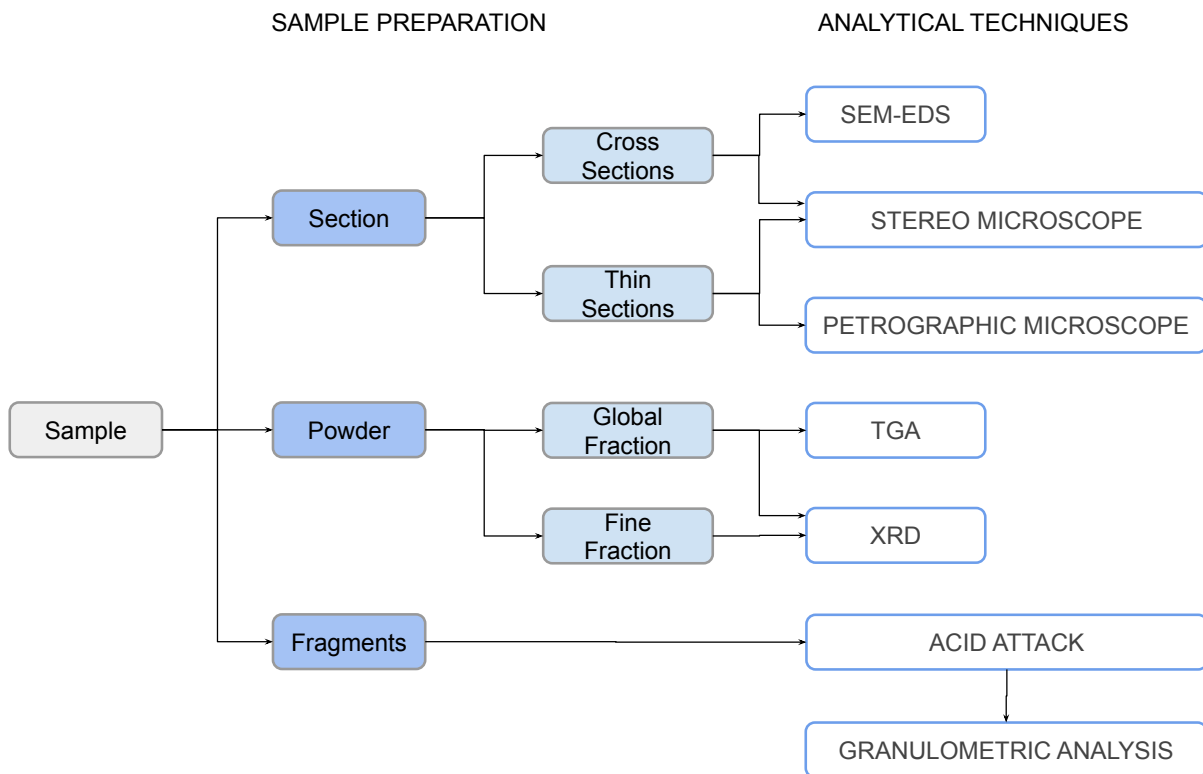


Figure 3.3: Sample preparation diagram.

Table 3.1: Sample function and locations.

| Sample | Function | Location | Notes |
|------------|----------------|--------------------|---------------------------|
| MHT-1 | Render (Mural) | Passage | |
| MHT-2 | Filling | Passage | |
| MHT-3 | Render (Mural) | Cenatio Aestivalis | |
| MHT-4 | Filling | Cenatio Aestivalis | |
| MHT-5 | Render (Mural) | Large Peristyle | |
| MHT-6 | Filling | Large Peristyle | Thin Wall of Peristyle |
| MHT-7 | Filling | Large Peristyle | |
| MHT-8 | Render | Large Peristyle | Mixed Ceramic |
| MHT-9 | Render (Mural) | Small Peristyle | |
| MHT-10 | Render (Mural) | Small Peristyle | Weathered, Tank |
| MHT-11 | Filling | Small Peristyle | |
| MHT-12 | Filling | Cubiculum | Weathered, Big Wall |
| MHT-13 | Render (Mural) | Cubiculum | |
| MHT-14 | Filling | Cubiculum | |
| MHT-15-EXT | Render | Hypocaust | Internal Hypocaust |
| MHT-16 | Filling | Hypocaust | Adjacent Interior Apophse |
| MHT-17 | Filling | Triclinium | Double Wall Part |
| MHT-18 | Filling | Triclinium | Double Wall Part |

3.3 SAMPLE PREPARATION

3.3.1 Cleaning for Visual Inspection

The surfaces of the samples were cleaned using brushes with plastic or metal bristles to remove dirt and biological organisms before any form of sample preparation. It was generally not possible to remove all the dirt at once; therefore, the samples were placed into the drying cabinet at a temperature of 51°C overnight. The brushing and drying processes were repeated two to three times until the dirt was sufficiently removed for

visual analysis. After photographing with a scale, the samples with large fragments were hammered to make small fragments for further preparation.

3.3.2 Sample Preparation for Optical Microscopy and SEM-EDS—Cross and Thin Sections

Relatively large pieces of samples that represent the stratigraphy of the mortar were picked to fit inside silicone cylinder specimen containers. about the diameter of three centimeters. Then resin in its liquid form was poured into the container for impregnation of sample fragments. The silicone containers were lined with a thin coating of vaseline beforehand to ease the removal of resin after hardening. The resin mixture was prepared using EpoFix Resin and EpoFix Hardener both from a manufacturer, Struers ApS. The ratio of the mixture is 25g EpoFix Resin: 3g EpoFix Hardener. The weight of each liquid was measured using a digital scale and a plastic cup. Once both liquids were inside the cup with the correct measurement, the mixture was stirred carefully not to make air bubbles using a wood stick. The mixture was then poured into the specimen containers with the sample fragments inside. After pouring this resin, the samples with labels were left overnight to allow the resin to solidify.

Once the resin hardened, the impregnation was removed out of the container. The side(s) of the impregnation was cut off using a diamond saw to expose the maximum cross-section area of the sample. Samples were then let dry overnight due to the water from the saw. After the samples were completely water-free, the surface with the maximum cross section was thinly coated using an additional resin mixture of the same formula. After the resin on the surface completely solidified, the surface was manually ground on sandpaper Buehler CarbiMet Grit 220 [P240]. The resin on the surface was ground against the sand sheet by moving in the number 8 or an infinity shape to ensure the surface was equally ground. The samples were ground for about an hour each until the surface of the impregnated mortar samples was exposed. The surface was observed using a magnifier to see if it reached the surface of the mortar. After grinding, the samples

were washed with water to remove the excess ground resin. After drying with paper towels, the samples were left to dry at room temperature.

Glass slides of thickness from 1.30 - 1.50 mm were ground by Discoplan-TS (Struers) to achieve a thickness of 1.16 mm. This process is to roughen the surface of the glass slides so that glue can hold onto the surface. After the impregnated samples dried, they were glued to the ground surface of the glass slides using Araldite (Huntsman).

Araldite consists of two components: resin and hardener. They were mixed in equal parts with a plastic spatula and applied on the ground surface of impregnated samples. The glass slide was approached slowly from 45 degrees to avoid air bubbles staying in the glue mixture. When the surface of the glass completely covered the surface of impregnation, it was put under a sample holder Plactronic (J. P. Selecta) to put pressure in order to glue correctly. It takes 12 hours for this mixture to dry. MHT-4 had a broken glass slide due to the process of drying glue and needed to be repeated. After the glue dried, the excess impregnation was removed by a cut-off saw CS10 (Logitech), leaving a few millimeters of the samples on the glass slides.

The samples were then divided into two groups, MHT-1 to MHT-9 and MHT-10 to MHT-18, due to the availability of the equipment. The first group was ground by Discoplan-TS (Struers). The second group was ground by an automatic grinder, PM5 (Logitech). In either scenario, the samples were ground to a thickness of 1.29 mm, including 1.16 mm of the glass slide and 0.04 mm of glue. The sample itself, therefore, has a thickness of 0.09 mm. The thickness was measured using a Digimatic Outside Micrometer without a data output function (Mitutoyo).

After ground by Discoplan or PM5 to 1.29mm, the final thickness of all the samples was adjusted by grinding further by hand to achieve 0.35mm of thickness, using sand sheet P240. The sample was ground to a thickness so that the quartz should appear white or grey in color when observed by an optical microscope. Once the thickness is achieved, all the samples were polished using P2500 to improve the visibility of the minerals.

3.3.3 Sample Preparation for X-Ray Diffraction (XRD) and Thermogravimetric Analysis (TGA) - Powders

Small fragments of the sample under 5mm after hammering were collected to measure approximately 10 mL of volume to powder using a mill machine (Retsch). The 10 mL of fragments were placed in a bowl of a mill machine along with 3 identical-sized balls and milled into powder at 500 rpm for ten to twenty minutes depending on the sample until the powder obtained a flour-like, fine-ground texture. This sample preparation method represents mortar as a whole that includes both binder and aggregates.

Another method of using a sieve was used to separate samples that are under 125 μm from larger particles. The sieved particles under 125 μm were placed into individual Eppendorf tubes. This method represents binder, as fine fractions under 125 μm tend to be crushed binder and aggregates are often sized over 125 μm .

3.3.4 Sample Preparation for Acid Attack and Granulometric Analysis – Fractions

The samples with large fragments were hammered using a rubber hammer to divide them into small pieces of approximately 5 -10 mm. Some of these fragments were used based on if they are similar and representing the samples. The pieces that have mural paintings were not included to ensure the samples represent the mortar and not to include the pigments. Two groups of 10 g each per sample of such fragments were measured on a scale (Adam Equipment PGL 3002) for the acid attack.

3.4. EXPERIMENTAL CONDITIONS

3.4.1 Experimental Conditions for Petrographic Analysis

Petrographic analysis was executed using Leica DM2700 P Polarization Microscope. The microscope was coupled with Leica MC170 HD digital camera to record photographs.

Leica Microsystems Application Suite X software was used for the recording. Each thin section was observed and recorded in plane polarized light (PPL) and cross polarized light (XPL) to observe different properties of minerals and other materials.

3.4.2 Experimental Conditions for X-Ray Diffraction (XRD)

Both the fine global fractions and fine fractions were analyzed using Bruker D8 Discover X-Ray Diffractometer. The powdered samples were placed in XRD sample holders using clean steel spatulas and flattened by pushing down a glass slide against the surface so that the powder was flat and level to the height of the sample holder. The sample holder was then secured in a metal holder and placed inside XRD for analysis. The X-Ray Generator voltage was set at 40 kV and the current at 40mA and 1600W. The scan type was set as Coupled Two Theta/Theta, scan mode as Continuous PSD fast, Steps at 1438, Total time at 1496 [s], therefore at 1000 time/steps [s]. The diffraction angle, two thetas, was set at 3.0001 and 74.9971. Software DIFFRAC.SUITE EVA was used for the analysis.

3.4.3 Experimental Conditions for Thermogravimetric Analysis (TGA-DTG)

Thermogravimetric analysis was carried out using DTA-TGA Jupiter (NETZSCH) equipped with Alphagaz compressed N₂ and (Air Liquide) and a water bath F 25-MA (Julabo).

Before each experiment, a cleaning run was executed to stabilize the instrument. In the cleaning run, the initial temperature was set as $T_i = 40^{\circ}\text{C}$, at a constant heating rate of 20°C increase per minute, and the final temperature reaches $T_f = 1000^{\circ}\text{C}$. After the cleaning run is finished, samples were analyzed in the following condition: the initial temperature was set as $T_i = 40^{\circ}\text{C}$, at a constant heating rate of 10°C increase per minute, to reach the final temperature of $T_f = 1000^{\circ}\text{C}$. All the thermogravimetric analysis were performed under an inert atmosphere of Nitrogen with a flow rate of 70 mL/min.

Two platinum crucibles were used for this analysis: crucibles 1 and 2. Although these crucibles are identical in appearance, they need to be distinguished as the blank analysis results of the two would differ. The crucible used were noted on each sample analysis,

and the blank analysis of appropriate crucibles were subtracted from the results to obtain correct information on the samples. The results are recorded using Proteus software (NETZSCH).

3.4.4 Experimental Conditions for Variable Pressure Scanning Electron Microscopy (VP-SEM-EDS)

Variable pressure Scanning Electron Microscope HITACHI S-3700N coupled with a Bruker X-Flash 5010 with a Silicon Drift Detector (SDD) Energy Dispersive X-ray Spectrometer was used for this analysis in backscattering (BSE) mode, with an accelerating voltage of 20 kV and chamber pressure of 40 Pa.

Samples prepared into thin sections were used for this analysis. The thin sections were not coated on the surface to not interfere with the elemental analyses.

3.4.5 Experimental Conditions for Acid Attack and Granulometric Analysis

3.4.5.1 Acid Attack

Two groups (A and B) of 10 grams of each sample were placed inside a beaker (VWR borosilicate glass, 1000 mL) respectively. A and B are in interchangeable conditions and are duplicates. This is to ensure the homogeneity of the samples, as fractions of mortars are often not similar materials. Only MHT-9B did not have enough sample to make 10 grams; therefore, the group was 3.942 grams instead.

Before the experiment, using a glass bar, the fragments of samples were tapped gently to make sure they are in separate pieces. A magnetic stirring bar was placed in each beaker along with the samples, and 120 mL of the HCl aqueous solution was poured into the beakers. To make the aqueous acid solution needed for the procedure, one part of the acid and three parts of distilled water were used. 666 mL of distilled water and 333 mL of concentrated HCl (33%) were combined in a 1000 mL volumetric flask that was placed in a container filled with ice to remove heat from the mixture. The solution was left in ice until it cooled down for two to three hours. Once at room temperature, water distilled

was added up to 1000 mL. After this solution was added, the sample was then left at room temperature until the reaction stops or no more gas is produced, approximately for 5 to 15 minutes, depending on the condition of each sample. The carbonate compounds such as the binder, shells, and lime lumps will dissolve in acid at this step, and only non-carbonated aggregates should remain. Once the reaction stopped, the beakers were placed on the magnetic stirrer / hot plate (VWR) to be stirred and heated at around 100°C. After the solution started boiling, the mixture was further stirred for 10 minutes with the heat still on. After 10 minutes, the beakers were removed from the hot plate to let cool to room temperature. Then distilled water was added, so that the solution to be disposed of would be thinner in acid and safer to handle during the filtering process.

The solution was filtered using a ceramic Büchner funnel and a Kitasato flask. Two filter papers (VWR) were stacked on top of each other and placed inside the funnel, and they were wet with a small amount of distilled water before the filtering process. The Kitasato was connected to a vacuum pump tube for air suction, and the mixture was filtered to catch the tiny particles dissolved in the solution. Once the solution is gone, the magnetic bar was removed. After, more distilled water was added to the beaker to filter the rest of the large grains left at the bottom of the beaker. Once the beaker is completely empty and cleaned out, the filtered insoluble grains left on the filter paper were washed with distilled water. The soluble left in Kitasato was disposed of. The insoluble residue was then placed inside the oven at the temperature of 70°C for 24 hours to dry.

3.4.5.2 Granulometric Analysis

After the acid attack, the insoluble residues were sieved using seven different sizes of ASTM test sieves (Gravimeta): 4, 2, 1, 0.5, 0.25, 0.125, and 0.063 mm. This system of sieves stacked vertically divides samples into eight groups: >4 mm, 4-2 mm, 2-1 mm, 1-0.5 mm, 0.5-0.25mm, 0.25-0.125mm, 0.125-0.063mm, and <0.063mm. The total of the sample and each divided group were respectively weighed on a scale to record the mass (g).

4. RESULTS

4.1 VISUAL INSPECTION

By visual inspection with an unassisted eye, colors of the binders, homogeneity, texture, porosity, types of aggregates, etc. were identified as preliminary assessments before other techniques (Table 4.1). The samples were also compared with each other to see if there were any similarities. As mentioned in chapter 3.2, the samples were taken from different walls as well as different functional parts of the walls such as render or filling. The information on the sample location and function was taken into consideration when comparing the samples with the naked eyes.

Among the render mortar samples (MHT-1, MHT-3, MHT-5, MHT-8, MHT-9, MHT-10, MHT-13, and MHT-15-EXT), MHT-1, MHT-3, MHT-5, MHT-9, and MHT-15-EXT had visible indications that they were painted on the surface with pigments of different colors. MHT-8, MHT-10, and MHT-13 were unclear whether they had mural paintings or not; however, using a stereo microscope, MHT-10 and MHT-13 were further identified that they had pigments on surface (appendix vi). The binders seem to be divided into two different colors. MHT-1, MHT-3, MHT-5, MHT-8, and MHT-15-EXT showed very similar white preparation surfaces for mural painting. MHT-15-EXT seemed to have a gray to blue color on the surface, but it was unclear whether the color came from a pigment. These five samples were similar in appearance; however, only MHT-15-EXT was very fragile and powdery in texture, while the rest were more durable with fine aggregates in the preparation layers and medium to large aggregates in the rest of the sample. Most of the render appeared to have red or black pigments, while only MHT-15-EXT had a blueish grey color.

The rest of the render mortars, MHT-9, MHT-10, and MHT-13 had beige-colored binders. MHT-9 and MHT-13 shared a grayish tone to the binder. MHT-10 shared similarity in the beige color, except it did not have the same gray tone as MHT-9 and MHT-13. MHT-9

and MHT-10 had similar medium aggregate sizes, while MHT-13 had much larger aggregates. All the render mortars seemed to be dense and had low porosity.

Among the filling mortars (MHT-2, MHT-4, MHT-6, MHT-7, MHT-11, MHT-12, MHT-14, MHT-16, MHT-17, and MHT-18), there was a clear color distinction between white and beige mortars. MHT-4, MHT-6, MHT-12, MHT-17, and MHT-18 were white. MHT-2, MHT-7, MHT-11, MHT-14, and MHT-16 were beige. Within the beige, MHT-16 was reddish (darker) beige. MHT-11 appears to contain both beige and reddish beige layers, possibly indicating that the beige mortar was recycled by binding the pieces with the reddish beige mortar. MHT-4, MHT-6, MHT-12, MHT-14, and MHT-18 appeared to have larger porosity in comparison to all the other samples.

Furthermore, MHT-8 and MHT-18 possibly had ceramic fragment-like aggregates.

In all the samples, except MHT-4, MHT-5, MHT-6, MHT-7, MHT-9, and MHT-10, lime lumps were visible, which usually represents that not enough amount of water was added in the hydration process of mortar production (Elsen, 2006).

Table 4.1: Visual inspection results.

| Sample | Function | Aggregates | Porosity | Lime Lump | Fragile | Color | Other Descriptions |
|------------|-----------------|------------------------------|---------------|-----------|---------|-------------|---|
| MHT-1 | Render (Mural) | Fine grains on surface layer | Low | Yes | | White | Two layers: Render and filling |
| MHT-3 | Render (Mural) | Fine grains on surface layer | Low | Yes | | White | Two layers: Render and filling |
| MHT-5 | Render (Mural) | Medium Quartz | Low | | | White/Beige | Two layers: Low porosity surface (white) and high filling |
| MHT-9 | Render (Mural) | Medium | Low to Medium | | | Gray-Beige | Two layers: Render and filling |
| MHT-10 | Render (Mural?) | Fine to Medium | Low | | Yes | Beige | Includes fiber-like materials |
| MHT-13 | Render (Mural?) | Large Quartz | Low | Yes | | Gray-Beige | Layers of grey and beige matrix mixed together |
| MHT-8 | Render | Ceramic / Quartz, Medium | Low | Yes | | White | White color similar to MHT-4 |
| MHT-2 | Filling | Large grains | Low | Yes | | Beige | Homogenous size of aggregates |
| MHT-4 | Filling | Large Quartz | Medium | | | White | The binder color is bright white |
| MHT-6 | Filling | Medium Quartz | Medium | | | White | Attached to a piece of red brick |
| MHT-17 | Filling | Medium Quartz | Low | Yes | | White | Attached to a piece of red brick |
| MHT-15-EXT | Render (Mural?) | Fine Quartz | Low | Yes | Yes | White | White matrix with fine aggregates |
| MHT-7 | Filling | Large Pebbles | Low | | | Beige | Includes very large to small pebbles |
| MHT-12 | Filling | Fine to Medium | Low to Medium | Yes | | White | Low porosity on one side and high on the opposite side |
| MHT-14 | Filling | Fine to Medium | Medium | Yes | | Beige | Two layers: Low porosity on surface and high in filling |
| MHT-16 | Filling | Medium to large, pebbles | Low | Yes | | Red-Beige | With black pebbles |
| MHT-11 | Filling | Medium to large, Quartz | Low | Yes | | Mix Beige | Mix of white and red matrix |
| MHT-18 | Filling | Large Pebbles | Low to Medium | Yes | | White | Includes ceramic-like fragments |

4.2 PETROGRAPHIC MICROSCOPE

From petrographic analysis, taking into account the main aggregates present in the mortars, two compositional groups were considered: basic/ultrabasic group and granitic group. The basic/ultrabasic group is characterized by the significant presence of iron-magnesium minerals such as olivines (+/- serpentized), pyroxenes and amphiboles, and fragments of gabbroic rocks. The group also contains metamorphic rocks such as quartzite. Of all the samples, five samples (MHT-7, MHT-12, MHT-14, MHT-15-EXT, and MHT-16) belong to this group (Table 4.2).

The granitic group contains minerals such as quartz, feldspars, and biotite. The observed feldspars were alkali feldspar rich in potassium (K-feldspar), sodium-rich plagioclase such as albite, or intergrowth of both (perthite). Perthite refers to the intergrowth of two minerals, potassic feldspar (K-feldspar) and sodic feldspars (plagioclase). If K-feldspar is predominant in the rock, it is considered perthite. If Na-rich plagioclase is dominant, it is antiperthite (Haldar, 2020). Eleven samples (MHT-1 to MHT-6, MHT-8 to MHT-10, MHT-13, and MHT-17) are in this granitic group. It should be noted that either the basic or granitic group can contain minerals from the other group, and the petrography of both groups is similar. However, the samples contain more signature minerals in their own group when compared to the other group (Figure 4.1).

The last group, the mixed group, contained both minerals from basic and granitic groups. Epidote was identified in this group by its bright colors in XPL (Table 4.3 D). This group consists of two samples: MHT-11 and MHT-18. Both samples demonstrated black and white mortar layers to the unaided eye (Figure 4.2). In MHT-11, the white mortar included fine angular quartz and round basic minerals, while in MHT-18, the white mortar was mainly only lime without aggregates. In MHT-11, the black mortar included micas such as biotite, whereas the black mortar in MHT-18 included angular quartz, feldspars, and gabbroic aggregates in large sizes. It is possible that this “layer” trait could be a signature of the mixed group.

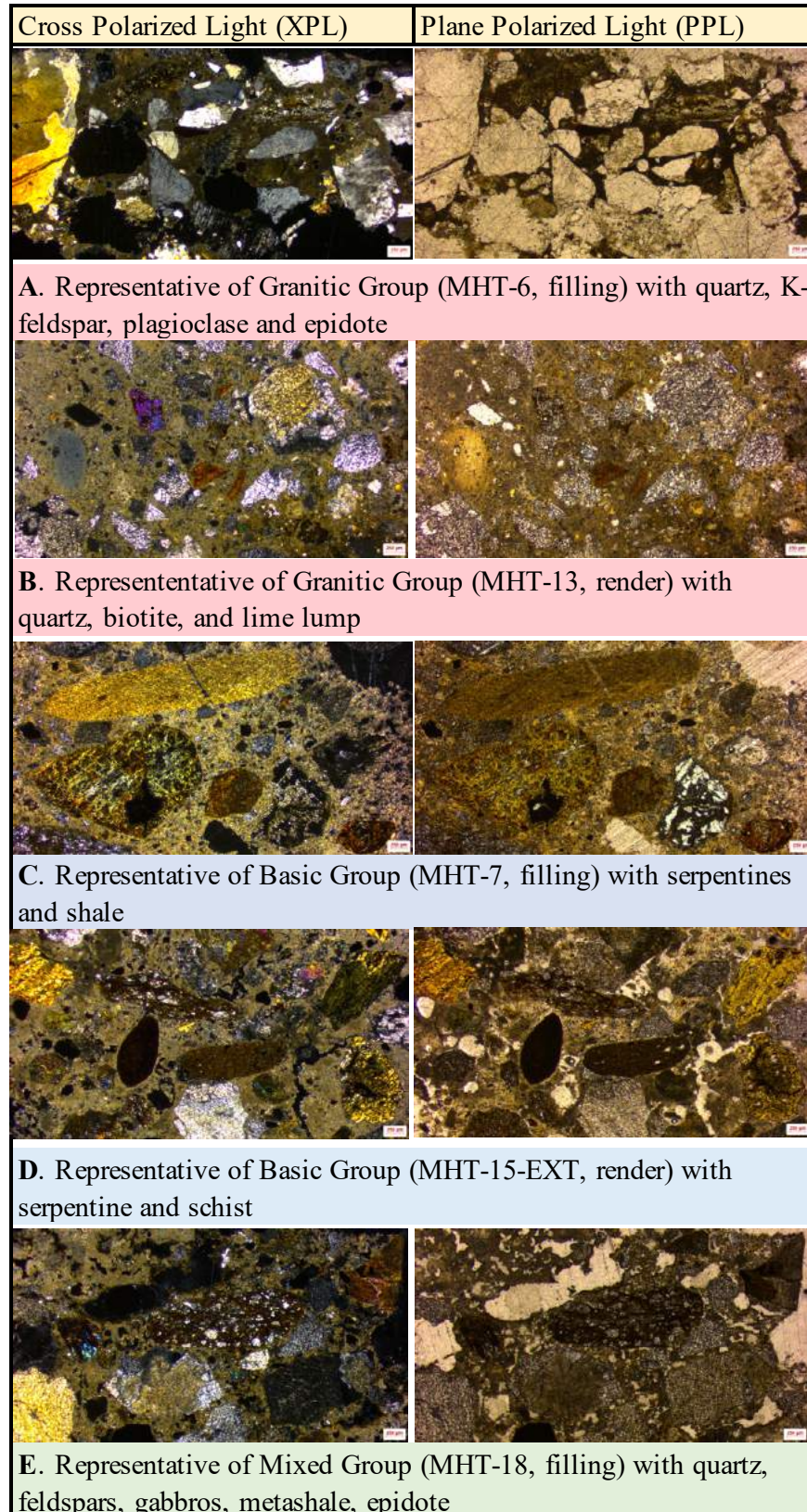


Figure 4.1: Representative micrographs of granitic, basic, and mixed groups.

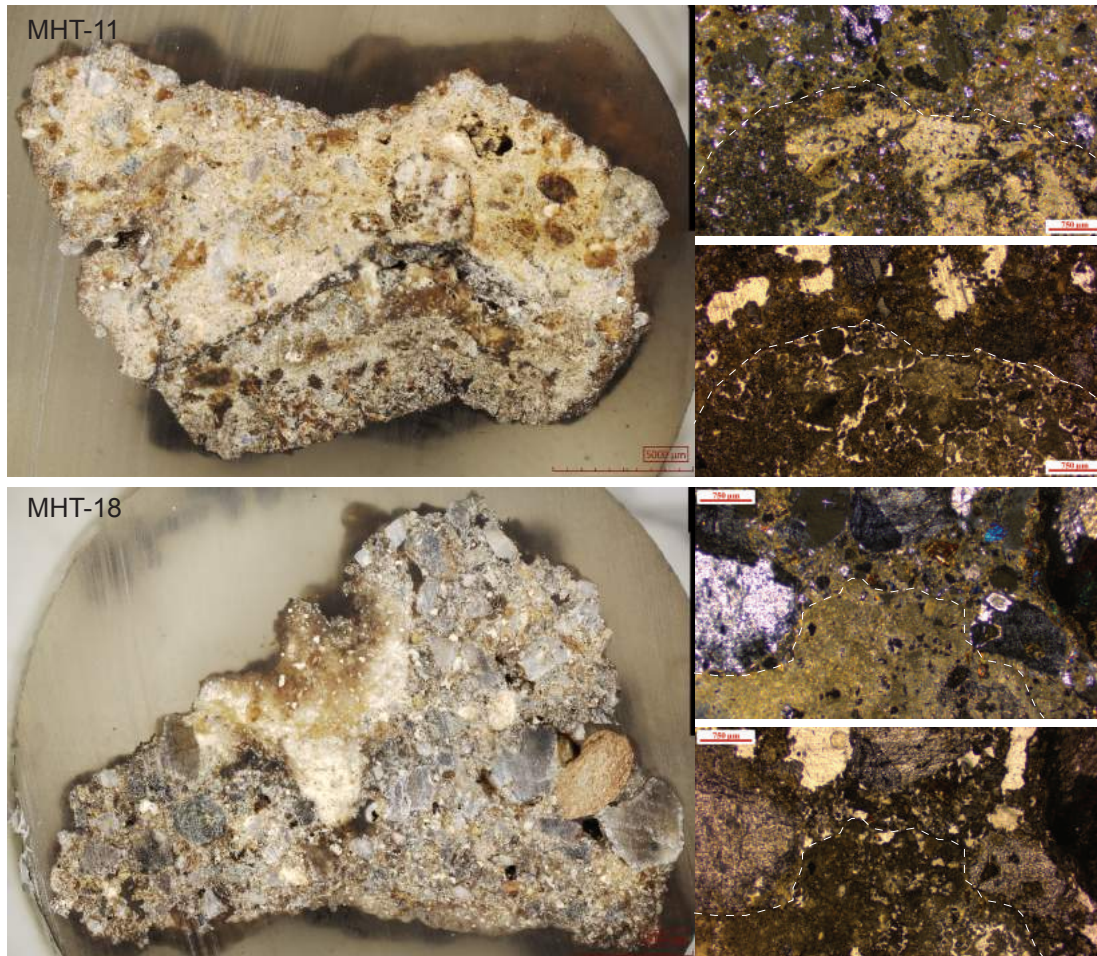


Figure 4.2: Mixed group samples demonstrating different layers in cross section (left) and thin sections (right).

Moreover, in several samples, some lime-related materials were found. In MHT-2, MHT-4, MHT-5, and MHT-11, fragments of calcite were found (Table 4.3 J and K). Calcite was especially abundant in MHT-11. These fragments originate from either marble fragments mixed as aggregate or limestone that became crystallized during the production process of mortar.

MHT-4, MHT-7, MHT-9, and MHT-11 included fine-grained fragments of non-calcined limestone, an unburned raw material of lime (Table 4.3 M). The preserved limestone in these samples indicates that the firing temperature during the production did not reach the calcination temperature at around 750°C - 900°C.

Furthermore, all the samples contained lime lumps (Table 4.3 L). These lime-related inclusions can contribute to finding out the provenance of the raw materials of the mortars and the technological level of the production (Elsen, 2006).

The relationship between the mortar sample locations and the grouping is indicated on Figure 4.3.

Table 4.2: Type of minerals and rocks found in petrographic analysis in comparison to the function of mortar.

| Sample | Function | Type of Inclusions | Group |
|------------|--------------|--|----------|
| MHT-1 | Render Mural | quartz, k-feldspar, (perthite), albite, biotite | Granitic |
| MHT-3 | Render Mural | quartz, k-feldspar, (perthite), albite, biotite | Granitic |
| MHT-5 | Render Mural | quartz, feldspar, biotite, schist, shell fragments, epidotes, unburned limestone | Granitic |
| MHT-9 | Render Mural | quartz, k-feldspar, (perthite), albite, biotite | Granitic |
| MHT-10 | Render Mural | quartz, k-feldspar, (perthite), albite, biotite | Granitic |
| MHT-13 | Render Mural | quartz, k-feldspar, (perthite), albite, biotite | Granitic |
| MHT-15-EXT | Render Mural | olivine (serpentine), amphibole, quartzite, meta-shale | Basic |
| MHT-8 | Render | quartz, k-feldspar, (perthite), albite, biotite | Granitic |
| MHT-2 | Filling | quartz, k-feldspar, (perthite), albite, biotite | Granitic |
| MHT-4 | Filling | quartz, k-feldspar, (perthite), albite, biotite | Granitic |
| MHT-6 | Filling | quartz, k-feldspar, (perthite), albite, biotite | Granitic |
| MHT-7 | Filling | olivine (serpentine), amphibole, quartzite, meta-shale | Basic |
| MHT-11 | Filling | lime lumps, shale, amphibole, feldspar, quartzite, calcite crystals | Mixed |
| MHT-12 | Filling | olivine (serpentine), amphibole, quartzite, meta-shale | Basic |
| MHT-14 | Filling | olivine (serpentine), amphibole, quartzite, meta-shale | Basic |
| MHT-16 | Filling | basalt, olivine (serpentine), amphibole, quartzite, meta-shale | Basic |
| MHT-17 | Filling | quartz, k-feldspar, (perthite), albite, biotite | Granitic |
| MHT-18 | Filling | olivine, amphibole, basic rocks such as gabbros, feldspars, quartz | Mixed |

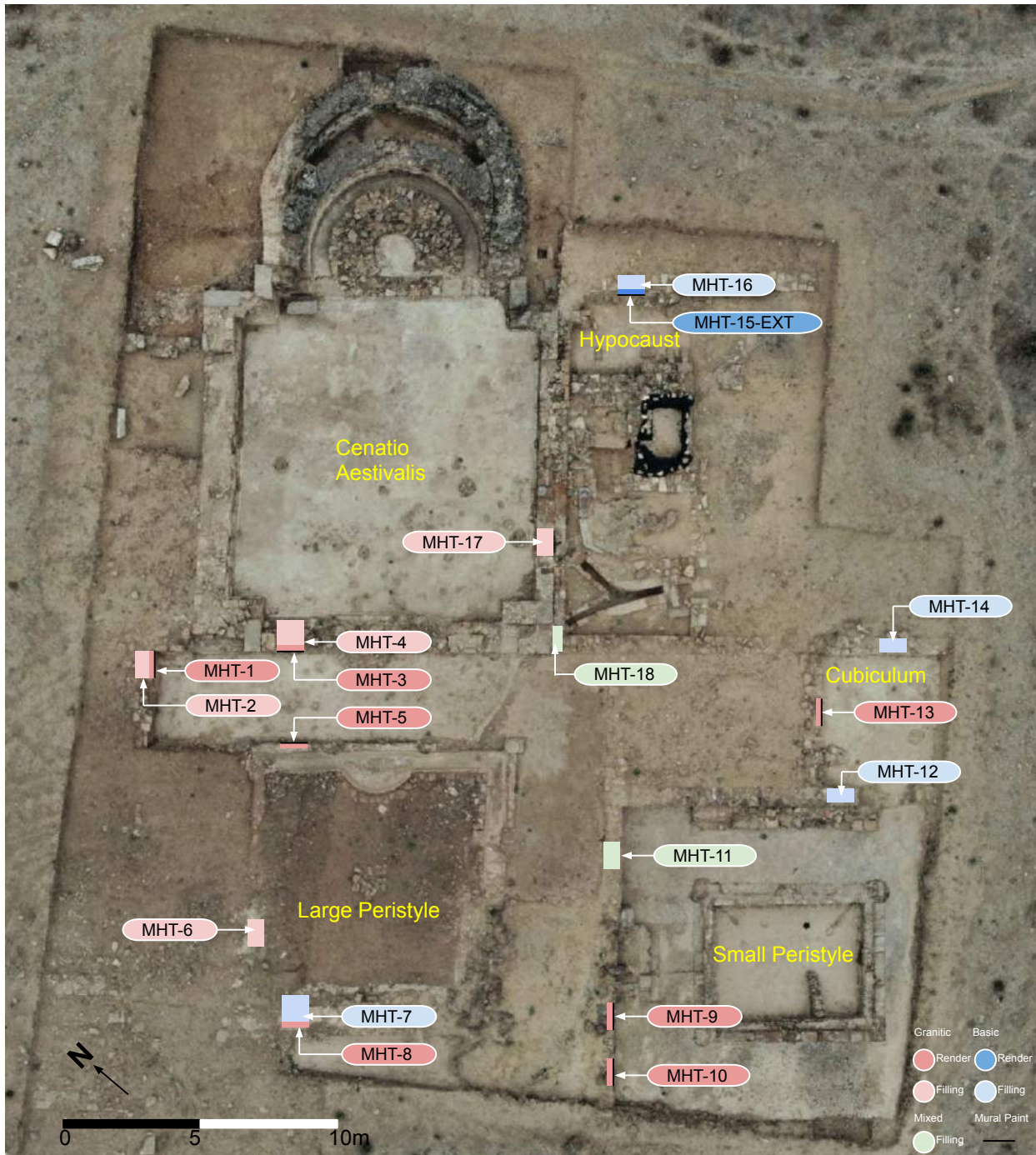
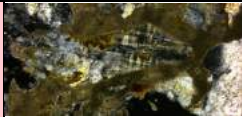
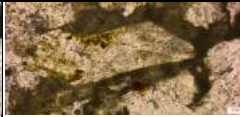
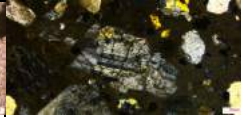
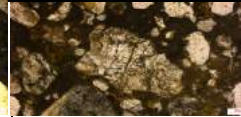
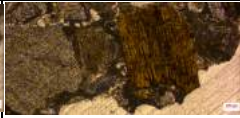
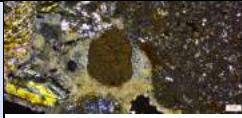
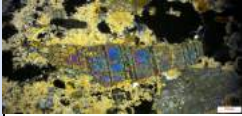
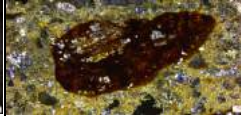
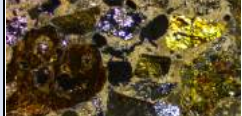


Figure 4.3: Sample locations indicating sample groups and functions based on the petrographic analysis.

Table 4.3: Individual minerals observed by petrographic microscope in cross polarized light (xpl) [left] and plane polarized light (ppl) [right]. Thin sections are thick to preserve binder.

| | | | | |
|---|---|---|--|---|
| Granitic Group |  |  |  |  |
| | A. K-Feldspar MHT-6 | | B. Plagioclase MHT-6 | |
| |  |  |  |  |
| | C. Biotite MHT-4 | | D. Epidote MHT-6 | |
| Basic Group |  |  |  |  |
| | E. Olivine MHT-15 | | F. Quartzite MHT-3 | |
| |  |  |  |  |
| | G. Amphibole MHT-11 | | H. Metashale MHT-11 | |
| |  |  | | |
| I. Pyroxene MHT-15 | | | | |
| Others |  |  |  |  |
| | J. Calcite (Crystallized Limestone) MHT-11 | | K. Calcite Grain MHT-2 | |
| |  |  |  |  |
| | L. Lime Lump MHT-1 | | M. Unburned Limestone MHT-11 | |
|  |  | | | |
| N. Lime Layer MHT-1, Mural Paint | | | | |

4.3 VARIABLE PRESSURE SCANNING ELECTRON MICROSCOPY COUPLED TO ENERGY DISPERSIVE X-RAY SPECTROSCOPY (VP-SEM-EDS)

With VP-SEM-EDS, acquisitions of surface texture and detection and color coding of chemical elements were performed using the elemental mapping function. In the object function, quantification of elements was performed on a point of specific objects, such as binders and individual aggregates, to be analyzed.

During the analysis, it was noted that the elements carbon, C and oxygen, O were often abundant with C from the chamber itself and O from the oxygen in the atmosphere and silicate minerals (SiO_2). Chlorine, Cl, and Sulfur, S, were often due to the resin used to bind the samples rather than from the samples themselves. In all the samples analyzed on SEM-EDS, aggregates and binders were differentiated by mapping Silicon, Si, and Calcium, Ca. Si is the dominant element in aggregates which is abundant in silicate minerals and Ca is the main binder element which is abundant in calcareous lime binder. In the mapping analysis, the binders of all samples showed dominantly Ca and not Magnesium, Mg, indicating that the raw material was limestone and not dolomite. This is important to clarify in SEM-EDS analysis because calcite (limestone-originated binder) and magnesium calcite (dolomite-originated binder) demonstrate the same peaks on the powder diffractograms obtained by XRD analysis. The absence of Mg was also confirmed by the Thermogravimetric analysis except MHT-7, MHT-9, MHT-12, MHT-15-EXT, and MHT-16.

MHT-1 and MHT-9 shared similarities in having layers: a lime layer that seems to be a preparation layer for mural painting which consists of smaller and rounder aggregates, and an inner layer that includes larger and angular aggregates (Figure 4.4 B). The lime layer was also seen in the petrographic analysis (Table 4.3 N), and the SEM-EDS confirmed that the layer is dominantly calcium with little magnesium. It is expected that the render mortars will have a higher percentage of CaCO_3 in TGA and acid attack analysis due to the lime layers. Another similarity in these samples is that they have angular calcareous fragments observed near the preparation lime layer (Figure 4.4 B).

This information agrees with the petrographic analysis where fine-grained fragments of non-calcined limestones were often observed.

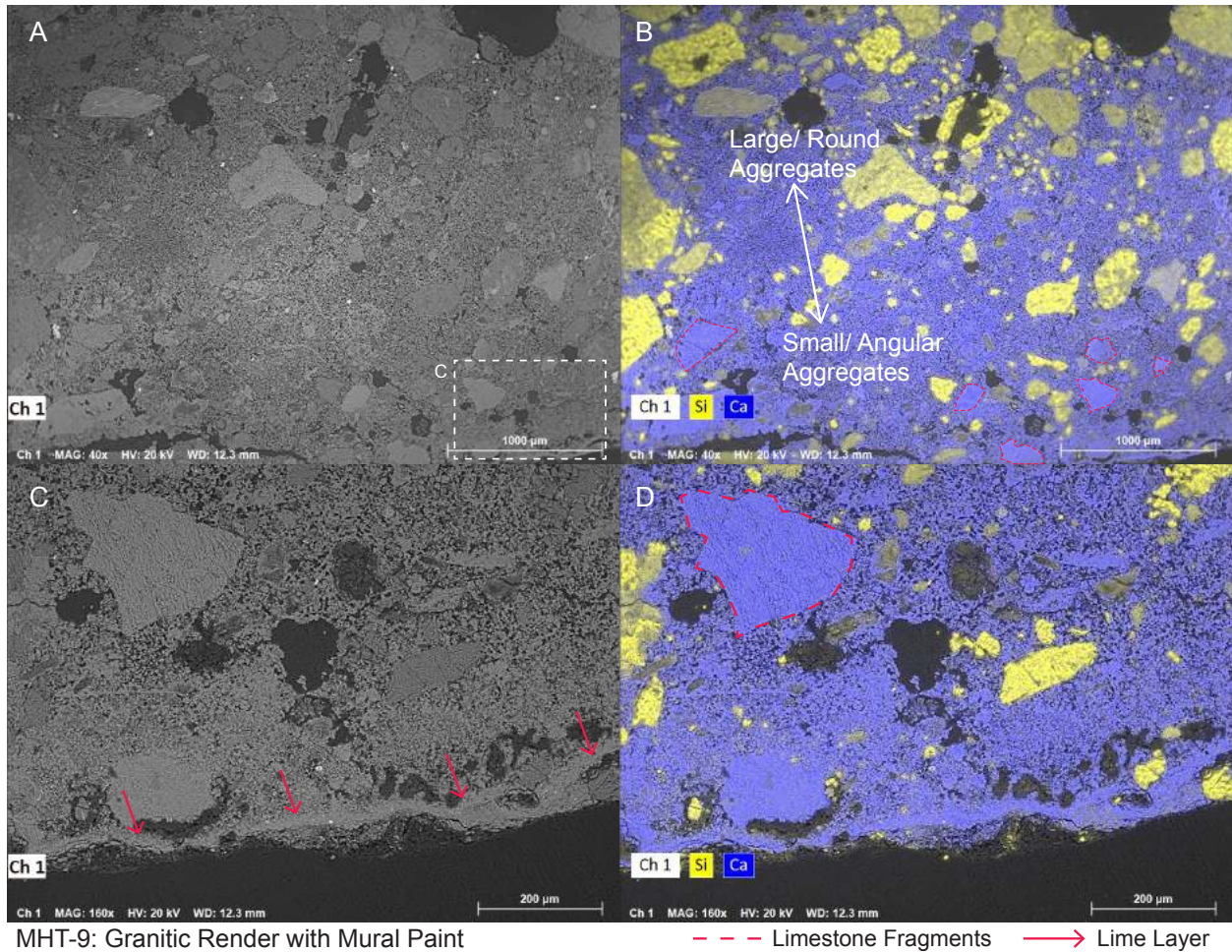


Figure 4.4: Representative micrographs of mural render mortar (MHT-9). Red arrows indicate lime layer. Dashed lines indicate limestone fragments.

In these samples, the feldspar (K-feldspar, plagioclase, perthite) fragments were much smaller in comparison to granitic filling samples such as MHT-6 (Figure 4.5 D). This trait seems to differentiate the render granitic group from the filling granitic group.

Samples such as MHT-6 included granitic minerals such as serpentine, feldspars, and quartz (Figure 4.5 D), which also agrees with the granitic group from the petrographic results.

Samples such as MHT-12, MHT-14, and MHT-18 included mafic/ ultramafic minerals such as olivine, pyroxene, and amphibole that confirms the basic-filling mortar group assessed by the petrographic analysis.

MHT-11 and MHT-18 can become a group by themselves, sharing a similarity in the mixed varieties in aggregate minerals including both characteristic minerals from granitic and basic groups, such as quartz, feldspars, and pyroxenes (Figure 4.5 J).

In MHT-12 and MHT-18, the presence of ilmenite was seen containing Fe, Ti, and Mn. Overall, quartz and feldspars were abundant in all groups.

Furthermore, on the mural surface of MHT-15-EXT, Cu and Zn (brass) were observed. During the initial visual inspection, only MHT-15-EXT appeared to have blue-grayish pigment on the surface.

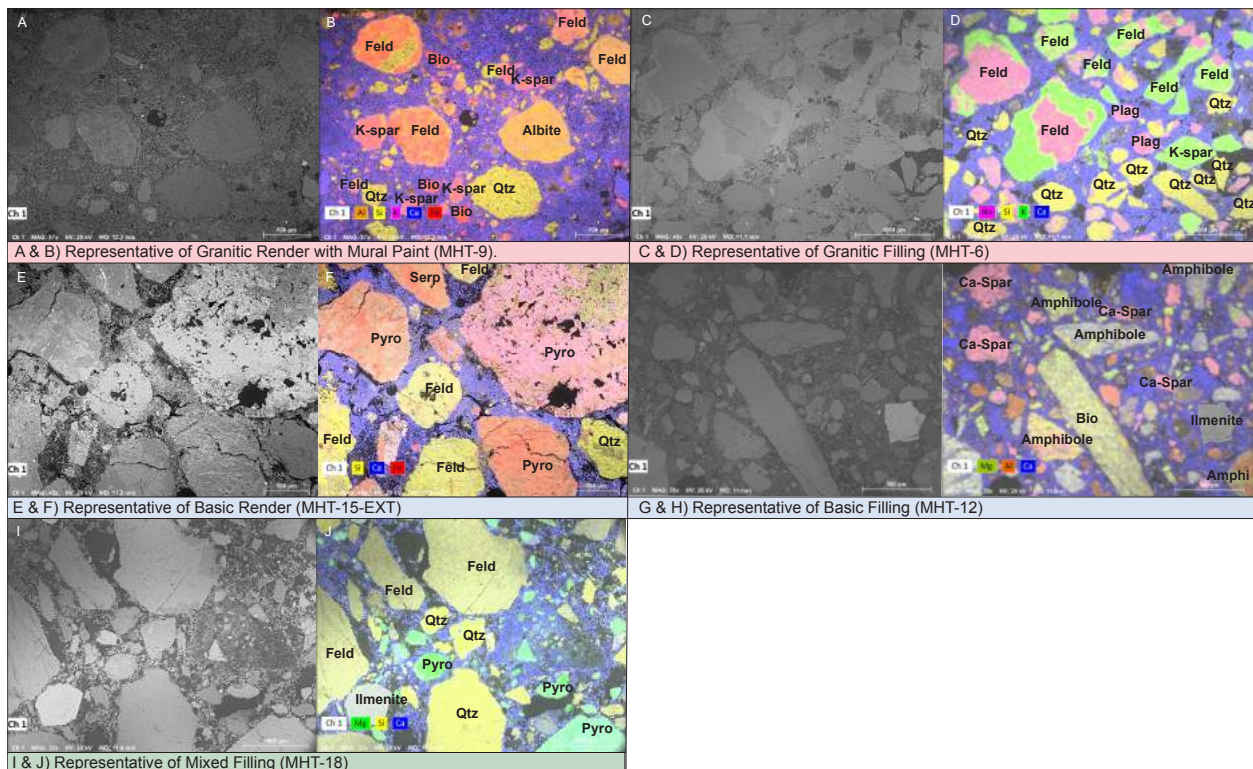


Figure 4.5: SEM-EDS representative images of granitic, basic, and mixed groups. BSE images and elemental map distribution.

4.4 THERMOGRAVIMETRIC ANALYSIS (TGA)

It is possible to identify mortar compositions by interpretation of the thermograms in different temperature ranges. According to Borsoi et al., 2019, there are four stages of mass losses in a calcareous binder: at 25–120 °C, 120–200 °C, 200–600 °C, and 600–900 °C, significant weight losses would occur. Generally, the first three stages of weight loss under 650°C are associated with loss of water, and a loss above 650°C is due to decomposition of calcium carbonates (Cardoso et al., 2014). At 25–120 °C, the mass loss is associated with the dehydration of water on the surface of material particles. Between 120–200 °C, the weight loss is less significant, losing the crystallization water of hydrated salts. At 200–600 °C, water chemically bound in hydraulic compound structure will be lost. The reaction at this temperature range is due to the materials mixed to improve the hydraulic property of mortar, such as pozzolan or other volcanic ashes. Finally, the weight loss at 600–900 °C is a signature of CaCO₃ decomposition (Figure 4.6 D) which is normally associated with the loss of binder component (Borsoi et al., 2019). At T = 600-900 °C, decomposition of calcium carbonate (Calcite, CaCO₃) occurs as following:



1 mol of CaCO₃ = Ar(Ca) + Ar(C) + 3Ar(O) = 100,082 g (molar mass)

1 mol of CO₂ = Ar(C) + 2Ar(O) = 44,02 g (molar mass)

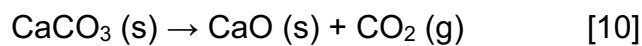
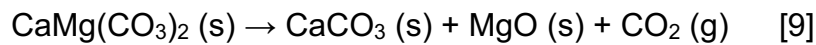
The thermal decomposition of 1 mol of CaCO₃ (100.082g/mol) produces 1 mol of CaO (56,077 g/mol) and 1 mol of CO₂ (44.02g/mol). From the thermogravimetric analysis information on the percentage of CO₂ that escaped, the percentage of CaCO₃ in the entire sample can be determined. For example, in the case of MHT-9, since the CO₂ is 8.56 % from the TGA result, the calculation is as follows:

1 mol CaCO₃ : 1 mol CO₂ = 100,082 g : 44.02 g = X : 8.56 % (from TGA result)

X=0.195 (19.5%) = Percentage of CaCO₃ in the sample interpreted as binder

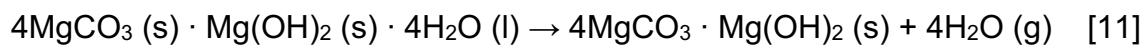
As the binder is interpreted as approximately 20% of the sample, the binder: aggregate ratio of MHT-9 is now determined as 1:4. The calculated percentage of CaCO₃ based on the mass variation at 600°C-900°C for each sample is listed in Table 4.4.

Analyzing the TG and DTG curves, MHT-7, MHT-12, MHT-15-EXT, and MHT-16 showed two steps during the decomposition at temperatures around 700°C, which can be a characteristic of dolomite [CaMg(CO₃)₂] (Figure 4.6 B and E). It should be noted that all these samples belong to the basic group assessed by the petrographic analysis. The two steps are associated with the decomposition of CaMgO(CO₃)₂ [9] which occurs between 700°C-800°C and decarbonation of CaCO₃ [10] near 900°C (Valverde et al., 2015).



Following up on this result in XRD analysis, in the diffractograms of these samples, dolomite only appeared in the automatic search of MHT-16. However, in MHT-7, MHT-12, and MHT-15-EXT, the diffractogram peaks seem to fit the peaks of dolomite; therefore, dolomite was manually added to all. In any case, the two characteristic peaks of dolomite in all four samples were small, with a loss of less than 1%. Dolomite was not clearly identified in SEM-EDS or petrography.

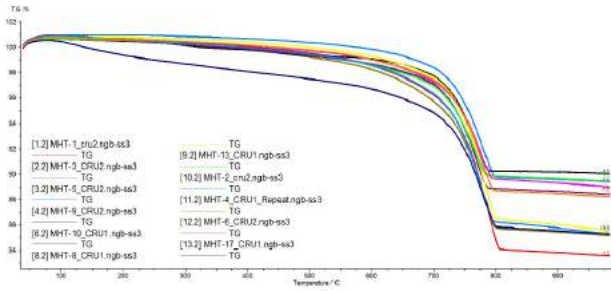
The result of MHT-9 showed three steps in the range of 200-650°C (Figure 4.6 F), which is normally a trait of hydromagnesite (Mg₅(CO₃)₄(OH)₂ · 4H₂O) and magnesite (MgCO₃). The decomposition process is as follows:



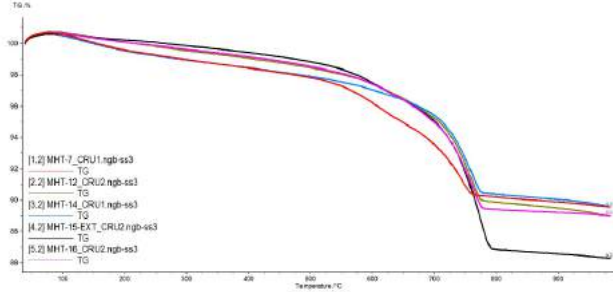
The first step represented by [11] is dehydration, where the removal of water molecules occurs at 200- 340°C. The second step [12] explains dihydroxylation, the removal of the

hydroxyl (OH) group at 340-450°C. The third step [13] is decarbonation of magnesites which occurs at 450-550°C (Bruni et al., 1998; Cardoso et al., 2014).

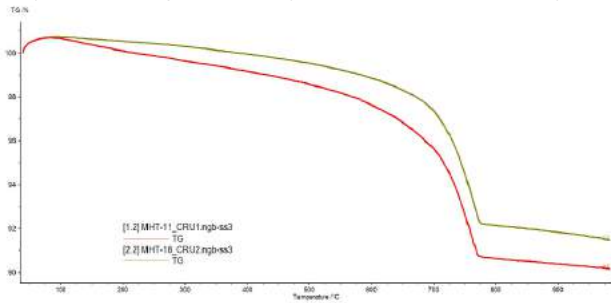
It is important to note that in petrographic microscope, SEM-EDS, and XRD, no significant amount of magnesium was identified in MHT-9. In the XRD diffractogram, hydromagnesite can be added manually and matches its peaks with the sample. Hydromagnesite was not suggested on the automatic search list.



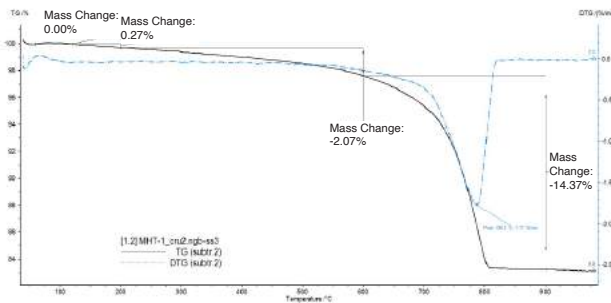
A) Granitic Group TG Curves (MHT-1,2,3,4,5,6,8,9,10,13,17).



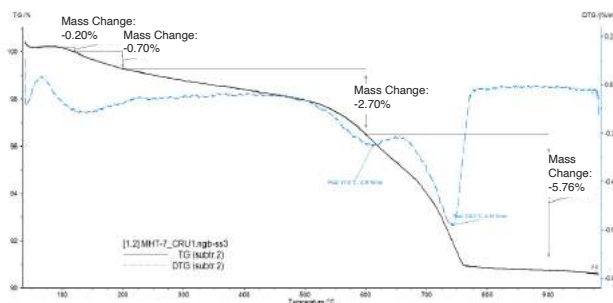
B) Basic Group TG Curves (MHT-7,12,14,15-EXT,16).



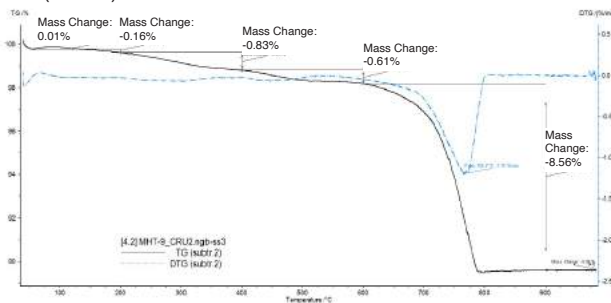
C) Mixed Group TG Curves (MHT-11,18).



D) Representative of TG/DTG Curves with one step at 700-900°C (MHT-1).



E) Representative of TG/DTG Curves with two steps at around 700°C (MHT-7).



F) Representative of TG/DTG Curves with three steps at 200-650°C (MHT-9).

Figure 4.6: TG Curve Comparisons by Granitic, Basic and Mixed Groups (A, B, and C) and TG/DTG Curves of Different Steps (C, D, and E).

The granitic group samples assessed by the petrographic analysis (Table 4.2) (MHT-1 to MHT-6, MHT-8 to MHT-10, MHT-13, and MHT-17) all showed one-step mass losses at

600°C - 900°C, with the calculated CaCO₃ percentage ranging from 19.10-32.67% (Table 4.4). The average is higher compared to the basic group that ranges from 13.10-17.82%, except for the render mortar, MHT-15-EXT at 24.01%.

It should be noted that the basic filling group demonstrated a clear distinction from the granitic group, with the percentage of CaCO₃ in all the samples being similar and lower at the average (15.64%) than the granitic filling average (24.09%). This result agrees with the preliminary grouping based on the petrographic analysis. Within the mixed group, MHT-11 and MHT-18, which are both filling mortars, demonstrated almost identical values to each other, respectively 15.10% and 15.16%. The mixed group average (15.13%) was closer to the basic filling group average (15.64%) than the granitic filling group (24.09%). On average, the render mortars were high in carbonates (24.6%) in comparison to the filling mortars (18.9%.) This seems a reasonable result considering that the render mortars can contain more lime layers as mural preparation layers (Table 4.3 N)

Finally, MHT-1, MHT-2, MHT-3, and MHT-8 showed similar and higher values of calcium carbonate percentage, with an average of 29.55%. MHT-11, MHT-12, MHT-14, MHT-16, and MHT-18 have lower values at the average of 15.47%. All the others (MHT-4, MHT-5, MHT-6, MHT-9, MHT-10, MHT-13, MHT-15-EXT, and MHT-17) were at intermediate values, with an average of 21.84%. This may have a relation to the location of the samples as the first group is located at the northwest of the site while the low-value group is at southeast (Figure 3.2).

Table 4.4: TGA mass loss (%) according to temperature range.

| Sample | Type | Group | Mass Loss (%) | | | | CaCO ₃ (%) | Binder : Aggregate Ratio |
|------------|--------------|----------|---------------|-----------|-----------|-----------|-----------------------|--------------------------|
| | | | 60-120°C | 120-200°C | 200-600°C | 600-900°C | | |
| MHT-1 | Render Mural | Granitic | 0.00 | 0.27 | 2.07 | 14.37 | 32.67 | 1 : 2 |
| MHT-3 | Render Mural | | 0.02 | 0.30 | 2.21 | 12.47 | 28.35 | 1 : 3 |
| MHT-5 | Render Mural | | -0.12 | 0.05 | 1.05 | 9.95 | 22.62 | 1 : 3 |
| MHT-9 | Render Mural | | -0.01 | 0.16 | 1.44 | 8.56 | 19.46 | 1 : 4 |
| MHT-10 | Render Mural | | -0.12 | 0.06 | 1.15 | 9.48 | 21.55 | 1 : 4 |
| MHT-13 | Render Mural | | -0.15 | 0.01 | 1.31 | 8.40 | 19.10 | 1 : 4 |
| MHT-8 | Render | | -0.21 | -0.08 | 0.83 | 12.67 | 28.80 | 1 : 2 |
| MHT-2 | Filling | | -0.01 | 0.26 | 2.02 | 12.49 | 28.40 | 1 : 3 |
| MHT-4 | Filling | | -0.14 | 0.03 | 0.91 | 9.96 | 22.64 | 1 : 3 |
| MHT-6 | Filling | | -0.03 | 0.19 | 1.56 | 9.39 | 21.35 | 1 : 4 |
| MHT-17 | Filling | | 0.24 | 0.76 | 2.00 | 10.54 | 23.96 | 1 : 3 |
| MHT-15-EXT | Render Mural | | 0.10 | 0.34 | 2.71 | 10.56 | 24.01 | 1 : 3 |
| MHT-7 | Filling | | Basic | 0.20 | 0.70 | 2.78 | 5.76 | 13.10 |
| MHT-12 | Filling | 0.13 | | 0.56 | 2.66 | 7.53 | 17.12 | 1 : 5 |
| MHT-14 | Filling | 0.20 | | 0.65 | 1.87 | 6.39 | 14.53 | 1 : 6 |
| MHT-16 | Filling | 0.18 | | 0.51 | 2.65 | 7.84 | 17.82 | 1 : 5 |
| MHT-11 | Filling | Mixer | 0.04 | 0.34 | 1.83 | 6.64 | 15.10 | 1 : 6 |
| MHT-18 | Filling | | -0.01 | 0.22 | 1.64 | 6.67 | 15.16 | 1 : 6 |

4.5 X-RAY DIFFRACTION (XRD) – POWDER XRD

4.5.1 Diffractograms

The diffractograms obtained from XRD analysis are very similar to each other which means that the mineral phases of global fractions are similar. Therefore, it is difficult to identify the grouping by XRD analysis alone. However, referencing the results from other techniques such as optical microscope and TGA, the analysis of the XRD patterns can divide the samples into three groups. The first group (MHT-4, MHT-5, MHT-6, MHT-8, MHT-9, MHT-10, MHT-13, and MHT-17) have similar results, and especially MHT-4, MHT-5, and MHT-6 showed almost identical diffractogram patterns (Figure 4.7). These samples all belong to the granitic group, one of the preliminary groups created based on the petrographic analysis (Table 4.3 A). The diffractogram patterns of MHT-1, MHT-3, MHT-5, MHT-9, MHT-10, and MHT-13 agree with each other, and they can create a subgroup within the granitic group as a granitic render group with mural paintings.

MHT-2, MHT-7, MHT-12, MHT-14, MHT-15-EXT, and MHT-16 all demonstrated similar diffractogram patterns (Figure 4.7 D). This group matches the basic group based on the petrographic analysis.

MHT-11 and MHT-18 diffractograms are almost identical to each other and create a group on their own, although they could possibly fit in either granitic or basic groups (Figure 4.7 G). This mixed aggregate group shows similar minerals with both granitic and basic groups. While this group demonstrated clear peaks of amphibole such as pargasite or hornblende which are peaks usually found in the basic group, it also has a slightly larger amount of feldspar minerals such as microcline which are found in the granitic group.

In diffractograms of fine fractions of MHT-6 and MHT-18, a peak at 11.5° was detected, which matches apophyllite, a secondary mineral of basalt.

As all the above results of all diffractograms are quite similar to each other, it is not so clear to identify the grouping by XRD analysis alone. Therefore, it is necessary to confirm the grouping with other techniques.

Dolomite was suggested by the automatic search database list only in MHT-16. All the others can match dolomite when added manually. All these samples belong to the basic group assessed by the petrographic analysis. Following the result of TGA, hydromagnesite was added to MHT-9 interpretation by the manual name search.

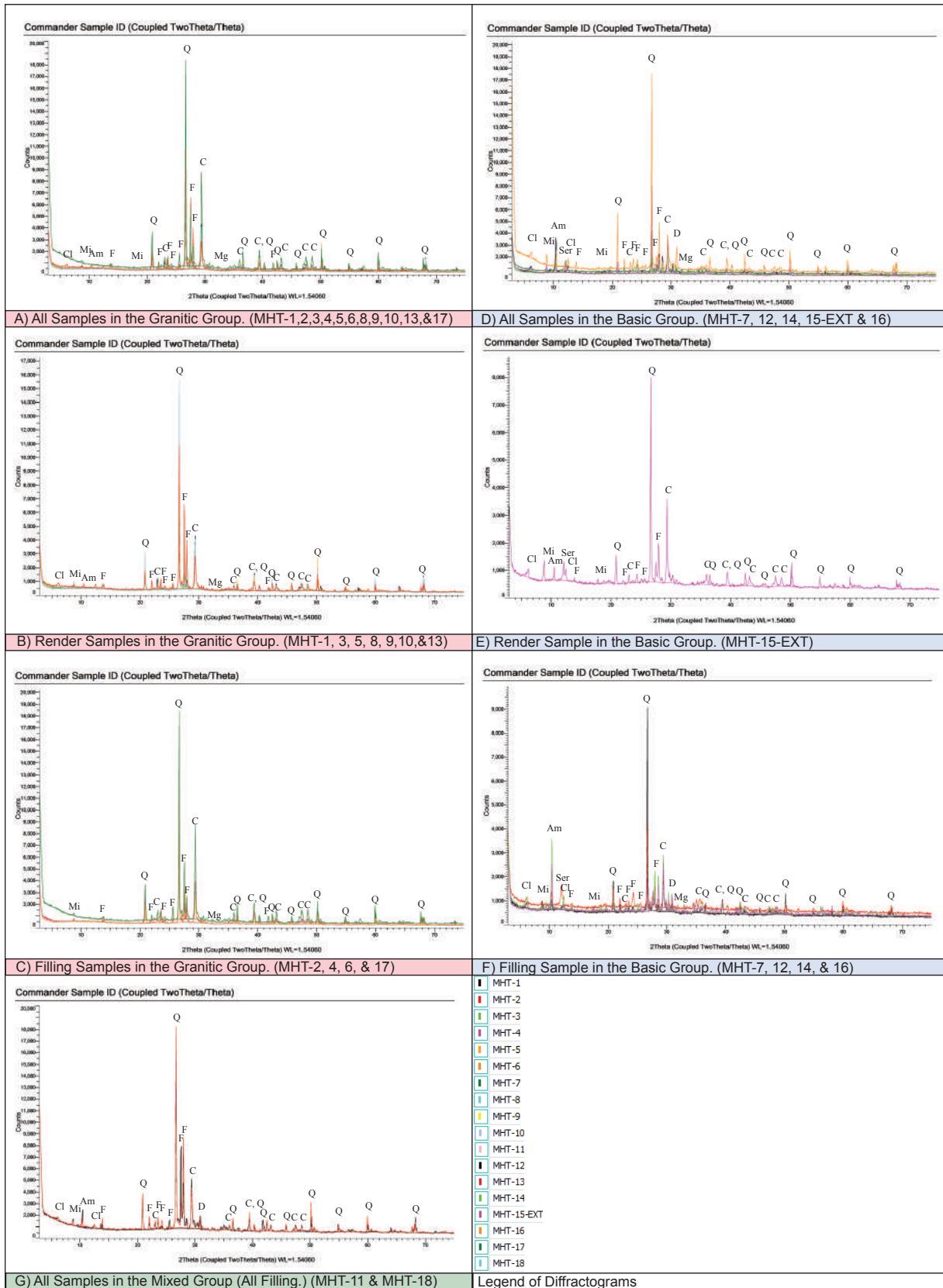


Figure 4.7: Diffractograms by groups (granitic, basic, and mixed) and functions (render and filling).

4.5.2 Semi-Analytical Quantification

Semi analytical quantification was performed using DIFFRAC.EVA software (Bruker). Using the crystalline phases in the samples listed in percentage in the software, a Table was created indicating the predominance of the minerals (Table 4.5).

Table 4.5: Mineralogical composition of the global fractions assessed by XRD.

| Sample (GF) | Type | Group | Quartz | K-Feldspars | Albite | Calcite | Micas | Amphiboles | Chlorite | Pyroxine | Serpentine | Olivine | Dolomite | Epidote | Hydromagnesite | Zeolite | |
|-------------|--------------|----------|--------|-------------|--------|---------|-------|------------|----------|----------|------------|---------|----------|---------|----------------|---------|---|
| MHT-1 | Render Mural | Granitic | +++ | ++ | ++ | +++ | + | + | - | - | - | - | - | - | - | - | |
| MHT-3 | Render Mural | | +++ | ++ | +++ | ++ | + | + | + | - | - | - | - | - | - | - | - |
| MHT-5 | Render Mural | | +++ | +++ | +++ | ++ | + | + | + | - | - | - | - | - | - | - | - |
| MHT-9 | Render Mural | | +++ | ++ | ++ | ++ | ++ | + | - | - | - | - | - | - | ++ | - | - |
| MHT-10 | Render Mural | | +++ | +++ | ++ | ++ | ++ | - | - | - | - | - | - | - | - | - | - |
| MHT-13 | Render Mural | | +++ | +++ | +++ | ++ | + | ++ | + | - | - | - | - | - | - | - | - |
| MHT-8 | Render | | +++ | +++ | ++ | +++ | + | + | - | - | - | - | - | - | - | - | - |
| MHT-2 | Filling | | +++ | ++ | ++ | +++ | + | - | + | - | - | - | - | - | - | - | - |
| MHT-4 | Filling | | +++ | +++ | +++ | ++ | + | + | - | - | - | - | - | - | - | - | - |
| MHT-6 | Filling | | +++ | +++ | +++ | ++ | ++ | + | - | - | - | - | - | - | Tr | - | - |
| MHT-17 | Filling | +++ | +++ | ++ | ++ | ++ | + | + | - | - | - | - | - | - | - | - | |
| MHT-15-EXT | Render | Basic | +++ | ++ | ++ | ++ | ++ | ++ | + | + | + | + | + | - | - | ? | |
| MHT-7 | Filling | | ++ | ++ | +++ | ++ | + | ++ | ++ | ++ | + | + | ++ | - | - | ? | |
| MHT-12 | Filling | | ++ | ++ | ++ | ++ | + | +++ | ++ | ++ | + | + | + | - | - | - | |
| MHT-14 | Filling | | ++ | ++ | ++ | ++ | + | ++ | ++ | ++ | + | + | ++ | - | - | - | |
| MHT-16 | Filling | | +++ | ++ | ++ | ++ | + | ++ | + | + | + | + | ++ | - | - | ? | |
| MHT-11 | Filling | Mixed | +++ | ++ | +++ | ++ | + | ++ | + | + | + | + | - | + | - | - | |
| MHT-18 | Filling | | +++ | ++ | ++ | ++ | + | ++ | + | ++ | + | + | - | + | - | - | |

In most of the samples in the granitic group, abundance in quartz, feldspars such as K-feldspar, albite, and calcite were demonstrated. These minerals were also common in the basic group, although they were less in percentage. Micas were found in all samples, with a majority in a few samples in the granitic group and MHT-15-EXT, the only render sample in the basic group. Amphibole, chlorite, and pyroxene were found in the basic and the mixed group ranging from major to minor. Serpentine and olivine were also found in these groups though in small amounts. Epidote was found in several samples, including the entire mixed group.

It is apparent that the granitic group contains more acidic minerals, and the basic group contains more basic minerals. The mixed group shares the characteristics of both groups, having more quartz and feldspars while having more amphiboles and pyroxenes. However, the dolomite was not detected in these samples, indicating there may be a difference from the basic group.

4.6 ACID ATTACK AND GRANULOMETRIC ANALYSIS

4.6.1 Acid Attack

Acid attack was performed to determine the ratio between the soluble fraction and the insoluble residue. The results of each sample were determined by taking the average value between the two duplicates (Appendix VII). These results of soluble fraction are comparable with the results of TGA, as both TGA and acid attack analyses demonstrate the amount of lost CaCO_3 (Table 4.4).

Overall, the ratio of soluble fraction and insoluble residue was quite similar throughout all samples, with the average percentage of soluble fraction ranging between 25.5% - 40.9% and the average insoluble residue ranging between 59.1% - 74.5% (Figure 4.8 and Figure 4.9). The average percentage of the soluble fraction of the granitic group ranges between 26.9%-40.9% while the average insoluble residue was between 59.1% - 73.1%. The soluble fraction of the basic group ranged from 25.5% - 31.8% and insoluble residue was between 68.2% - 74.5%. The average percentage of soluble fractions is slightly higher than the granitic group.

The two samples in the mixed group (MHT-11 and MHT-18) were close values to each other, with the soluble fraction of MHT-11 at 33.9% and MHT-18 at 37.6%. These values are closer to the average of the granitic filling group (33.5%) than the basic group (29.8%) (Table 4.6). Since the mixed group only consists of filling mortars, it is more accurate to compare with the average of only filling mortars. The mixed group is more like the granitic

filling than the basic filling group. This differs from the TGA results, as the carbonate percentage was closer to the basic group (Table 4.6).

The render mortars overall were higher in the soluble fraction (average 35.1%) in comparison to the filling mortars (32.5%.) This was expected because the lime layers were seen during the petrographic analysis on the surface of render mortars as a preparation layer for mural painting. The lime layers would have increased the percentage of calcium carbonates. This difference between the render and filling mortars was most apparent in the basic group (Table 4.6). The render mortars having a higher soluble fraction agree with the TGA results, in which the average carbonates for the render mortar were 24.6% while the filling mortar was 18.9% (Table 4.6).

Furthermore, MHT-2, MHT-3, and MHT-8 demonstrated almost identical values for both acid attack soluble fraction (38.3% - 39.4%) and TGA carbonates (28.3% - 28.8%). MHT-9, MHT-10, MHT-11, MHT-12, MHT-13, MHT-14, and MHT-16 have very close percentage values to each other in both soluble fractions (30.0% - 33.9%) and TGA carbonates (14.5% - 21.6%). This can indicate a correlation with the location of the walls where the samples were taken from. The first group is located on the northwest of the site, and the second group is located on the southeast side of the site (Figure 3.2).

Table 4.6: Simplified compositions of the mortars determined according to the Jedrzejewska method. Soluble fraction (Jedrzejewska) = 100 – [(IR (from acid attack) + calcium carbonate (from TGA))].

| Sample | Type | Group | Acid Attack | | TGA Carbonates (%) | SF(Jedrzejewska) 100-(IR+Carbonates) | Total Aggregates in Sample (%) | Binder to Aggregate Ratio |
|------------|--------------|----------|----------------------|-----------------------|--------------------|--------------------------------------|--------------------------------|---------------------------|
| | | | Soluble Fraction / % | Insoluble Residue / % | | | | |
| MHT-1 | Render Mural | Granitic | 40.9 | 59.1 | 32.7 | 8.2 | 67.3 | 1 : 2 |
| MHT-3 | Render Mural | | 38.3 | 61.7 | 28.3 | 10.0 | 71.7 | 1 : 3 |
| MHT-5 | Render Mural | | 32.6 | 67.4 | 22.6 | 10.0 | 77.4 | 1 : 3 |
| MHT-9 | Render Mural | | 30.0 | 70.0 | 19.5 | 10.5 | 80.5 | 1 : 4 |
| MHT-10 | Render Mural | | 33.3 | 66.7 | 21.6 | 11.7 | 78.4 | 1 : 4 |
| MHT-13 | Render Mural | | 30.3 | 69.7 | 19.1 | 11.2 | 80.9 | 1 : 4 |
| MHT-8 | Render | Granitic | 39.3 | 60.7 | 28.8 | 10.5 | 71.2 | 1 : 2 |
| MHT-2 | Filling | Granitic | 39.4 | 60.6 | 28.4 | 11.0 | 71.6 | 1 : 3 |
| MHT-4 | Filling | | 36.1 | 63.9 | 22.6 | 13.5 | 77.4 | 1 : 3 |
| MHT-6 | Filling | | 26.9 | 73.1 | 21.3 | 5.5 | 78.7 | 1 : 4 |
| MHT-17 | Filling | | 31.8 | 68.2 | 24.0 | 7.8 | 76.0 | 1 : 3 |
| MHT-15-EXT | Render | Basic | 36.3 | 63.7 | 24.0 | 12.3 | 76.0 | 1 : 3 |
| MHT-7 | Filling | Basic | 25.5 | 74.5 | 13.1 | 12.4 | 86.9 | 1 : 7 |
| MHT-12 | Filling | | 31.3 | 68.7 | 17.1 | 14.2 | 82.9 | 1 : 5 |
| MHT-14 | Filling | | 30.5 | 69.5 | 14.5 | 16.0 | 85.5 | 1 : 6 |
| MHT-16 | Filling | | 31.8 | 68.2 | 17.8 | 14.0 | 82.2 | 1 : 5 |
| MHT-11 | Filling | | Mixed | 33.9 | 66.1 | 15.1 | 18.8 | 84.9 |
| MHT-18 | Filling | 37.6 | | 62.4 | 15.2 | 22.4 | 84.8 | 1 : 6 |

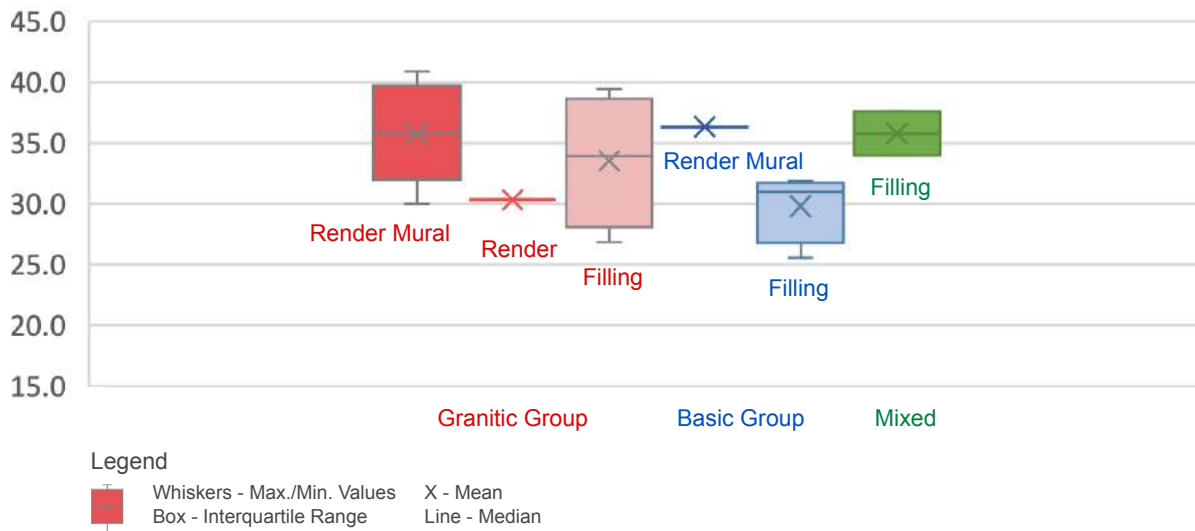


Figure 4.8: Soluble fraction (%) compared by groups and functions.

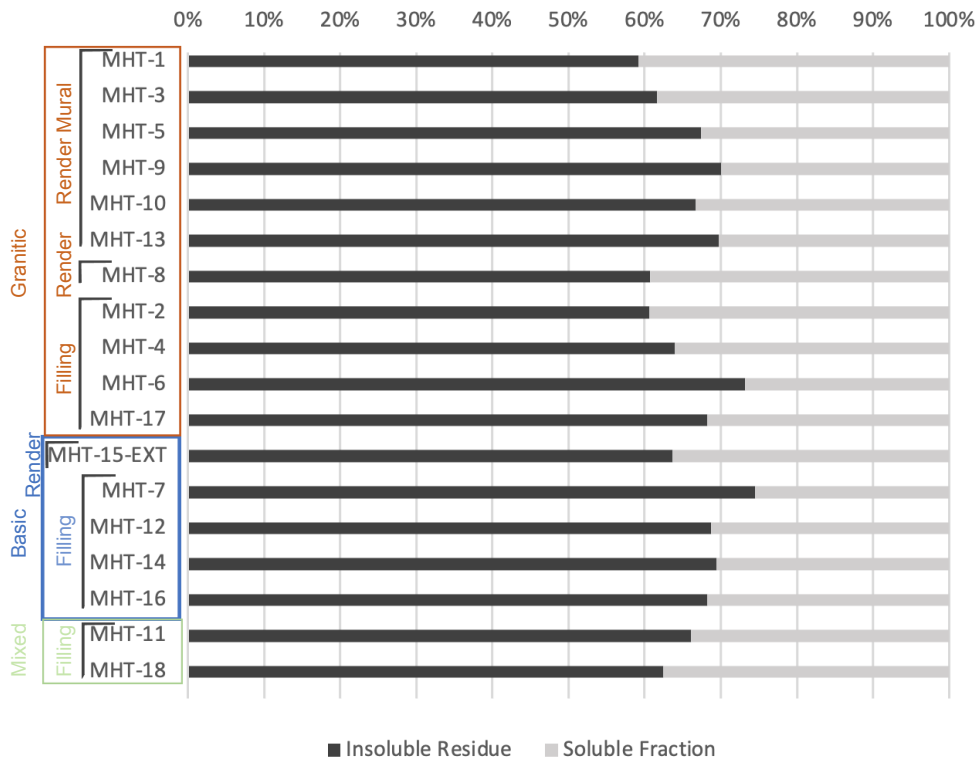


Figure 4.9: Average percentage of insoluble residue and soluble fraction from acid attack analysis.

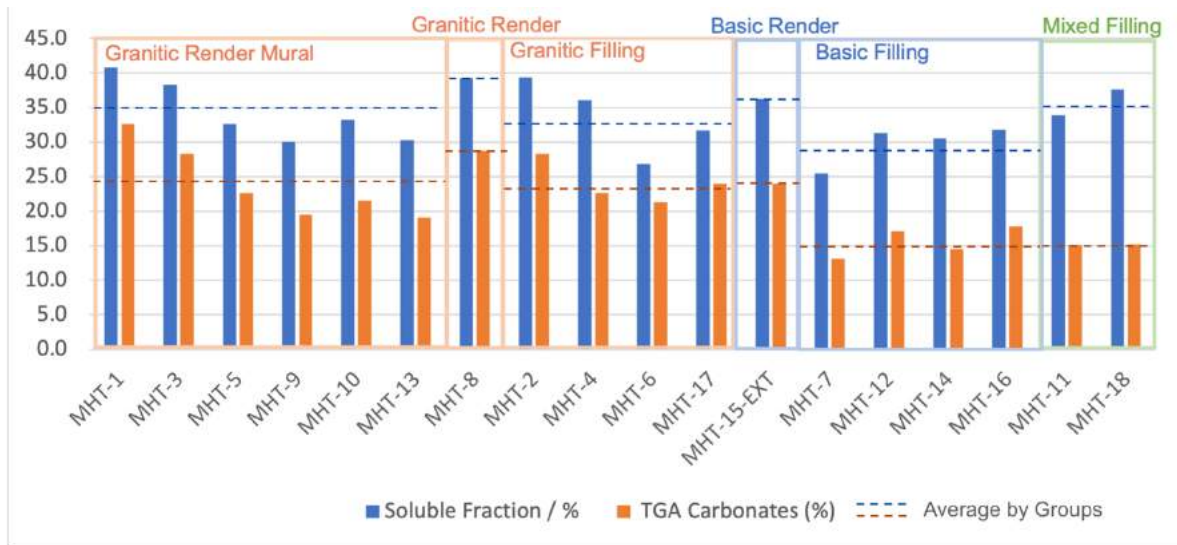


Figure 4.10: Comparison between acid attack soluble fractions and TGA carbonates (%) by groups and functions.

4.6.2 Granulometric Analysis

In the results of granulometric analysis, respectively in pairs, MHT-1 and MHT-3, MHT-4 and MHT-5, MHT-9 and MHT-10, and MHT-12 and MHT-14 demonstrated nearly identical results in percentage (Figure 4.11). The grain size 1-2 mm was predominant in MHT-4, MHT-5, MHT-8, MHT-13, MHT-15-EXT, MHT-17, and MHT-18. All these samples are in the granitic group except MHT-18 which is from the mixed group. In the basic filling group, MHT-12, MHT-14, and MHT-16 are characterized by higher percentages of 0.250-0.125mm and 0.125-0.063mm grains in comparison to the granitic group. MHT-11 from the mixed group also showed similar traits to these samples. Therefore, MHT-11 from the mixed group demonstrates more similarities with the basic filling group than the granitic group. However, it should be noted that this characteristic was also seen in MHT-9 and MHT-10 from the granitic group. Thus MHT-9, MHT-10, MHT-11, MHT-12, MHT-14, and MHT-16 may create a subgroup. This information can be coherent with the location of the walls where the samples were taken from (Figure 3.2).

Samples such as MHT-5, MHT-6, and MHT-8 did not include any particles of size larger than 4mm. This can either be due to the large fragments not being present in the collected samples or dissolving during the acid attack if they were carbonates.

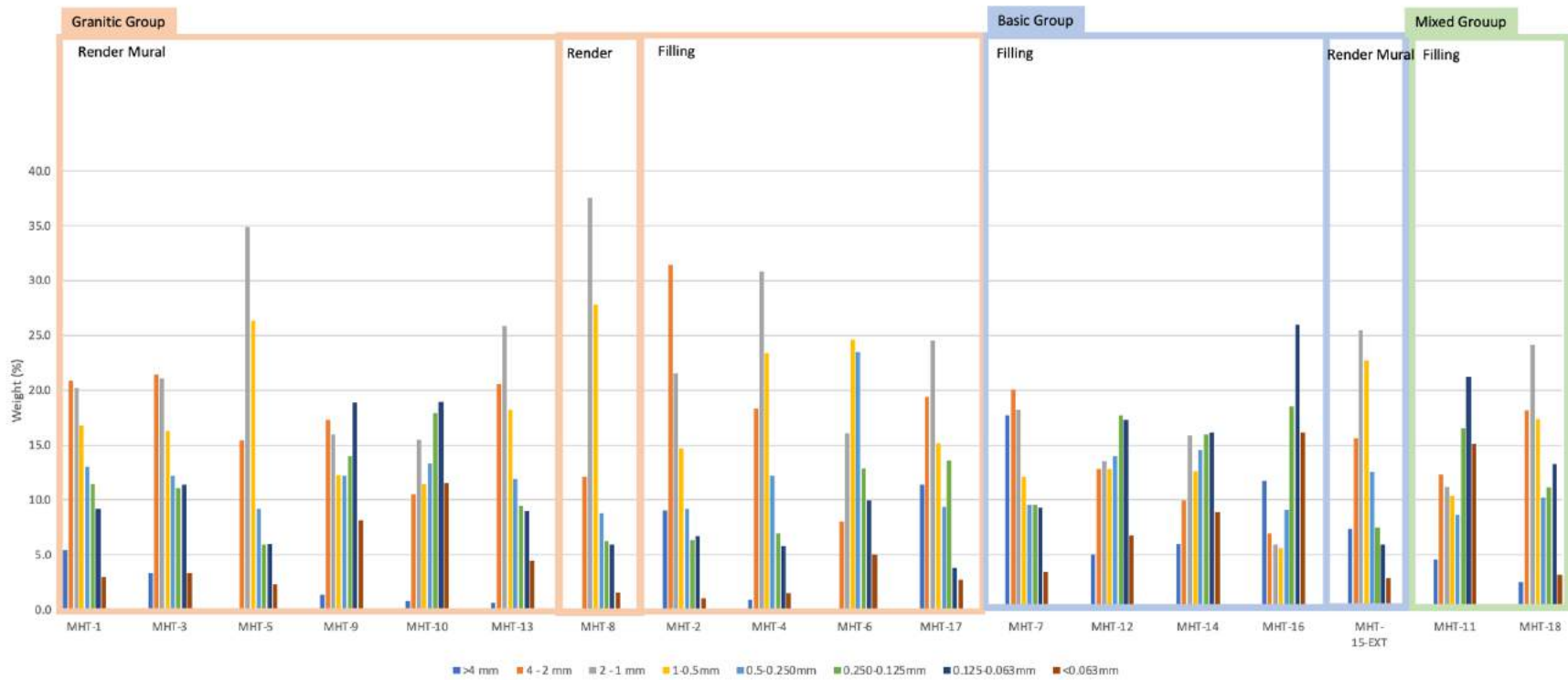


Figure 4.11: Grain size distribution grouped by granitic, basic, and mixed groups and their functions.

To further analyze the insoluble fractions, GRADISTAT, a particle size analysis software based on Microsoft Excel and created by S. Blott (2000), was employed. The software provides information on the insoluble residue samples such as the mode of fractions, sorting, and textural group. In this software, it is also possible to calculate the sieving error caused by samples lost during the sieving by comparing the original weight with the total of the sieved fractions (Table 4.7). The software also provides a gravel/mud/sand diagram demonstrating the distribution of the particles (Figure 4.12). This chart determines the textural groups of the samples.

The render mural samples of the granitic group (MHT-1, MHT-3, MHT-5, MHT-9, MHT-10, and MHT-13) were bimodal except MHT-1 and MHT-13 being unimodal. The basic group also contains both unimodal and bimodal types. Filling mortars (MHT-7, MHT-12, MHT-14, MHT-16) are bimodal except MHT-7 as unimodal. The two samples in the mixed group, MHT-11 and MHT-18, are both bimodal. It is possible that the mixed group tends to be more like the basic filling group than granitic filling; however, the results of basic filling and granitic filling are fairly similar (Table 4.7). It is difficult to identify whether the mode has clear relations to the samples' groups and functions.

In terms of sorting, most samples are categorized as poorly sorted, with exceptions of MHT-9, MHT-10, MHT-11, MHT-12, MHT-14, and MHT-17 being very poorly sorted. The samples are mostly gravelly sand in texture, with the exceptions of MHT-2 as sandy gravel, meaning it is more gravel-like than sand compared to the rest, and MHT-10, MHT-11, MHT-14, and MHT-17 as gravelly muddy sand, indicating they contain more mud than the rest. In the granitic group, render mural samples (MHT-1, MHT-3, MHT-5, MHT-9, MHT-10, and MHT-13) were all gravelly sand except MHT-10 as gravelly muddy sand. As seen in the Gravel-Sand-Mud Diagram, gravelly sand, gravelly muddy sand, and sandy gravel are all similar to each other, and the distribution of the samples in texture is mostly uniform (Figure 4.12).

Overall, the results of the granulometric analysis show similar results in mode, sorting, and textural groups regardless of the groups or the functions of the samples.

Table 4.7: Results from GRADISTAT particle size analysis software showing sieving errors and descriptions of insoluble fractions in each sample.

| SAMPLE | FUNCTION | GROUP | SIEVING ERROR | MODE | SORTING | TEXTURAL GROUP |
|------------|--------------|----------|---------------|----------|--------------------|---------------------|
| MHT-1 | Render Mural | Granitic | 0.8% | Unimodal | Poorly Sorted | Gravelly Sand |
| MHT-3 | Render Mural | | 2.2% | Bimodal | Poorly Sorted | Gravelly Sand |
| MHT-5 | Render Mural | | 1.2% | Bimodal | Poorly Sorted | Gravelly Sand |
| MHT-9 | Render Mural | | 1.8% | Bimodal | Very Poorly Sorted | Gravelly Sand |
| MHT-10 | Render Mural | | 2.7% | Bimodal | Very Poorly Sorted | Gravelly Muddy Sand |
| MHT-13 | Render Mural | | 2.4% | Unimodal | Poorly Sorted | Gravelly Sand |
| MHT-8 | Render | | 1.1% | Unimodal | Poorly Sorted | Gravelly Sand |
| MHT-2 | Filling | | 1.6% | Bimodal | Poorly Sorted | Sandy Gravel |
| MHT-4 | Filling | | 0.7% | Unimodal | Poorly Sorted | Gravelly Sand |
| MHT-6 | Filling | | 1.7% | Unimodal | Poorly Sorted | Gravelly Sand |
| MHT-17 | Filling | | 2.6% | Bimodal | Very Poorly Sorted | Gravelly Muddy Sand |
| MHT-7 | Filling | Basic | 1.2% | Unimodal | Poorly Sorted | Sandy Gravel |
| MHT-12 | Filling | | 0.9% | Bimodal | Very Poorly Sorted | Gravelly Sand |
| MHT-14 | Filling | | 2.2% | Bimodal | Very Poorly Sorted | Gravelly Muddy Sand |
| MHT-16 | Filling | | 1.9% | Bimodal | Poorly Sorted | Gravelly Sand |
| MHT-15-EXT | Render | | 1.2% | Unimodal | Poorly Sorted | Gravelly Sand |
| MHT-11 | Filling | Mixed | 2.8% | Bimodal | Very Poorly Sorted | Gravelly Muddy Sand |
| MHT-18 | Filling | | 1.1% | Bimodal | Poorly Sorted | Sandy Gravel |

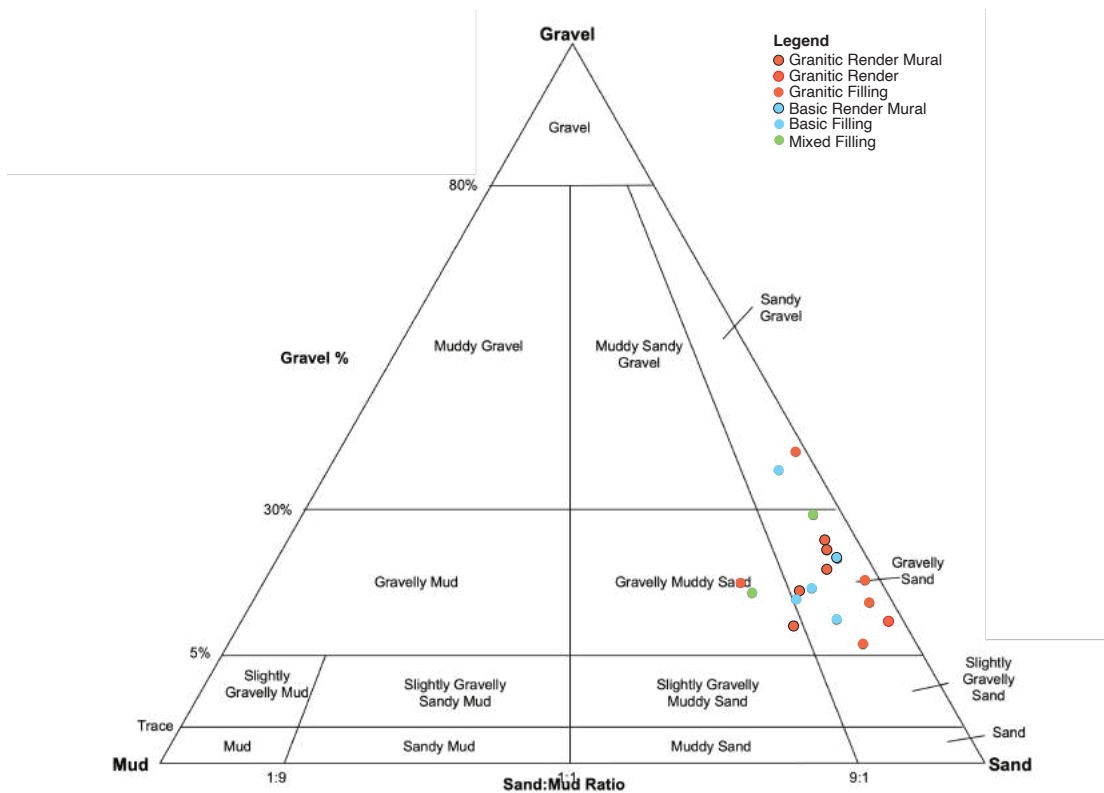


Figure 4.12: Gravel sand mud diagram obtained using GRADISTAT.

The insoluble residues that were sieved after the acid attack were visually analyzed and photographed using a Stereozoom Microscope (Hirox) (Appendix VI). The samples can be roughly divided into three groups: a white and transparent group that corresponds with the granitic group, a black and green group that are all in the basic group, and a mix of white, black, and transparent fragments that applies to the mixed group (Table 4.8). Within the granitic group, in MHT-1, MHT-2, MHT-3, MHT-13, and MHT-17, almost all the fragments are white or transparent (Table 4.9). MHT-4, MHT-5, MHT-6, and MHT-8 included some colored fragments such as light orange or light pink (Table 4.10). MHT-9 and MHT-10 have brown-transparent fragments (Table 4.11). All the basic group samples appeared very dark in color with the mafic/ ultramafic rocks and minerals (Table 4.12). The mixed group demonstrated a mixture of the white/ transparent minerals and the mafic/ultramafic minerals (Table 4.13).

Table 4.8: Colors and shapes of aggregates based on insoluble residues obtained by stereozoom microscopy.

| Sample | Type | Group | Color of Aggregates | Shape of Aggregates |
|-----------|--------------|----------|---|---------------------|
| MHT-1 | Render Mural | Granitic | White and Transparent | Angular |
| MHT-3 | Render Mural | | White and Transparent | Angular |
| MHT-5 | Render Mural | | White, Orange, and Transparent | Angular |
| MHT-9 | Render Mural | | White, Brown, Green, and Transparent | Angular |
| MHT-10 | Render Mural | | White, Brown, Yellow, and Transparent | Semi-Angular |
| MHT-13 | Render Mural | | White and Transparent | Angular |
| MHT-8 | Render | | White, Orange, and Transparent | Angular |
| MHT-2 | Filling | | White and Transparent | Angular |
| MHT-4 | Filling | | White, Orange, and Transparent | Semi-Angular |
| MHT-6 | Filling | | White, Orange, and Transparent | Angular |
| MHT-17 | Filling | | White and Transparent | Round |
| MHT-15-EX | Render | Basic | Black Green, Orange | Round |
| MHT-7 | Filling | | Black and Green | Round |
| MHT-12 | Filling | | Black and Green | Round |
| MHT-14 | Filling | | Black, Green, and Yellow | Semi-Angular |
| MHT-16 | Filling | | Black and Green | Round |
| MHT-11 | Filling | Mixed | White, Black, Brown, Green, and Transparent | Angular |
| MHT-18 | Filling | | White, Black, and Transparent | Semi-Angular |

Table 4.9: Representative samples of granitic group with only white and transparent fragments.

| | | |
|---|---|--|
| MHT-1 (Granitic Render Mural) Set A |  |  |
| | > 4mm | 4-2 mm |
|  |  |  |
| 2-1 mm | 1-0.5 mm | 0.5-0.25 mm |
|  |  |  |
| 0.25-0.125mm | 0.125-0.063 mm | < 0.063 mm |

Table 4.10: Representative samples of granitic group with light-orange or light-pink fragments.

| | | |
|---|---|--|
| MHT-4 (Granitic Filling) Set A |  |  |
| | > 4mm | 4-2 mm |
|  |  |  |
| 2-1 mm | 1-0.5 mm | 0.5-0.25 mm |
|  |  |  |
| 0.25-0.125mm | 0.125-0.063 mm | < 0.063 mm |

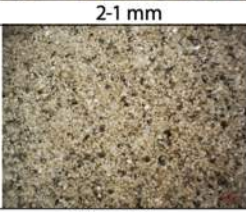
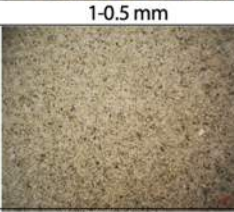
Table 4.11: Representative samples of granitic group with brown fragments.

| | | |
|---|---|--|
| MHT-9 (Granitic Render Mural) Set A |  |  |
| | > 4mm | 4-2 mm |
|  |  |  |
| 2-1 mm | 1-0.5 mm | 0.5-0.25 mm |
|  |  |  |
| 0.25-0.125mm | 0.125-0.063 mm | < 0.063 mm |

Table 4.12: Representative samples of basic group with dark-colored fragments.

| | | |
|---|---|--|
| MHT-12 (Basic Filling) Set B |  |  |
| | > 4mm | 4-2 mm |
|  |  |  |
| 2-1 mm | 1-0.5 mm | 0.5-0.25 mm |
|  |  |  |
| 0.25-0.125mm | 0.125-0.063 mm | < 0.063 mm |

Table 4.13: Representative samples of mixed group with white/transparent and black/green fragments.

| | | |
|---|---|--|
| <p>MHT-18 (Mixed Filling) Set A</p> |  |  |
|  |  |  |
|  |  |  |
| <p>0.25-0.125mm</p> | <p>0.125-0.063 mm</p> | <p>< 0.063 mm</p> |

5. DISCUSSION

5.1 SUMMARY OF RESEARCH AIMS

This research aimed to address the construction phases of the Horta da Torre Roman Villa, the production technology engaged in the construction of the Villa, types and provenance of raw materials used for producing mortar. During the site visit and the visual inspection of the site, the double wall on the south-east of the *cenatio aestivalis* (Figure 3.2, the wall of MHT-17 and MHT-18) suggested that there may have been different construction phases of the villa, as one wall visually seem to be added to another afterward. This may apply not only to the double wall, but also to the entire construction of the Villa. Studying the mortars may form a hypothesis on the construction phases. The study may also indicate the raw materials and their possible origins in comparison to geological data of the area. It can also suggest the quality and the production techniques of the mortars at Horta da Torre. These aspects of Horta da Torre Roman Villa were considered binders and aggregates of the eighteen wall mortar samples were characterized by the multi-analytical approach.

5.2 KEY FINDINGS

5.2.1 Construction Phases based on Aggregate Groups

5.2.1.1. Granitic, Basic, and Mixed Group

The research indicates that there are three types of mortars at the site based on their aggregates: granitic, basic, and mixed of both. According to the preliminary assessment of groups by the petrographic analysis, MHT-1 to MHT-6, MHT-8 to MHT-10, MHT-13, and MHT-17 belong to the granitic group, MHT-7, MHT-12, MHT-14, MHT-15-EXT, and MHT-16 belong to the basic group, and MHT-11 and MHT-18 belong to the mixed group. The results of all analyses generally agree with this grouping.

Since sample MHT-7 is a filling mortar that belongs to the basic group, and MHT-8 is a granitic render mortar that covered the surface of the filling mortar MHT-7, it is possible to construct a hypothesis that the basic group is the earlier construction phase in relative to the granitic group. Even if they were in the same construction phase, it is indicated that the basic group was created before the granitic group.

The mixed group could represent another construction phase apart from these two phases. Some of the results suggested that the mixed group may belong to either the granitic or the basic group; however, considering all the results, it was not possible to clearly determine whether the group was a part of the granitic or the basic. What seems to be clear is that MHT-11 and MHT-18 are very similar to each other in all results. Therefore, the mixed group may suggest a third construction phase.

Furthermore, the wall of the hypocaust where MHT-15-EXT was taken can be another construction phase, as render mortar with basic aggregates was only found here.

5.2.1.2. Subgroups

Although the samples were divided into three groups in this research, it should be noted that the samples can possibly be divided further into smaller subgroups within the suggested groups (granitic, basic, and mixed). For example, in the thermogravimetric analysis, MHT-1, MHT-2, MHT-3, and MHT-4 demonstrated similar and higher values of calcium carbonate percentage with an average of 29.55%. MHT-11, MHT-12, MHT-14, MHT-16, and MHT-18 had lower values at the average of 15.47%. All the others (MHT-5, MHT-6, MHT-9, MHT-10, MHT-13, MHT-15-EXT, and MHT-17) were at intermediate values between the previous two groups, with an average of 21.84%. This may have a relation to the location of the samples as the first group is located at the northwest of the site while the low-value group is in the southeast.

Comparing this data with acid attack, MHT-2, MHT-3, and MHT-8 demonstrated almost identical values for both acid attack soluble fraction (38.3% - 39.4%) and TGA carbonates (28.3% - 28.8%). MHT-9, MHT-10, MHT-11, MHT-12, MHT-13, MHT-14, and MHT-16

also demonstrated almost identical values to each other in both soluble fractions (30.0% - 33.9%) and TGA carbonates (14.5% - 21.6%). This can again indicate a correlation with the location of the walls where the samples were taken from. The first group is located on the northwest of the site, and the second group is located on the southeast side of the site (Figure 3.2). Finally, in the granulometric analysis, MHT-1 and MHT-3, MHT-4 and MHT-5, MHT-9 and MHT-10, and MHT-12 and MHT-14 in pairs, demonstrated nearly identical results in grain size distribution. MHT-9 and MHT-10 differed from the rest of the render mural group, showing similarities to the basic samples such as MHT-12, MHT-14, MHT-16. MHT-12, MHT-14, MHT-16 may have a strong relation to each other with acid attack value close, granulometric similar with all bimodal, and grain size distribution similar with predominant. Again, this information can be coherent with the location of the walls where the samples were taken from (Figure 3.2).

The information from stereomicroscope also suggested that within the granitic group, in MHT-1, MHT-2, MHT-3, MHT-13, and MHT-17, almost all the fragments were white or transparent (Table 4.9). MHT-4, MHT-5, MHT-6, and MHT-8 included some colored fragments such as light orange or light pink (Table 4.10).

In conclusion, four subgroups had almost consistent results in every analysis: Group A (MHT-1, MHT-2, and MHT-3), Group B (MHT-4, MHT-5, and MHT-6), Group C (MHT-9 and MHT-10), and Group D (MHT-12, MHT-14, and MHT-16.) Group A-C belong to the granitic group, and group D belongs to the basic group (Table 5.1). All the other samples (MHT-7, MHT-8, MHT-11, MHT-13, MHT-15-EXT, MHT-17, and MHT-18) were not consistent enough in results that it was not possible to classify into these four subgroups. These subgroups seem to have ties to the wall locations, which may indicate that some parts of the Roman Villa were constructed earlier or later than the other parts, even if in the same construction phase.

From this information, it should be noted that the groups and construction phases could be more complex than the suggested three groups (Granitic, Basic, and Mixed). It is also possible that these only suggest different batches of mix in the same construction phase,

which resulted in mortars with the same raw materials but slightly different consistency. Further research may be needed to clarify what these smaller categories might suggest and address the relationship between these groups, whether chronologically or functionally.

Nonetheless, the results are in line with the early hypothesis that there were different construction phases at Horta da Torre. In conclusion, this research suggests that there are different construction phases of the villa. The excavated part of the villa as of July 2023 was possibly built in three to four different construction phases.

Table 5.1: Samples by functions, aggregate groups, subgroups, and binder types.

| Sample | Type | Aggregate Group | Subgroup | Binder |
|------------|--------------|-----------------|----------|-----------------------------|
| MHT-1 | Render Mural | Granitic | A | Calcitic |
| MHT-2 | Filling | Granitic | A | Calcitic |
| MHT-3 | Render Mural | Granitic | A | Calcitic |
| MHT-4 | Filling | Granitic | B | Calcitic |
| MHT-5 | Render Mural | Granitic | B | Calcitic |
| MHT-6 | Filling | Granitic | B | Calcitic |
| MHT-7 | Filling | Basic | N/A | Presense of Dolomite? |
| MHT-8 | Render | Granitic | N/A | Calcitic |
| MHT-9 | Render Mural | Granitic | C | Presense of Hydromagnesite? |
| MHT-10 | Render Mural | Granitic | C | Calcitic |
| MHT-11 | Filling | Mixed | N/A | Calcitic |
| MHT-12 | Filling | Basic | D | Presense of Dolomite? |
| MHT-13 | Render Mural | Granitic | N/A | Calcitic |
| MHT-14 | Filling | Basic | D | Calcitic |
| MHT-15-EXT | Render | Basic | N/A | Presense of Dolomite? |
| MHT-16 | Filling | Basic | D | Presense of Dolomite? |
| MHT-17 | Filling | Granitic | N/A | Calcitic |
| MHT-18 | Filling | Mixed | N/A | Calcitic |

5.2.2 Raw Materials of Binders

The dominance of calcite in the samples indicates that all samples have calcareous aerial binders. This was suggested by the crystal phase of calcite identified in XRD analysis in

all samples, the peak mass loss at 600–900 °C in TGA, and the point analyses performed by SEM-EDS. Moreover, in several samples in the petrographic analysis, fragments of calcite were observed (Table 4.3 J and K). These fragments originate from marble fragments mixed as aggregate.

The TGA and XRD analyses also suggested the presence of dolomite in MHT-7, MHT-12, MHT-15-EXT, MHT-16, and hydromagnesite in MHT-9. Compared the XRD results with the thermogravimetric analysis results, there is a possibility that dolomite exists in MHT-7, MHT-12, MHT-15-EXT, and MHT-16 (Figure 4.7 D). The TGA result suggested hydromagnesite in MHT-9. Hydromagnesite was added to MHT-9 interpretation of XRD by the manual name search. However, it should be noted that the steps in TGA results that characterize dolomite and hydromagnesite are a small variation of less than 1%. In addition, dolomite and hydromagnesite were not confirmed by other techniques such as SEM-EDS and petrographic analysis.

Furthermore, it is indicated that even if there was a presence of dolomite, it was probably added as aggregate, because of the absence of Mg while observing binders with point analysis using SEM-EDS in these four samples. This information reassures that all the samples have calcareous aerial binders, and the raw material used to produce the binder was likely calcite and not dolomite.

5.2.3 Provenance of Materials

The information on the identified rocks and minerals obtained by the multi-analytical techniques agrees with the geology of the area in comparison to the geological surveys (Figure 2.8). The site is within a kilometer of the area in the north where schists, graywackes, and quartzites are available. These materials were often mixed in any of the mortar samples. Two kilometers to the north, serpentized ultramafic rocks or mafic and ultramafic rocks are abundant. As shown in the results, these types of rocks were more abundant in the basic group samples, possibly characterizing a different phase of construction. On the other hand, in about 3.5 km south of the site, calc-alkaline to alkaline

granites such as biotite are abundant. Micaceous minerals such as biotite were found in most of the samples, but especially abundant in the granitic group.

According to the survey map (Figure 2.8), the rocks and minerals in the basic group come from the north of the Horta da Torre site, and the granitic group comes from the south. It should be noted that there is a creek by Horta da Torre, to the east of the site. As shown in Figure 2.8, the stream comes from the northeast and goes down to the southwest. The direction of the stream goes downward to the southwest, making Horta da Torre the right bank, considering the contour lines that show ground elevations on the map. The results suggest that the basic materials from the northwest were carried along the water to the site, making the mafic and ultramafic aggregates available to Horta da Torre. It is also suggested that the population obtained the sand from the stream nearby, especially for those mortars that belong to the basic group.

This hypothesis aligns with the information on the aggregate shapes obtained by the observation of insoluble residues using stereomicroscope (Table 4.8). The granitic group contained more angular aggregates whereas the basic group contained round-shaped aggregates. The granitic materials from the south came from the quarry which were sharper, while the mafic and ultramafic materials were weathered easily during the transportation in the water.

The site is also located in an area rich in key materials in mortar production, carbonate rocks such as limestone, which was most likely used to produce the binders. As the petrographic analysis suggested, MHT-4, MHT-7, MHT-9, and MHT-11 included unburned raw material of lime. These findings suggest that limestones were used for mortar production. The presence of limestone was also seen in SEM-EDS analysis. In the mapping analysis, the binders of all samples showed mainly Ca, indicating that the raw material was limestone and not dolomite. Although MHT-7, MHT-9, MHT-12, MHT-15-EXT, and MHT-16 showed a presence of dolomite in the TG curves, the steps were less than 1% each and not significant enough to prove that there was a presence of Mg

in these samples. However, if the dolomites exist in the samples, it would be also reasonable as dolomites are readily available in the same area.

5.2.4 Production Technology of the Horta da Torre

It is suggested from the results that the population in the region who constructed Horta da Torre Roman Villa had the fundamental skills and knowledge to produce mortar. For example, in visual and petrographic analyses, it was clear that all the mural paintings had lime layers which were used to prepare the surface for the pigments. This indicates that the population had a basic understanding of the preparation of mural painting. It also appears that at some point in time, the population was producing the mortars according to Vitruvius's recommendation of mortar at binder to aggregate ratio of 1:3 (Morgan, 1914), as the results of TGA and granulometric analysis suggested that all the samples belong to the granitic group and MHT-15-EXT had ratio close to 1:3, between 1:2 and 1:4 (Table 4.6).

The software GRADISTAT was employed to further analyze the insoluble fractions. The software provided information such as the mode of fractions, sorting, and textural group. The render mural samples of the granitic group (MHT-1, MHT-3, MHT-5, MHT-9, MHT-10, and MHT-13) were bimodal except MHT-1 and MHT-13 being unimodal. The basic group also contains both unimodal and bimodal types. Filling mortars (MHT-7, MHT-12, MHT-14, MHT-16) are bimodal except MHT-7 as unimodal. The two samples in the mixed group, MHT-11 and MHT-18, are both bimodal. It is possible that the mixed group tends to be more like the basic filling group than granitic filling; however, the results of basic filling and granitic filling are fairly similar (Table 4.7). It is difficult to identify whether the mode has clear relations to the samples' groups and functions.

In terms of sorting, most samples are categorized as poorly sorted, with exceptions of MHT-9, MHT-10, MHT-11, MHT-12, MHT-14, and MHT-17 being very poorly sorted. The samples are mostly gravelly sand in texture, with the exceptions of MHT-2 as sandy gravel, meaning it is more gravel-like than sand compared to the rest, and MHT-10, MHT-11,

MHT-14, and MHT-17 as gravelly muddy sand, indicating they contain more mud than the rest. In the granitic group, render mural samples (MHT-1, MHT-3, MHT-5, MHT-9, MHT-10, and MHT-13) were all gravelly sand except MHT-10 as gravelly muddy sand. As seen in the Gravel-Sand-Mud Diagram, gravelly sand, gravelly muddy sand, and sandy gravel are all similar to each other, and the distribution of the samples in texture is mostly uniform (Figure 4.12).

Overall, the results of the granulometric analysis show similar results in mode, sorting, and textural groups regardless of the groups or the functions of the samples (Table 4.7).. However, it is indicated that Vitruvius's rule was not followed completely since there were no signs of brittle marble near the preparation layer; instead, limestone fragments were found (Figure 4.4). The substitution of marble with limestone may be due to the availability of the material.

In addition, some of the results suggested that the studied mortars were in different qualities. For example, in the petrographic analysis, the results suggested that MHT-4, MHT-7, MHT-9, and MHT-11 included unburned raw material of lime (Table 4.2 M). The preserved limestone in these samples indicates that the firing temperature during the production did not reach the proper calcination temperature at around 750°C - 900°C. This can indicate that the population did not have the pyrotechnology to have a high firing temperature.

Furthermore, all the samples contained lime lumps (Table 4.2 L). This is often an indication of an insufficient amount of water added during the hydration process of mortar production (Elsen, 2006). A recent study shows that lime lumps may improve the durability of mortars (Seymour, et al., 2023).

5.3. FURTHER INTERPRETATION OF FINDINGS

5.3.1 Comparison with Existing Research

In previous research on mortars from Horta da Torre, it is stated that olivine (sometimes serpentized), pyroxene, allanite, quartzite, chlorite, amphibolite, quartz and feldspars were found in a masonry mortar sample HT-60 and that these materials came from the north of Horta da Torre (Ditta, 2017), which makes the sample a basic mortar. This information is agreeable with the sample MHT-15-EXT and MHT-16 which were both taken from the nearby walls of the hypocaust and belong to the basic group (Figure 5.1). It is also stated that HT-40 from the *cenatio aestivalis* contained granitic aggregates such as quartz and small feldspar grains. This is also coherent with the granitic samples found by the *cenatio aestivalis*, such as MHT-3, MHT-4, and MHT-17.

In another research of Horta da Torre, it is mentioned that minerals such as quartz, alkali feldspars (orthoclase and microcline), plagioclase feldspars (albite), amphiboles (hornblende), micas (muscovite and biotite), pyroxenes, olivine, and calcite were found in some samples (Madrid, 2019). In this research, it is also stated that the provenance of raw materials indicates local production according to the geology of the area, which agrees with this research. Specifically, for samples HHT-4 near the hypocaust in the small peristyle, which is a wall mortar sample, the presence of pyroxenes and olivine were mentioned in the discussion of aggregates.

HHT-4 containing the basic aggregates is consistent with Ditta's HT-60 having basic aggregates and MHT-15-EXT and MHT-16 in the hypocaust in this research having basic aggregates (Figure 5.1). On PHHT-6, a chromatic wall sample, it is stated that granitic aggregates such as quartz, K-feldspar, micas (biotite), and sandstones were found. This corresponds to MHT-9 and MHT-10, which are also render mural mortars with granitic aggregates.

To summarize, this research seems to be coherent with past research on Horta da Torre, adding more information to the existing set of results the previous studies have provided.

The previous results are coherent with this research, and they agree with the hypothesis of this research.



Figure 5.1: Horta da Torre Roman villa aerial view indicating Ditta's sample (Ditta, 2017) and Madrid's sample (Madrid, 2019) locations. Ditta's samples (HT-40 and HT-60) and Madrid's samples (HHT-4 and PHHT-6) are shown with red arrows.

5.3.2. Different Behavior of Aggregates in Mortars

In previously published research on the mechanical behavior of mortars, mortars that were created to repair existing heritage sites were designed to be as close as possible to

original mortars, as the use of cement mortars can harm the existing structures (Lanas, et al., 2004). These mortars were tested for their strengths based on different characteristics of both binders and aggregates. From these studies, it is known that different aspects of mortar affect its durability: the types of mortars (whether aerial or hydraulic,) binder: aggregate ratio, the aggregate sizes and shapes, and chemical compositions (Lanas, et al., 2004).

Mortars enriched in binder were always more durable, as suggested in Vitruvius's 1:3 ratio of aggregates and binder (Morgan, 1914). However, specifically in natural aerial mortars, a tendency to decrease its durability after setting for 182 days was observed in mortar samples that have a higher aggregate ratio of 1:3 and above. The mortars that contain aggregate size less than 2mm were more durable than those with coarser rock fragments (>2mm). Limestone aggregates create more durability while siliceous aggregates result in weaker mortars. When limestone is used as aggregate, the pore diameters created in mortars are smaller, making the mortar more durable. Angular aggregates tend to create stronger mortars, as they tend to have a better-packed structure. Round aggregates disrupt the creation of packed structure as the matrix does not attach to the aggregates as much as it does to angular aggregates, which results in larger porosity (Lanas, et al., 2004).

Based on this information, the stronger mortars at Horta da Torre may be the granitic group, considering all aspects that can have an impact on the strength of mortars (Table 5.2). The binder ratio of the granitic group was always higher in comparison to the basic and mixed groups. The percentage of large aggregate sizes >2mm was always lower in the granitic group, which also makes the mortars in this group more resistant. The aggregate shapes were mostly angular in the granitic group which means the mortar structure is more durable due to a higher adhesive characteristic of the shapes. It is possible that the population at Horta da Torre was aware of the different behaviors of mortars in accordance with the binder and aggregates and made conscious decisions on certain kinds of mortars where structural strengths may be needed.

Table 5.2: Samples compared by key aspects that effect on strength of mortar.

| Sample | Type | Group | B:AG ratio | AG Size >2mm | AG Shape | Porosity | Composition |
|-----------|--------------|----------|------------|------------------------------------|------------------------------------|----------------------------|-----------------------------------|
| MHT-1 | Render Mural | Granitic | 1 : 2 | <10% | Angular | Low | |
| MHT-3 | Render Mural | | 1 : 3 | <5% | Angular | Low | |
| MHT-5 | Render Mural | | 1 : 3 | 0% | Angular | Low | Calcite |
| MHT-9 | Render Mural | | 1 : 4 | <5% | Angular | Low to Medium | Limestone |
| MHT-10 | Render Mural | | 1 : 4 | <1% | Semi-Angular | Low | |
| MHT-13 | Render Mural | | 1 : 4 | <1% | Angular | Low | |
| MHT-8 | Render | Granitic | 1 : 2 | 0% | Angular | Low | |
| MHT-2 | Filling | Granitic | 1 : 3 | <10% | Angular | Low | Calcite |
| MHT-4 | Filling | | 1 : 3 | <1% | Semi-Angular | Medium | Limest./Cals. |
| MHT-6 | Filling | | 1 : 4 | 0% | Angular | Medium | |
| MHT-17 | Filling | | 1 : 3 | >10% | Round | Low | |
| MHT-15-EX | Render | Basic | 1 : 3 | <10% | Round | Low | |
| MHT-7 | Filling | Basic | 1 : 7 | >10% | Round | Low | Limestone |
| MHT-12 | Filling | | 1 : 5 | <10% | Round | Low to Medium | |
| MHT-14 | Filling | | 1 : 6 | <10% | Semi-Angular | Medium | |
| MHT-16 | Filling | | 1 : 5 | >10% | Round | Low | |
| MHT-11 | Filling | Mixed | 1 : 6 | <5% | Angular | Low | Limest./Cals. |
| MHT-18 | Filling | | 1 : 6 | <5% | Semi-Angular | Low to Medium | |
| | | | *From TGA | *From Granulometric Analysis | *From Granulometric Analysis | *From Visual Inspection | *From Petrographic Analysis |

5.4 LIMITATIONS OF THIS RESEARCH AND RECOMMENDATIONS

As mentioned earlier, this research may not cover all the different phases of construction, as the groups may be categorized further into smaller groups. It is also possible that some of the mortars were created in different times but with the same recipe and raw materials. It is not possible to address day-by-day construction phases; however, this research addressed the construction phases of the Roman Villa as a large picture that responds to the research aim. More importantly, further research shall be conducted on chronology, as this research only reveals the relative chronology of the wall constructions in relation to each other.

The nature of this research also does not cover whether the mortars had different recipes according to chronology or functionality. It is possible that some mortars were created following certain recipes to gain more durability to withstand certain structural designs

while it is also possible that different eras simply brought in different walls created with different recipes. There may even be more reasons as to why different types of mortars were utilized such as according to room functions. This may bring more insights into the construction and archeology of Horta da Torre Roman Villa.

6. CONCLUSION

Horta da Torre is an excavation site of a Roman villa that dates to 1500 - 2000 years ago, estimated to be constructed around the third and the fourth century A.D (Carneiro, 2019). The archaeological site is located near Cabeço de Vide (Fronteira), Alto Alentejo Region, Portugal. This area was a part of the Lusitania province during the Roman period. Located approximately halfway near Antonine Itinerary between two important ancient cities, current day Merida, Spain, and Lisbon, Portugal, the villa played a crucial role as a retreat for wealthy individuals. It is crucial to study Horta da Torre Roman Villa because of its significance in the location.

The samples were taken from different walls of the villa to compare the construction phases. Some of these samples were taken from the same wall but different parts and different functions of the mortars such as the filling mortars and the render mortars. Seven render mortars with mural paintings, one render, and ten filling mortars, in a total of eighteen mortars were sampled from twelve different walls across the excavated part of the villa. The samples were then analyzed using SEM-EDS, Stereo microscope, petrographic microscope, XRD, TGA, Acid attack, and granulometric analysis. Textural, chemical, and mineralogical characterization of the samples enabled to obtain information on the binders and aggregates.

In the early stage of analyses, petrographic analysis was executed, and samples were divided into three groups according to their aggregates: granitic, basic, and mixed. the basic group was always filling mortars except for MHT-15-EXT, and the granitic group was either filling or the render mortars (Table 4.2). In the case of MHT-8 (granitic render) and MHT-7 (basic filling), the samples come from the same wall which can indicate relative chronology that the basic group was created earlier than the granitic group.

From this information, a hypothesis was constructed that the basic group was associated with previous structures, and the granitic group was either used to render previous walls

as render mortars or associated with the construction of later structures as filling mortars. The mixed group can represent another construction phase apart from these two phases. Furthermore, the information on the minerals obtained by petrographic analysis aligns with the geology of the area in comparison to geological surveys. From this, it is likely that the raw materials were locally sourced. According to the survey, the aggregates in the basic group come from 2 km north of the site, the granitic group comes from 3.5 km south, and the limestone used for binder on site or within 1km of the site.

These key points were considered throughout the rest of the research, and as other analyses were completed, the results were compared to verify if they were coherent with the hypothesis. As explained in Results and Discussion, all data, from this research and past research on Horta da Torre Roman Villa, are consistent and support the hypothesis. To conclude this research, the data collected by this study suggest that there are different construction phases of the villa. The excavated part of the villa where the samples were taken from was most likely built in three construction phases. There are three types of mortars at the site based on the data obtained through multi-analytical approach: granitic, basic, and mixed of both. MHT-1 to MHT-6, MHT-8 to MHT-10, MHT-13, and MHT-17 belong to the granitic group, MHT-7, MHT-12, MHT-14, MHT-15-EXT, and MHT-16 belong to the basic group, and MHT-11 and MHT-18 belong to the mixed group. The collected data suggested that the basic group is the earlier construction phase in relative to the granitic group.

Furthermore, the wall of the hypocaust where MHT-15-EXT was taken from can be a later construction phase, as render mortar with basic aggregates was only found here.

The production technology of the mortars at Horta da Torre appears to have followed Vitruvius's recipe at some point in time, based on all samples in the granitic group (MHT-1 to MHT-6, MHT-8 to MHT-10, MHT-13, and MHT-17) and one sample from the basic group (MHT-15-EXT) having 1:3 aggregate to binder ratio. It is rather clear that the population had basic knowledge of mortar production; however, the recipe of the mortars was not always consistent, most likely being affected by the accessibility of the raw materials and conditions at Horta da Torre. In addition, adding brittle marble to the

preparation layer of mural paintings seemed to have been followed; however, not by using marble, but fragments of limestone.

The research aims of the construction phases of the Roman Villa of Horta da Torre, the production technology engaged in the construction of the Villa, and the types and provenance of raw materials used for producing mortar were addressed, giving insights to the further research at Horta da Torre where large part of the site remains underground and awaiting excavation.

7. BIBLIOGRAPHY

Arias, G. (2004). El Nuevo Miliario y El Miliario Extravagante. Boletín sobre vías Romanas, historia de los caminos y otros temas de geografía histórica. MAPA ÍNDICE DE VÍAS ROMANAS.

Borsoi, G., Silva, A. S., Menezes, P., Candeias, A., & Mirão, J. (2019). Analytical characterization of ancient mortars from the archaeological Roman site of Pisões (Beja, Portugal). *Construction and Building Materials*, 204, 597-608.

Bruni, S., Cariati, F., Fermo, P., Pozzi, A., & Toniolo, L. (1998). Characterization of ancient magnesian mortars coming from northern Italy. *Thermochimica Acta*, 321(1-2), 161-165.

Burnstock, A., & Jones, C. (2000). Scanning electron microscopy techniques for imaging materials from paintings. *Radiation in art and archeometry*, 202-231.

Cardoso, I., Macedo, M. F., Vermeulen, F., Corsi, C., Santos Silva, A., Rosado, L., ... & Mirao, J. (2014). A Multidisciplinary Approach to the Study of Archaeological Mortars from the Town of A mmaia in the R oman Province of L usitania (P ortugal). *Archaeometry*, 56(1), 1-24.

Carneiro, A. (2019, October). Horta da Torre Roman villa (Fronteira) and the Monumentalization in Lusitania's Rural Landscape. *Centro Interuniversitario di Studi sull'Edilizia abitativa tardoantica nel Mediterraneo (CISEM)*. P.527-538.

Carneiro, A. (2020). Adapting to Change in Rural Lusitania: Zooarchaeological Record in the Horta da Torre Roman Villa (Portugal). *European Journal of Post Classical Archaeologies* 10, P249-275.

Carneiro, A. (2022). The Fate of Villae: The Example of Horta da Torre (Fronteira). Paisajes, espacios y materialidades. *Arqueología rural altomedieval en la península ibérica* S. P166-177.

Carneiro, A., Sanchez, J. G., Stek, T. D., & Kalkers, R. (2020). 2020_The Late Roman villae of Horta da Torre and Monte de São Francisco and their rural context (North Alentejo, Portalegre district, Portugal). *Congreso Internacional Las Villas Romanas Bajoimperiales De Hispania – Actas, Palencia*, 15-17.

CEN: European Committee for Standardization. (2011). Cement - Part 1: Composition, Specifications and Conformity Criteria for Common Cements. *DIN EN 197-1*, Page 40.

Chever, L., Pavía, S. & Howard, R. (2010). Physical Properties of Magnesian Lime Mortars. *Mater Struct* 43, 283–296.

Gonçalves, F. (1973): Carta Geológica de Portugal 1:50.000, 32-B (Portalegre) Serviços Geológicos Portugal.

Gonçalves, F., Zbysewski, G. & Chelho, A. (1975): Carta Geológica de Portugal 1:50.000, 32-D (Sousel) Serviços Geológicos Portugal.

Ditta, A. (2017). Conservation of Architectural Heritage: Characterization and Provenance of Roman Mortars. P27-94.

Elsen, J. (2006). Microscopy of Historic Mortars—A Review. *Cement and Concrete research*, 36(8), 1416-1424.

Etiopo, G., Vance, S., Christensen, L. E., Marques, J. M., & da Costa, I. R. (2013). Methane in serpentized ultramafic rocks in mainland Portugal. *Marine and Petroleum Geology*, 45, 12-16.

Faria, P., & Martins, A. I. G. (2011). Influence of curing conditions on lime and lime-metakaolin mortars. In *XII DBMC-International Conference on Durability of Building Materials and Components, April 12th-15th, 2011*.

Haldar, S.K. (2020). Chapter 3 - Basic Mineralogy, *Introduction to Mineralogy and Petrology (Second Edition)*. Elsevier, 109-143.

Hughes, J. J., & Callebaut, K. (2007). 2.1 In-situ visual analysis and practical sampling of historic mortars. Report 28: Characterisation of Old Mortars with Respect to their Repair-State-of-the-Art Report of RILEM Technical Committee 167-COM, 28, 9.

Callebaut, K., Elsen, J., Van Balen, K., & Viaene, W. (2001). Nineteenth century hydraulic restoration mortars in the Saint Michael's Church (Leuven, Belgium): Natural hydraulic lime or cement?. *Cement and Concrete Research*, 31(3), 397-403. Khan, A., & Lemmen, C. (2013). Bricks and urbanism in the Indus Valley rise and decline. *arXiv preprint arXiv:1303.1426*.

Lanas, J., Arandigoyen, M., Alvarez, J. I., Bernal, J. P., & Bello, M. A. (2004). Mechanical behavior of masonry repair mortars: Aerial and hydraulic lime-based mixtures. In *10th International Congress on Deterioration and Conservation of Stones Stockholm*.

Le Maitre, R. W., Streckeisen, A., Zanettin, B., Le Bas, M. J., Bonin, B., & Bateman, P. (Eds.). (2005). *Igneous rocks: a classification and glossary of terms: recommendations of the International Union of Geological Sciences Subcommission on the Systematics of Igneous Rocks*. Cambridge University Press.

Madrid, D. (2019). Characterization of mortars associated with the hydraulic system of Roman villa Horta da Torre (Fronteira, Portugal). P57-62.

Marques, J., Maria Orquidia Neves, Ana Miller, et al. (2017). Water-rock Interaction Ascribed to Hyperalkaline Mineral Waters in the Cabeço de Vide Serpentinized Ultramafic Intrusive Massif (Central Portugal). *Procedia Earth and Planetary Science*. 17. 646-649.

Middendorf, B., Hughes, J. J., Callebaut, K., Baronio, G., & Papayianni, I. (2005). Investigative methods for the characterisation of historic mortars—Part 1: Mineralogical characterisation. *Materials and Structures* 38, 761-769.

Middendorf, B., Hughes, J., Callebaut, K., Baronio, G., & Papayianni, I. (2005). Investigative Methods for The Characterisation of Historic Mortars—Part 2: Chemical Characterisation. *Materials and Structures* 38, 771-780.

Morgan, M. H., & Warren, H. L. (1914). *Vitruvius: the ten books on architecture*.

Saleh, H. M., & Eskander, S. B. (2020). Innovative cement-based materials for environmental protection and restoration. In *New materials in civil engineering* (pp. 613-641). Butterworth-Heinemann.

Seymour, L. M., Maragh, J., Sabatini, P., Di Tommaso, M., Weaver, J. C., & Masic, A. (2023). Hot mixing: Mechanistic insights into the durability of ancient Roman concrete. *Science Advances*, *9*(1), eadd1602.

Torres, I., Gina Matias, Paulina Faria. (2020). Natural hydraulic lime mortars - The effect of ceramic residues on physical and mechanical Behaviour. *Journal of Building Engineering*, *Volume 32*, 101747.

Valverde, J. M., Perejon, A., Medina, S., & Perez-Maqueda, L. A. (2015). Thermal decomposition of dolomite under CO₂: insights from TGA and in situ XRD analysis. *Physical Chemistry Chemical Physics*, *17*(44), 30162-30176.

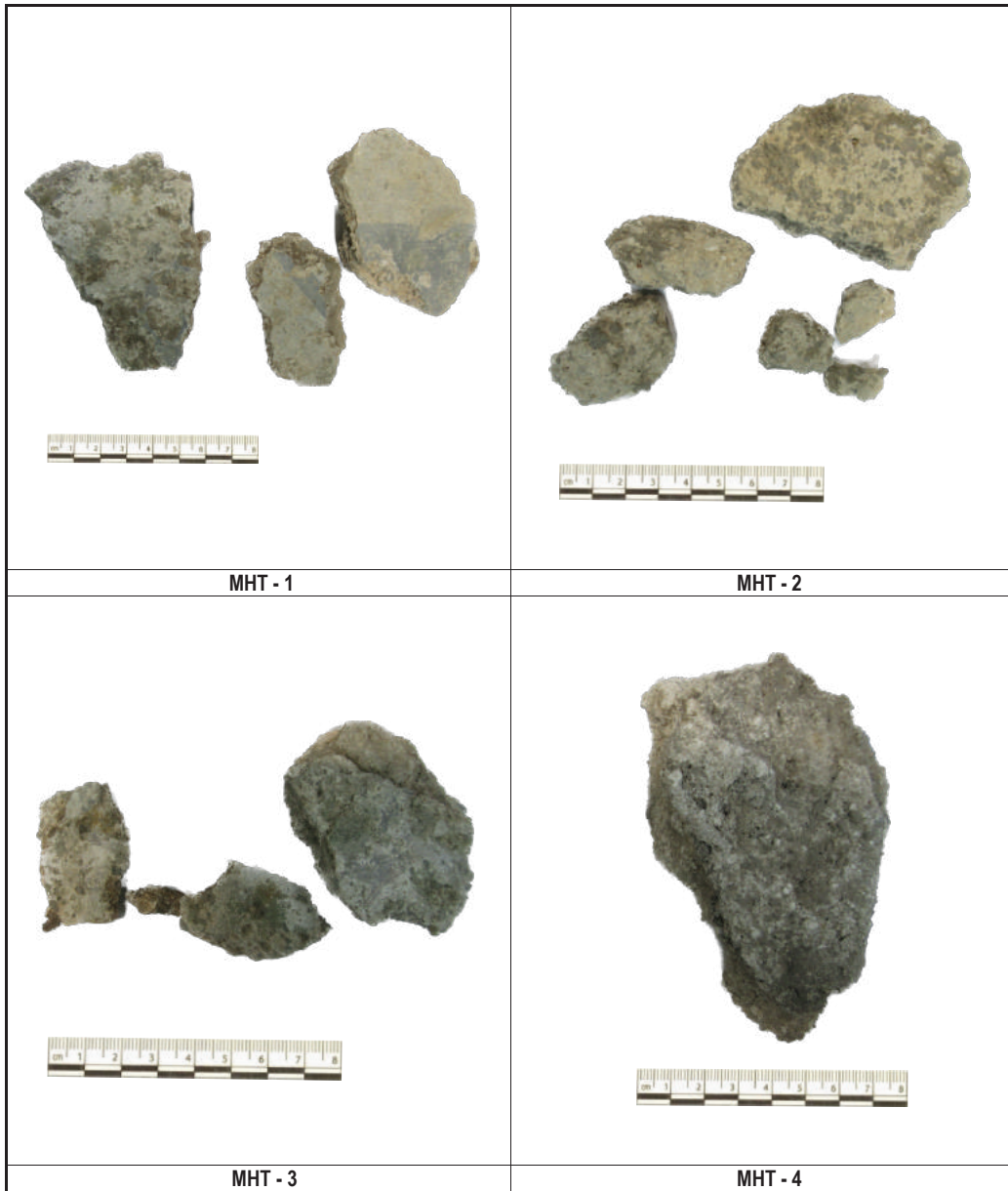
Wang, F. (2013). The birth and use of concrete and reinforced concrete. *Advanced Materials Research*, *712*, 955-960.

Zhang, D., Zhao, J., Wang, D., Xu, C., Zhai, M., & Ma, X. (2018). Comparative study on the properties of three hydraulic lime mortar systems: Natural hydraulic lime mortar, cement-aerial lime-based mortar and slag-aerial lime-based mortar. *Construction and Building Materials*, *186*, 42-52.

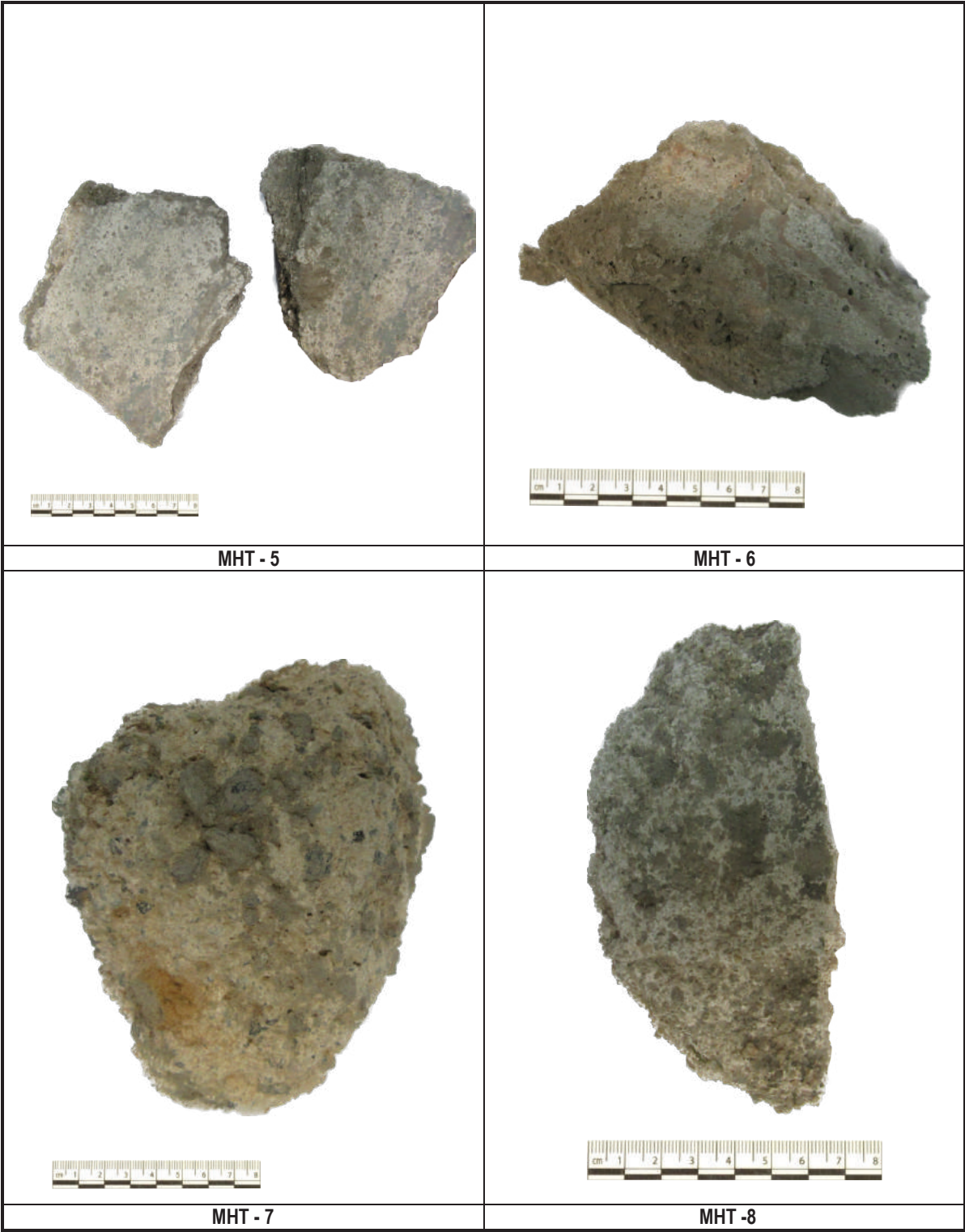
APPENDICES

APPENDICES

Appendix I. Photos of Samples from Horta da Torre.



APPENDICES



APPENDICES



MHT - 9



MHT - 10

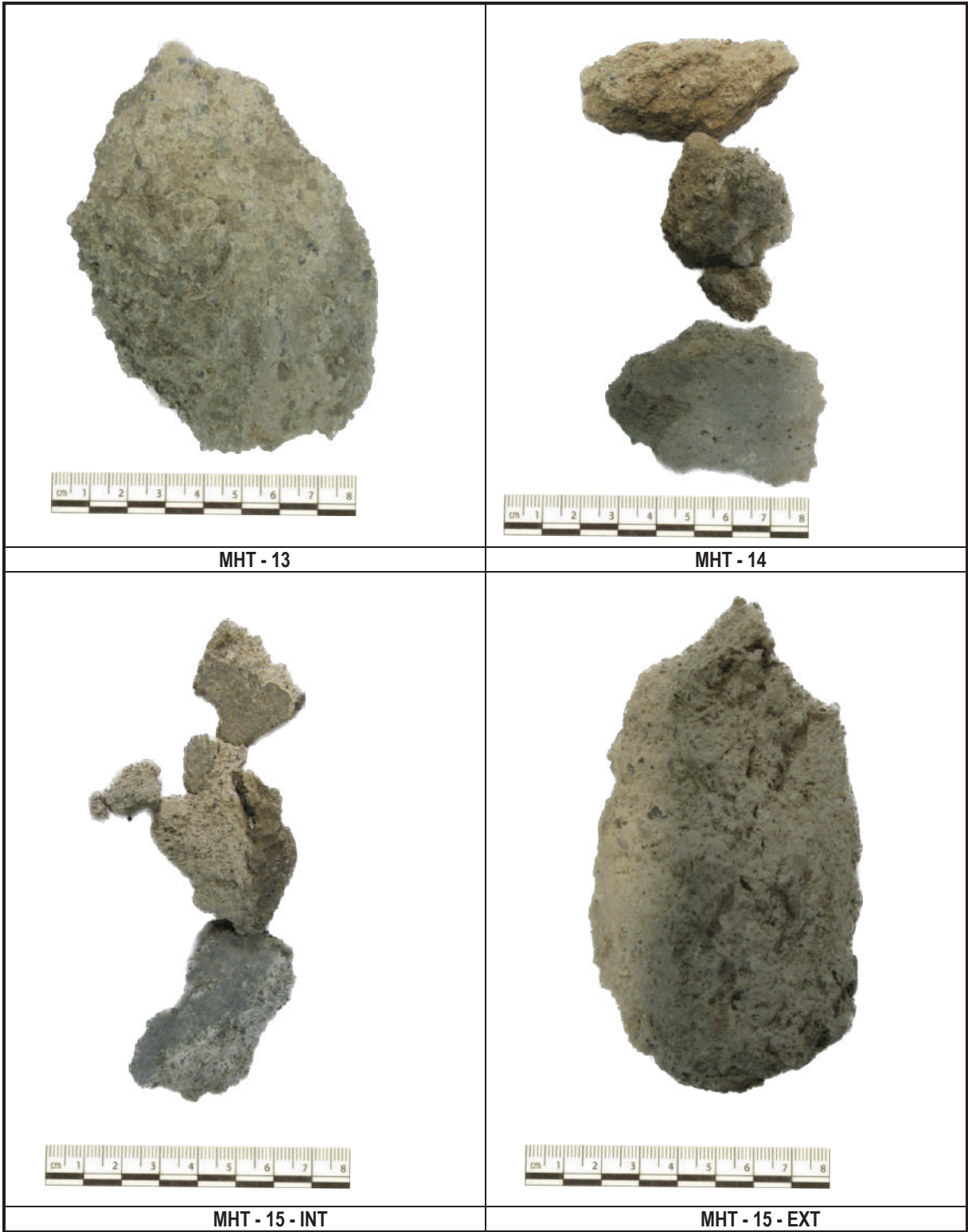


MHT - 11



MHT - 12

APPENDICES



APPENDICES



MHT - 16



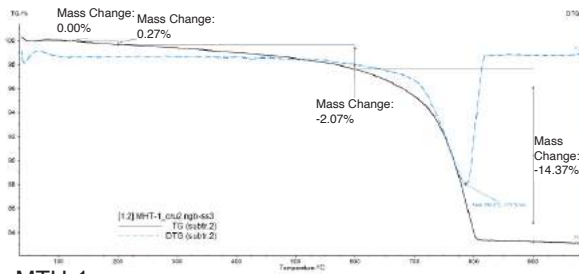
MHT - 17



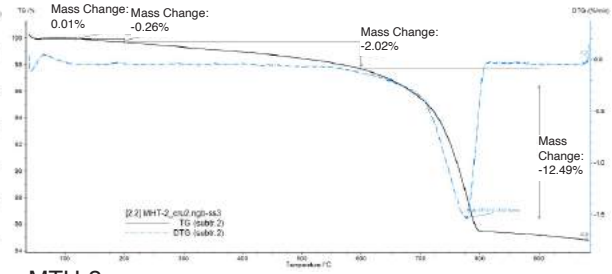
MHT - 18

APPENDICES

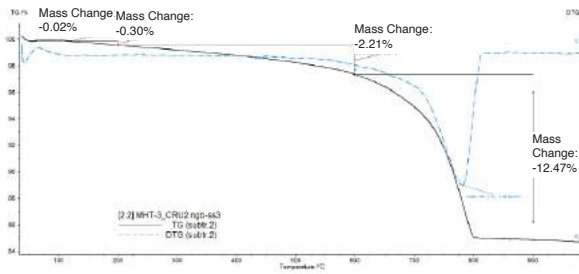
Appendix II: TG and DTG Curves.



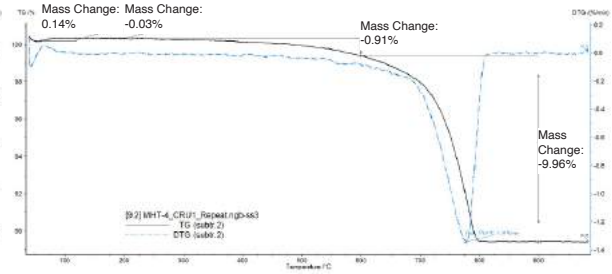
MTH-1



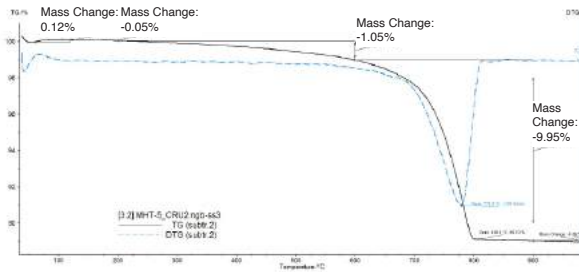
MTH-2



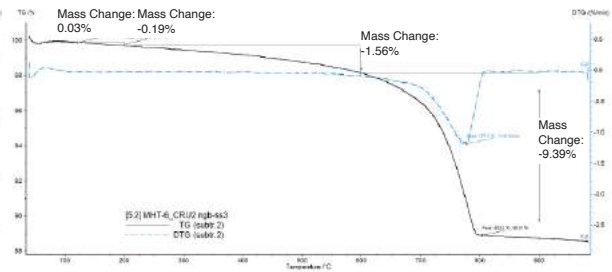
MTH-3



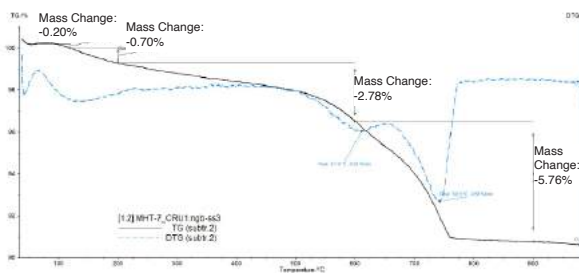
MTH-4



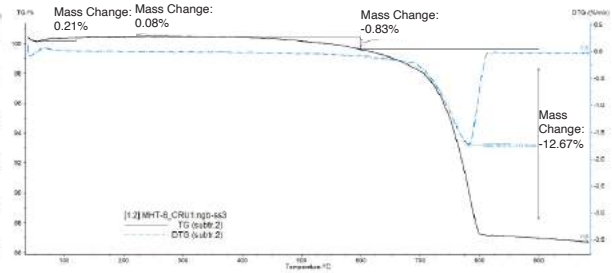
MTH-5



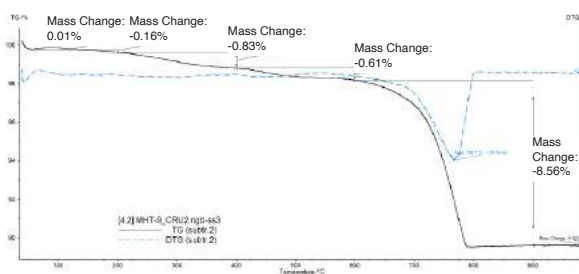
MTH-6



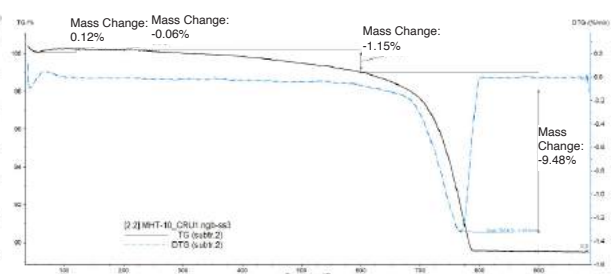
MTH-7



MTH-8

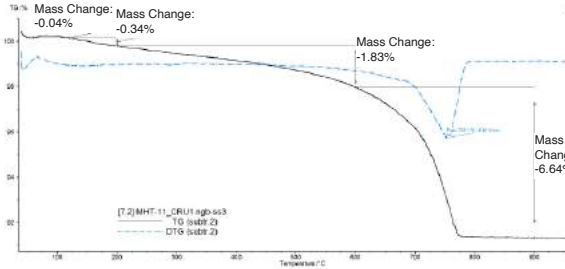


MTH-9

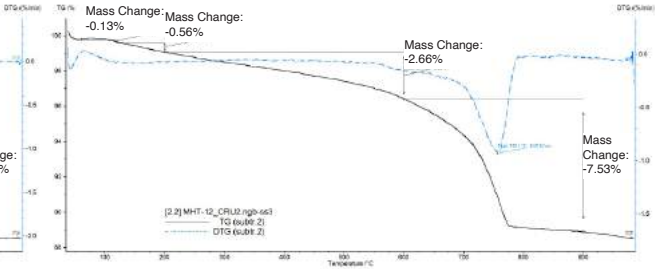


MTH-10

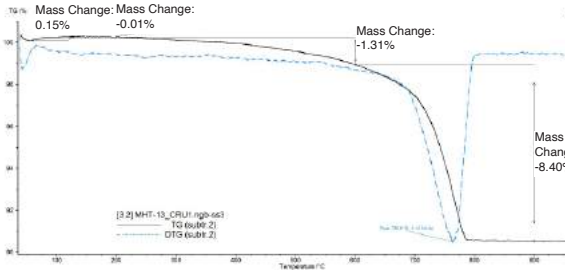
APPENDICES



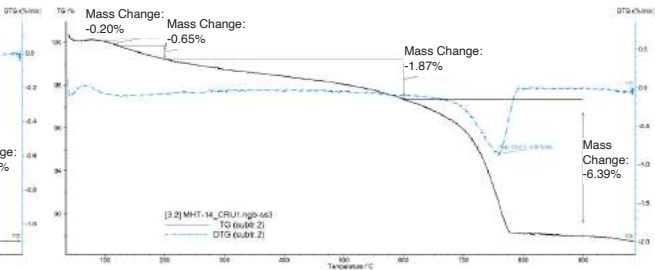
MTH-11



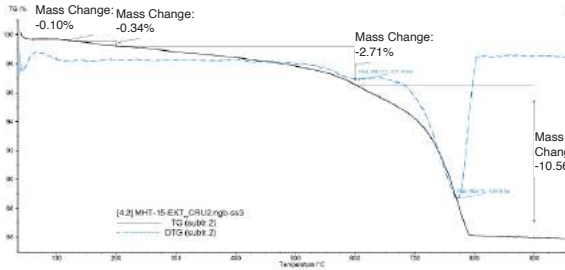
MTH-12



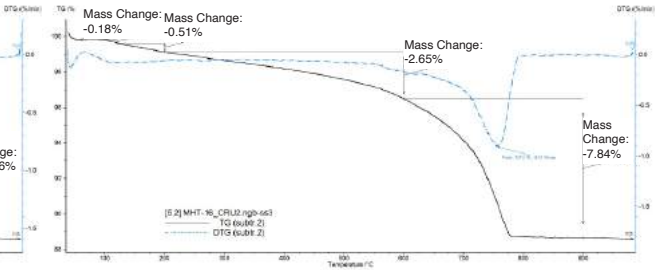
MTH-13



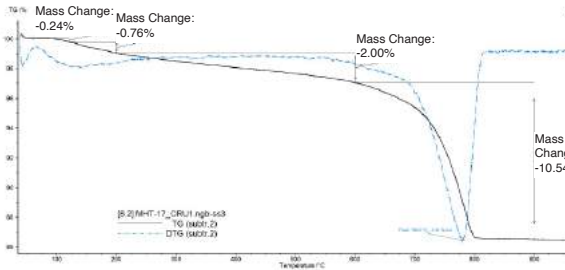
MTH-14



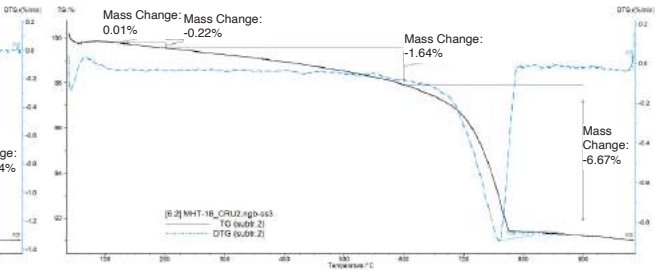
MTH-15



MTH-16



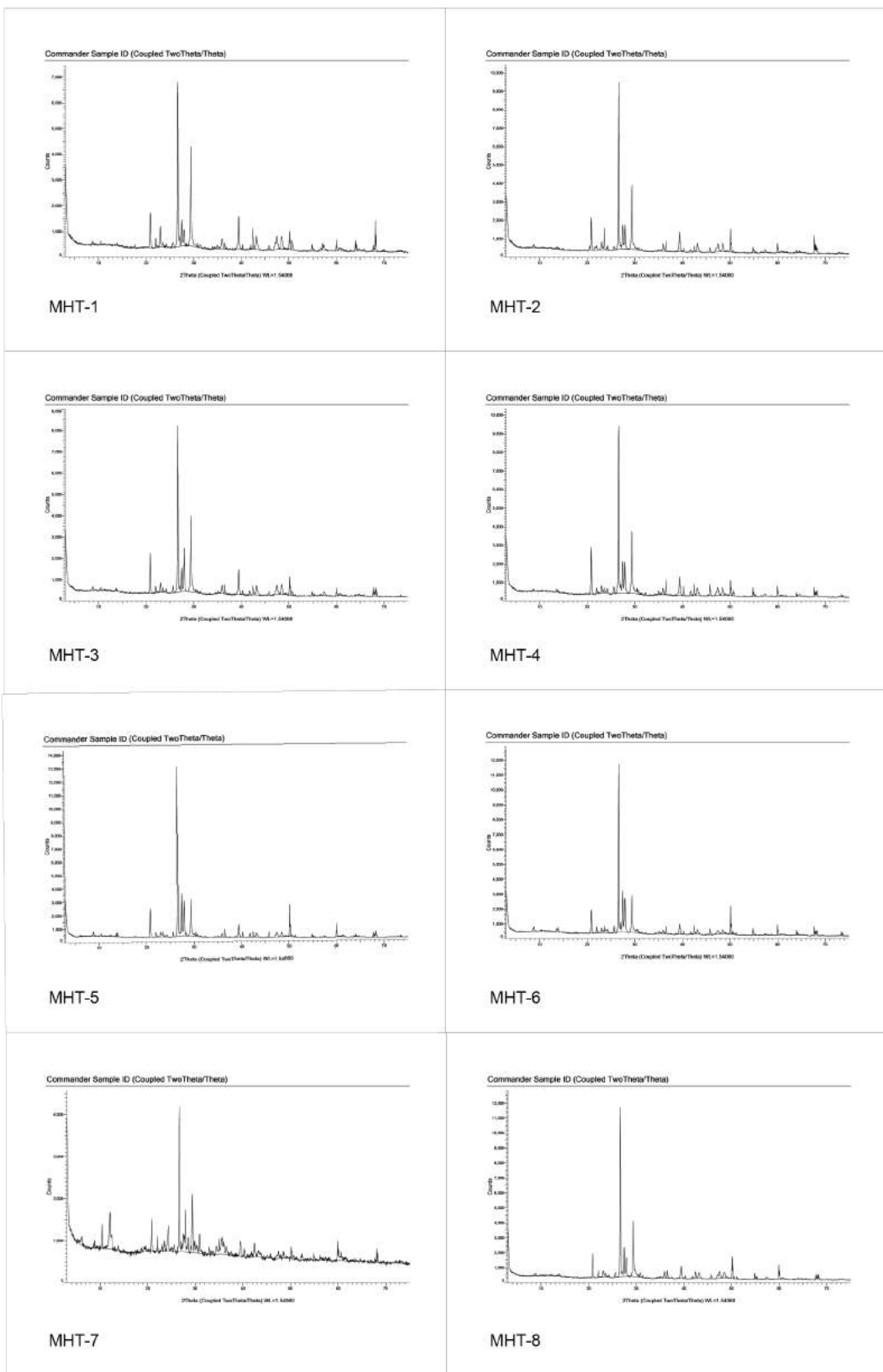
MTH-17



MTH-18

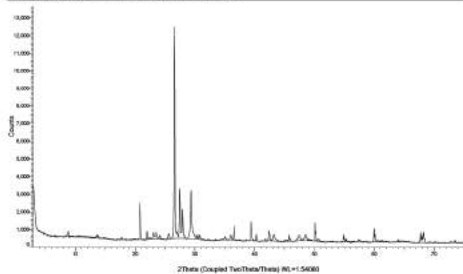
APPENDICES

Appendix III: X-Ray Diffractograms of Global Fractions.



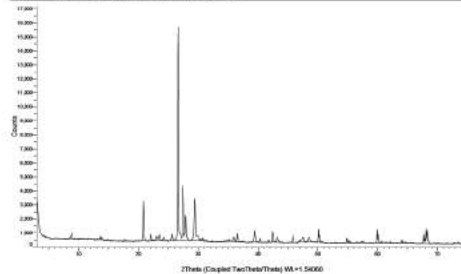
APPENDICES

Commander Sample ID (Coupled TwoTheta/Theta)



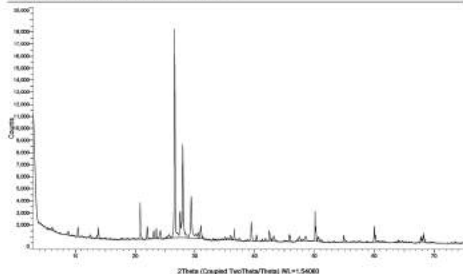
MHT-9

Commander Sample ID (Coupled TwoTheta/Theta)



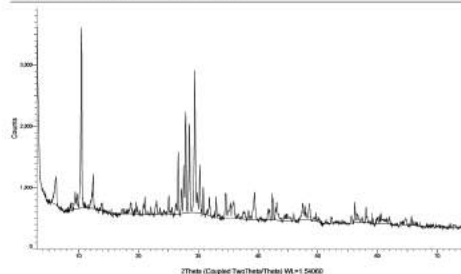
MHT-10

Commander Sample ID (Coupled TwoTheta/Theta)



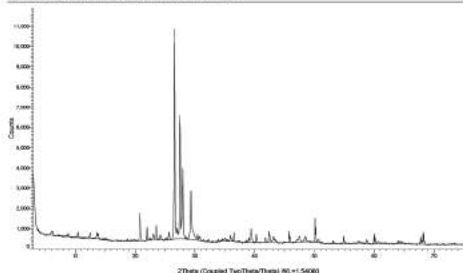
MHT-11

Commander Sample ID (Coupled TwoTheta/Theta)



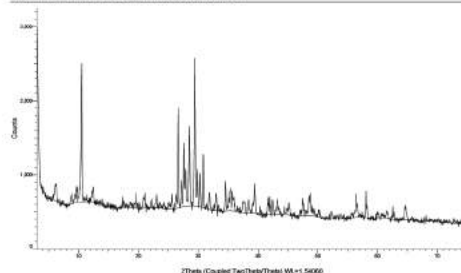
MHT-12

Commander Sample ID (Coupled TwoTheta/Theta)



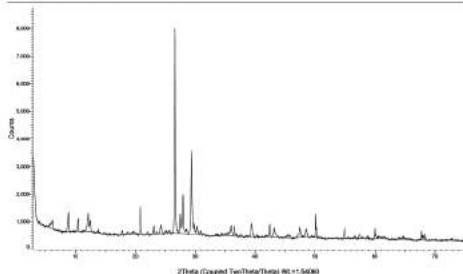
MHT-13

Commander Sample ID (Coupled TwoTheta/Theta)



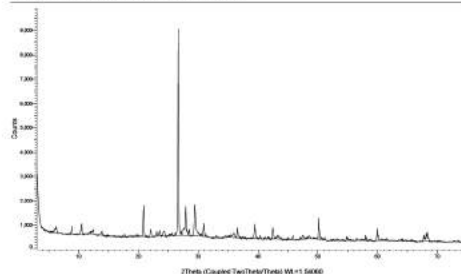
MHT-14

Commander Sample ID (Coupled TwoTheta/Theta)



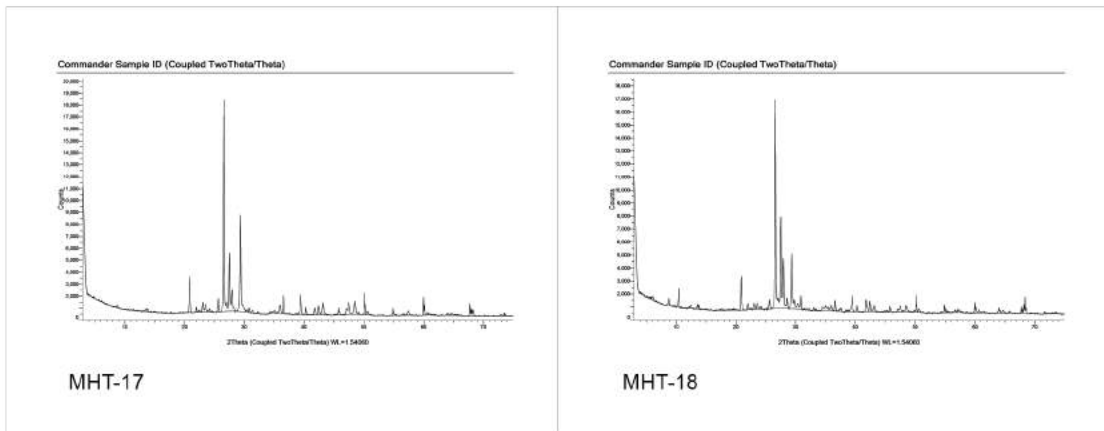
MHT-15

Commander Sample ID (Coupled TwoTheta/Theta)



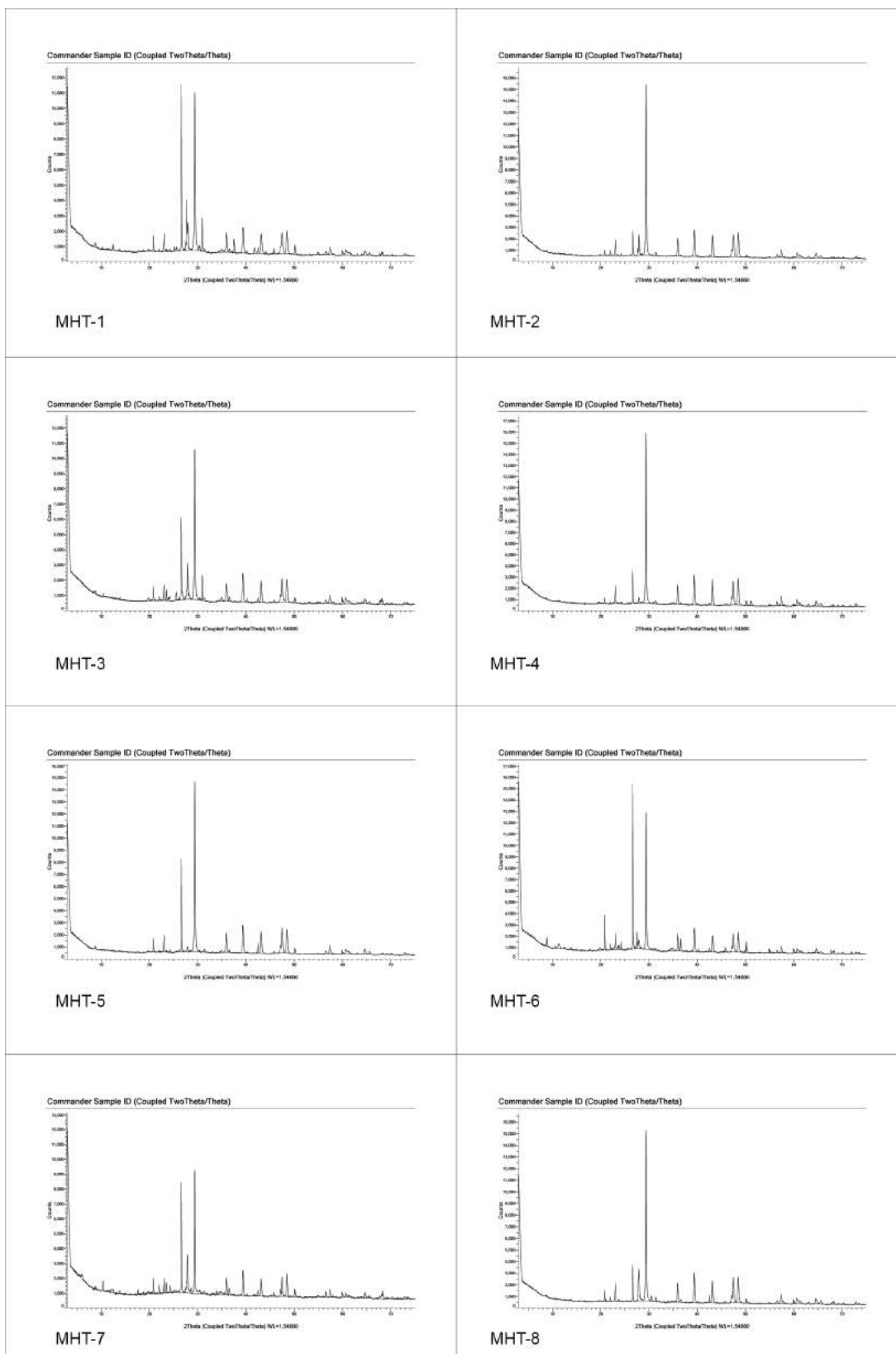
MHT-16

APPENDICES



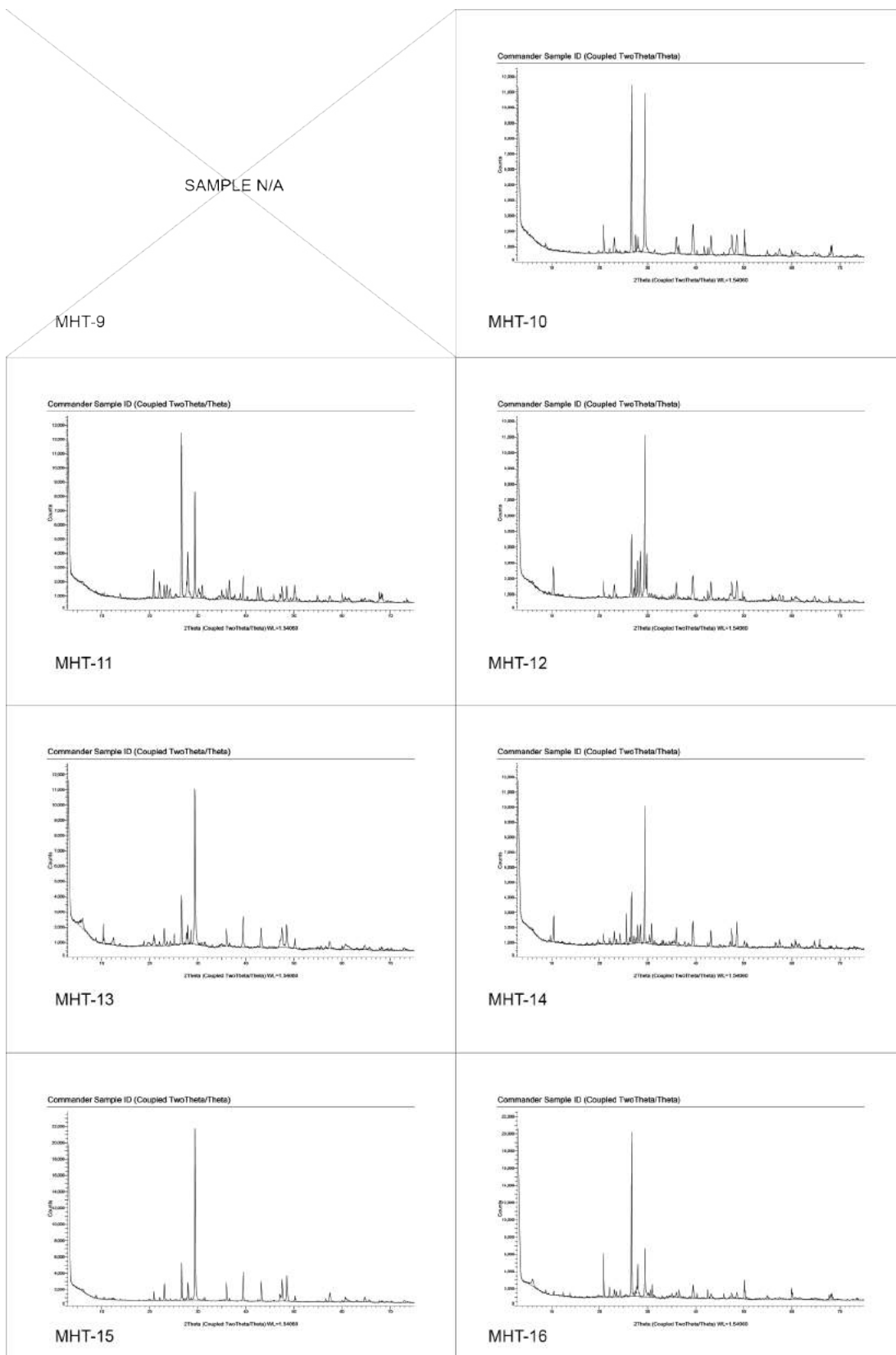
APPENDICES

Appendix IV: X-Ray Diffractogram of Fine Fractions.

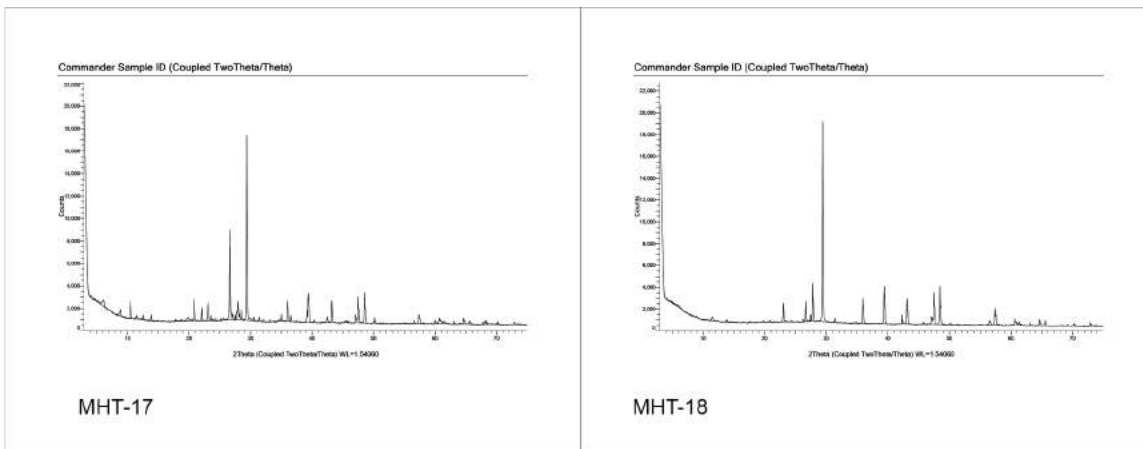


APPENDICES

Note: Not Enough Sample for MHT-9.

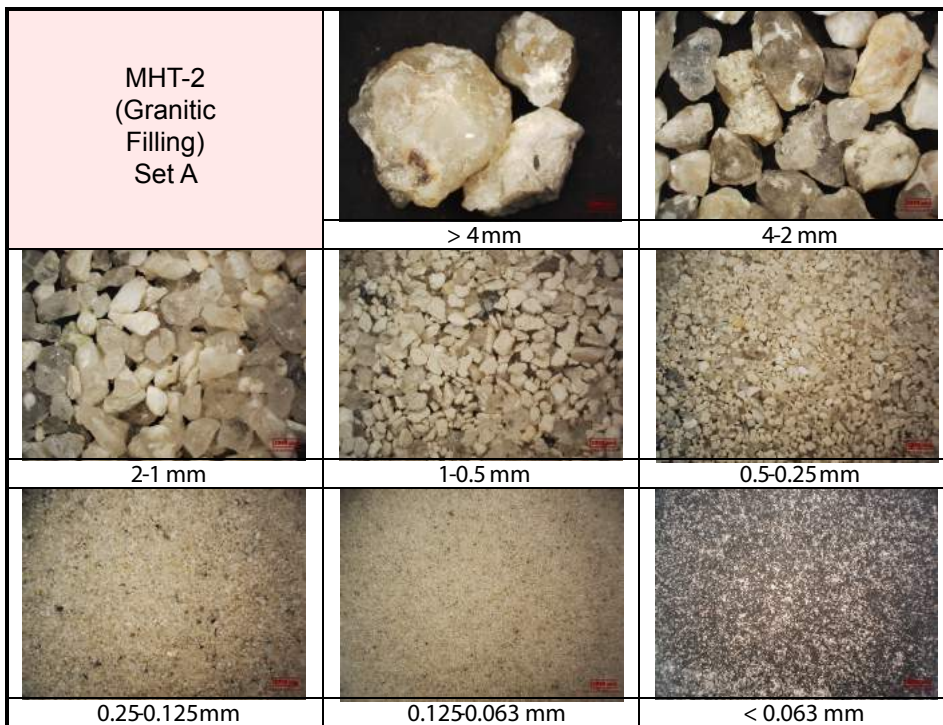
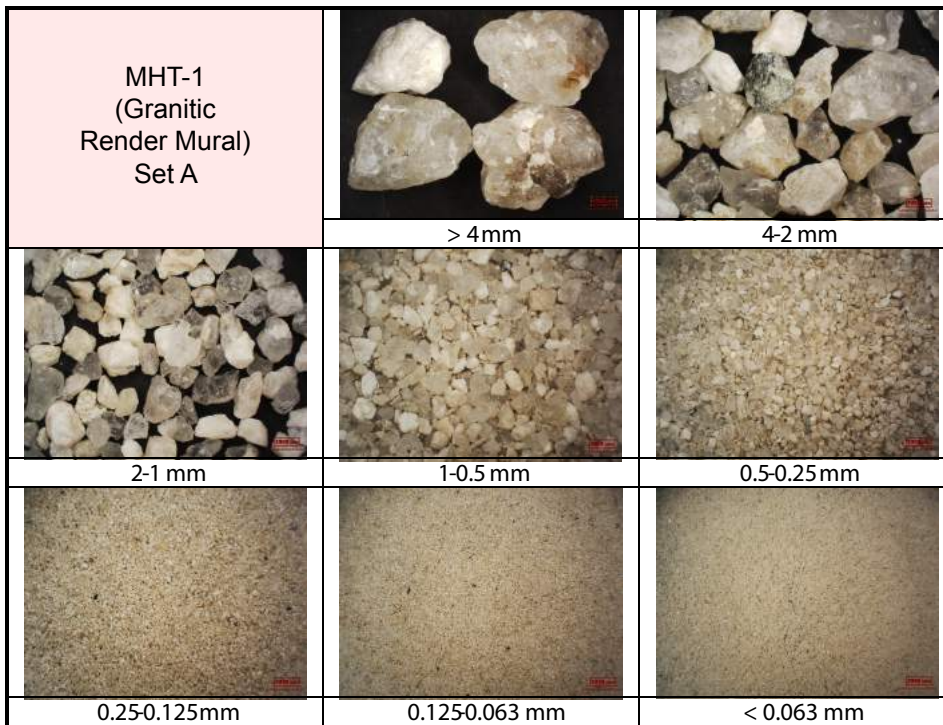


APPENDICES



APPENDICES

Appendix V: Insoluble Residues Sorted by Sieving System for Granulometric Analysis After Acid Attack.



APPENDICES

| | | |
|---|---|--|
| <p>MHT-3 (Granitic Render Mural) Set A</p> |  |  |
| | > 4mm | 4-2 mm |
|  |  |  |
| 2-1 mm | 1-0.5 mm | 0.5-0.25mm |
|  |  |  |
| 0.25-0.125mm | 0.125-0.063 mm | < 0.063 mm |

| | | |
|---|---|--|
| <p>MHT-4 (Granitic Filling) Set A</p> |  |  |
| | > 4mm | 4-2 mm |
|  |  |  |
| 2-1 mm | 1-0.5 mm | 0.5-0.25mm |
|  |  |  |
| 0.25-0.125mm | 0.125-0.063 mm | < 0.063 mm |

APPENDICES

| | | |
|---|---|--|
| MHT-5 (Granitic Render Mural) Set A | N/A |  |
| | > 4mm | 4-2 mm |
|  |  |  |
| 2-1 mm | 1-0.5 mm | 0.5-0.25mm |
|  |  |  |
| 0.25-0.125mm | 0.125-0.063 mm | < 0.063 mm |

| | | |
|---|---|--|
| MHT-6 (Granitic Filling) Set A | N/A |  |
| | > 4mm | 4-2 mm |
|  |  |  |
| 2-1 mm | 1-0.5 mm | 0.5-0.25mm |
|  |  |  |
| 0.25-0.125mm | 0.125-0.063 mm | < 0.063 mm |

APPENDICES

| | | |
|---|---|--|
| MHT-7 (Basic Filling) Set A |  |  |
| | > 4mm | 4-2 mm |
|  |  |  |
| 2-1 mm | 1-0.5 mm | 0.5-0.25mm |
|  |  |  |
| 0.25-0.125mm | 0.125-0.063 mm | < 0.063 mm |

| | | |
|---|---|--|
| MHT-8 (Granitic Render) Set A | N/A |  |
| | > 4mm | 4-2 mm |
|  |  |  |
| 2-1 mm | 1-0.5 mm | 0.5-0.25mm |
|  |  |  |
| 0.25-0.125mm | 0.125-0.063 mm | < 0.063 mm |

APPENDICES

| | | |
|---|---|--|
| <p>MHT-9 (Granitic Render Mural) Set A</p> |  |  |
| | > 4mm | 4-2 mm |
|  |  |  |
| 2-1 mm | 1-0.5 mm | 0.5-0.25mm |
|  |  |  |
| 0.250-0.125mm | 0.1250-0.063 mm | < 0.063 mm |

| | | |
|---|---|--|
| <p>MHT-10 (Granitic Render Mural) Set A</p> |  |  |
| | > 4mm | 4-2 mm |
|  |  |  |
| 2-1 mm | 1-0.5 mm | 0.5-0.25mm |
|  |  |  |
| 0.250-0.125mm | 0.1250-0.063 mm | < 0.063 mm |

APPENDICES

| | | |
|---|---|---|
| MHT-11 (Mixed Filling) Set A |  |  |
| | > 4mm | 4-2 mm |
|  |  |  |
| 2-1 mm | 1-0.5 mm | 0.5-0.25mm |
|  |  |  |
| 0.25-0.125mm | 0.125-0.063 mm | < 0.063 mm |

| | | |
|---|---|---|
| MHT-12 (Basic Filling) Set B |  |  |
| | > 4mm | 4-2 mm |
|  |  |  |
| 2-1 mm | 1-0.5 mm | 0.5-0.25mm |
|  |  |  |
| 0.25-0.125mm | 0.125-0.063 mm | < 0.063 mm |

APPENDICES

| | | |
|---|---|--|
| <p>MHT-13 (Granitic Render Mural) Set A</p> |  |  |
| | > 4mm | 4-2 mm |
|  |  |  |
| 2-1 mm | 1-0.5 mm | 0.5-0.25mm |
|  |  |  |
| 0.25-0.125mm | 0.125-0.063 mm | < 0.063 mm |

| | | |
|---|---|--|
| <p>MHT-14 (Basic Filling) Set A</p> |  |  |
| | > 4mm | 4-2 mm |
|  |  |  |
| 2-1 mm | 1-0.5 mm | 0.5-0.25mm |
|  |  |  |
| 0.25-0.125mm | 0.125-0.063 mm | < 0.063 mm |

APPENDICES

| | | |
|---|---|---|
| MHT-15-EXT (Basic Render) Set A |  |  |
| | > 4mm | 4-2 mm |
|  |  |  |
| 2-1 mm | 1-0.5 mm | 0.5-0.25mm |
|  |  |  |
| 0.250-0.125mm | 0.1250-0.063 mm | < 0.063 mm |

| | | |
|---|---|---|
| MHT-16 (Basic Filling) Set A |  |  |
| | > 4mm | 4-2 mm |
|  |  |  |
| 2-1 mm | 1-0.5 mm | 0.5-0.25mm |
|  |  |  |
| 0.250-0.125mm | 0.1250-0.063 mm | < 0.063 mm |

APPENDICES

| | | |
|---|---|--|
| MHT-17 (Granitic Filling) Set A |  |  |
| | > 4mm | 4-2 mm |
|  |  |  |
| 2-1 mm | 1-0.5 mm | 0.5-0.25mm |
|  |  |  |
| 0.25-0.125mm | 0.125-0.063 mm | < 0.063 mm |

| | | |
|---|---|--|
| MHT-18 (Mixed Filling) Set A |  |  |
| | > 4mm | 4-2 mm |
|  |  |  |
| 2-1 mm | 1-0.5 mm | 0.5-0.25mm |
|  |  |  |
| 0.25-0.125mm | 0.125-0.063 mm | < 0.063 mm |

APPENDICES

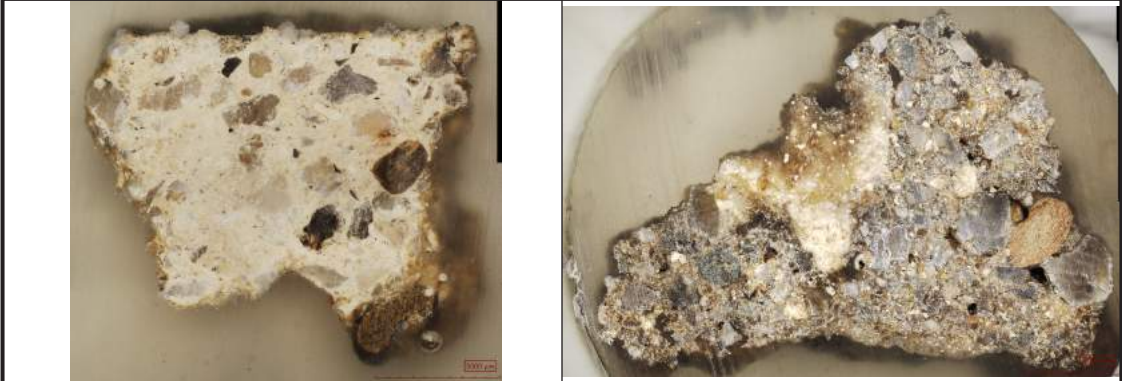
Appendix VI: Cross Section of Samples Taken by Stereozoom Microscope.

| | |
|---|--|
|  |  |
| MHT-1 | MHT-2 |
|  |  |
| MHT-3 | MHT-4 |
|  |  |
| MHT-5 | MHT-6 |
|  |  |
| MHT-7 | MHT-8 |

APPENDICES

| | |
|---|--|
|  |  |
| MHT-9 | MHT-10 |
|  |  |
| MHT-11 | MHT-12 |
|  |  |
| MHT-13 | MHT-14 |
|  |  |
| MHT-15 | MHT-16 |

APPENDICES



MHT-17

MHT-18

| | |
|--|--|
| | |
| | |
| | |
| | |
| | |
| | |
| | |
| | |
| | |
| | |

APPENDICES

Appendix VII: Acid Attack Results.

| Sample | | Weight | | Composition (%) | | Particle Size (mm) | | | | | | | |
|------------|-----|-------------|-----------|-------------------|------------------|--------------------|-------|-------|---------|------------|---------------|---------------|--------|
| Name | Set | Initial (g) | Final (g) | Insoluble Residue | Soluble Fraction | >4 | 4 - 2 | 2 - 1 | 1 - 0.5 | 0.5 - 0.25 | 0.250 - 0.125 | 0.125 - 0.063 | <0.063 |
| MHT-1 | A | 10.297 | 6.455 | 62.69 | 37.31 | 9.72 | 22.10 | 17.31 | 16.93 | 12.57 | 9.99 | 8.33 | 3.05 |
| | B | 10.68 | 5.939 | 55.61 | 44.39 | 1.09 | 19.67 | 23.18 | 16.64 | 13.41 | 12.99 | 10.02 | 2.99 |
| MHT-2 | A | 10.14 | 5.79 | 57.10 | 42.90 | 11.26 | 26.48 | 22.56 | 13.96 | 9.49 | 6.67 | 8.37 | 1.21 |
| | B | 10.127 | 6.487 | 64.06 | 35.94 | 6.81 | 36.36 | 20.57 | 15.42 | 8.85 | 5.99 | 5.02 | 0.97 |
| MHT-3 | A | 10.478 | 6.435 | 61.41 | 38.59 | 1.25 | 17.47 | 23.21 | 16.60 | 14.56 | 12.28 | 10.98 | 3.64 |
| | B | 10.027 | 6.208 | 61.91 | 38.09 | 5.41 | 25.32 | 18.93 | 15.88 | 9.76 | 9.87 | 11.75 | 3.07 |
| MHT-4 | A | 10.665 | 6.678 | 62.62 | 37.38 | 1.07 | 16.84 | 30.43 | 24.61 | 12.75 | 7.08 | 5.62 | 1.59 |
| | B | 10.242 | 6.678 | 65.20 | 34.80 | 0.80 | 19.89 | 31.27 | 22.15 | 11.57 | 6.87 | 5.96 | 1.50 |
| MHT-5 | A | 10.161 | 7.253 | 71.38 | 28.62 | 0.00 | 15.10 | 34.99 | 26.04 | 9.42 | 5.80 | 6.09 | 2.56 |
| | B | 10.699 | 6.782 | 63.39 | 36.61 | 0.00 | 15.73 | 34.74 | 26.64 | 9.00 | 6.03 | 5.86 | 2.00 |
| MHT-6 | A | 10.053 | 6.977 | 69.40 | 30.60 | 0.00 | 6.75 | 17.21 | 24.41 | 24.41 | 13.07 | 10.41 | 3.74 |
| | B | 10.009 | 7.696 | 76.89 | 23.11 | 0.00 | 9.30 | 14.93 | 24.78 | 22.56 | 12.67 | 9.48 | 6.29 |
| MHT-7 | A | 10.141 | 7.46 | 73.56 | 26.44 | 11.34 | 23.97 | 17.67 | 11.69 | 9.22 | 10.62 | 10.96 | 4.52 |
| | B | 10.087 | 7.608 | 75.42 | 24.58 | 24.04 | 16.10 | 18.79 | 12.56 | 9.92 | 8.48 | 7.66 | 2.44 |
| MHT-8 | A | 10.37 | 6.189 | 59.68 | 40.32 | 0.00 | 12.22 | 37.74 | 29.37 | 8.29 | 5.81 | 5.16 | 1.40 |
| | B | 10.25 | 6.326 | 61.72 | 38.28 | 0.00 | 11.94 | 37.38 | 26.22 | 9.32 | 6.73 | 6.71 | 1.69 |
| MHT-9 | A | 10.118 | 7.089 | 70.06 | 29.94 | 2.73 | 13.28 | 16.48 | 14.55 | 12.77 | 14.95 | 17.54 | 7.71 |
| | B | 3.942 | 2.757 | 69.94 | 30.06 | 0.00 | 21.35 | 15.38 | 9.91 | 11.59 | 13.10 | 20.15 | 8.52 |
| MHT-10 | A | 10.418 | 7.203 | 69.14 | 30.86 | 1.21 | 9.90 | 17.70 | 13.16 | 12.64 | 17.19 | 18.98 | 9.23 |
| | B | 10.49 | 6.744 | 64.29 | 35.71 | 0.40 | 11.24 | 13.30 | 9.74 | 14.01 | 18.63 | 18.92 | 13.78 |
| MHT-11 | A | 10.064 | 6.424 | 63.83 | 36.17 | 1.80 | 11.28 | 11.90 | 11.66 | 11.01 | 18.06 | 20.53 | 13.77 |
| | B | 10.708 | 7.313 | 68.29 | 31.71 | 7.35 | 13.31 | 10.51 | 9.12 | 6.27 | 15.05 | 21.94 | 16.46 |
| MHT-12 | A | 10.084 | 6.829 | 67.72 | 32.28 | 0.00 | 15.67 | 14.27 | 12.58 | 13.84 | 17.75 | 18.56 | 7.33 |
| | B | 10.114 | 7.047 | 69.68 | 30.32 | 10.05 | 10.00 | 12.78 | 13.03 | 14.20 | 17.66 | 16.10 | 6.18 |
| MHT-13 | A | 10.311 | 7.087 | 68.73 | 31.27 | 0.00 | 19.10 | 24.55 | 16.45 | 12.53 | 11.44 | 10.19 | 5.75 |
| | B | 10.605 | 7.493 | 70.66 | 29.34 | 1.22 | 22.05 | 27.12 | 19.97 | 11.32 | 7.42 | 7.81 | 3.09 |
| MHT-14 | A | 10.08 | 7.208 | 71.51 | 28.49 | 7.87 | 10.82 | 17.58 | 13.41 | 13.90 | 14.20 | 14.03 | 8.20 |
| | B | 10.127 | 6.829 | 67.43 | 32.57 | 4.08 | 9.07 | 14.13 | 11.89 | 15.27 | 17.69 | 18.20 | 9.68 |
| MHT-15-EXT | A | 10.788 | 6.93 | 64.24 | 35.76 | 11.56 | 14.55 | 25.64 | 23.14 | 10.23 | 6.66 | 5.54 | 2.68 |
| | B | 10.435 | 6.59 | 63.15 | 36.85 | 3.19 | 16.73 | 25.24 | 22.24 | 14.90 | 8.27 | 6.32 | 3.11 |
| MHT-15-INT | A | 10.269 | 6.327 | 61.61 | 38.39 | 1.36 | 9.31 | 23.45 | 25.94 | 14.46 | 10.02 | 9.60 | 5.85 |
| | B | 10.063 | 5.646 | 56.11 | 43.89 | 5.67 | 8.64 | 15.24 | 19.88 | 15.04 | 13.64 | 15.42 | 6.47 |
| MHT-16 | A | 10.376 | 7.323 | 70.58 | 29.42 | 16.23 | 5.92 | 5.96 | 4.42 | 9.63 | 17.72 | 24.88 | 15.25 |
| | B | 10.071 | 6.627 | 65.80 | 34.20 | 7.27 | 7.97 | 5.86 | 6.83 | 8.59 | 19.41 | 27.05 | 17.01 |
| MHT-17 | A | 10.548 | 7.007 | 66.43 | 33.57 | 10.82 | 21.46 | 24.42 | 15.98 | 9.82 | 7.42 | 7.26 | 2.81 |
| | B | 10.014 | 7.016 | 70.06 | 29.94 | 11.98 | 17.26 | 24.66 | 14.38 | 8.93 | 19.83 | 0.32 | 2.64 |
| MHT-18 | A | 10.047 | 5.284 | 52.59 | 47.41 | 1.37 | 17.06 | 25.35 | 18.24 | 10.57 | 10.59 | 12.96 | 3.85 |
| | B | 10.414 | 7.519 | 72.20 | 27.80 | 3.65 | 19.27 | 22.91 | 16.47 | 9.86 | 11.69 | 13.60 | 2.55 |